Chapter 13

Volcano Seismology

(Version August 2011; DOI: 10.2312/GFZ.NMSOP-2_ch13)

Joachim Wassermann

Geophysikalisches Observatorium der Ludwig-Maximilians Universität München, Ludwigshöhe 8, D-82256 Fürstenfeldbruck, Germany,
Tel.: +49 (0)89 2180 73962, E-mail: j.wassermann@lmu.de

page

13.1 Introduction 2
13.1.1 Why a different chapter? 3
13.1.2 Why use seismology when forecasting volcanic eruptions? 3
13.1.3 Why is a revised version needed? 4
13.2 Classification and source models of volcano-seismic signals 4
13.2.1 Transient volcano-seismic signals 5
13.2.1.1 Volcanic-Tectonic events (deep and shallow) 5
13.2.1.2 Low-Frequency events 9
13.2.1.3 Hybrid events, Multi-Phases events 12
13.2.1.4 Explosion quakes, very-low-frequency events, ultra-low-frequency events 13
13.2.2 Continuous volcanic-seismic signals 18
13.2.2.1 Volcanic tremor (low-viscous two-phase flow and eruption tremor) 19
13.2.2.2 Volcanic tremor (high-viscous - resonating gas phase) 21
13.2.2.3 Surface processes 23
13.2.3 Special note on noise 24
13.3 Design of a monitoring network 25
13.3.1 Station site selection 25
13.3.2 Station distribution 26
13.3.3 Seismic arrays in volcano monitoring 26
13.3.4 Arrays of seismic arrays 27
13.4 Analysis and interpretation 28
13.4.1 One-component single station 29
13.4.1.1 Spectral analysis 29
13.4.1.2 Envelope, RSAM and cumulative amplitude measurements 30
13.4.1.3 Failure Forecast Method (FFM) 33
13.4.2 Three-component single station 34
13.4.2.1 Polarization 35
13.4.2.2 Polarization filters 35
13.4.3 Network 37
13.4.3.1 Hypocenter determination by travel-time differences 37
13.4.3.2 Cross-correlation of diffuse wavefields 38
13.4.3.3 Amplitude - distance based hypocenter determination algorithm 39
13.4.4 Seismic arrays 42
13.4.4.1 f-k beamforming 43
13.4.4.2 Array polarization 45

13.4.4.3 Hypocenter determination using seismic arrays 45
13.4.5 Automatic classification/detection 46
13.4.6 Moment tensor inversion 47
13.4.6.1 Computation of Green´s function in 3D 48
13.4.6.2 Source modelling of complex processes 49
13.4.6.3 Limitations of Moment Tensor Inversion 50
13.4.7 Automatic analysis and databases 51
13.5 Other monitoring techniques 52
13.5.1 Infra sound 52
13.5.2 Ground deformation (D-GPS, P-InSAR, strain, tilt) 54
13.5.3 Micro-Gravimetry 57
13.5.4 Gas monitoring 57
13.5.5 Thermal and video recording 59
13.5.6 Meteorological parameters 59
13.6 Technical considerations 60
13.6.1 Site and vault 60
13.6.2 Sensors and digitizers 61
13.6.3 Digital telemetry and satellite communication 62
13.6.4 Power considerations 64
13.6.5 Data center 65
Acknowledgments 67
Recommended overview readings 67
References 68

13.1 Introduction

Volcanic eruptions and their impact on human society, following earthquakes and meteorological disasters, are the most severe natural hazards. Since the pioneering works of Omori (1911), Sassa (1936) and Imbo (1954), much attention was focused on the seismic signals preceding or accompanying a volcanic eruption. Soon after the start of more extensive seismic monitoring it became clear that volcanoes show a variety of different seismic signals, which often differ from those produced by common tectonic earthquake sources, i.e., double couple type sources.

Starting with the availability of small portable seismographs in the late 1960's to early 1970's, a tremendous number of observations were made at different volcanoes and during different stages of activity. At the same time, first attempts were made to explain some of the seismic signals recorded and to classify the different signals by their proposed (but still mostly unknown) source mechanisms. Following this very enthusiastic period the progress in the study of accelerated magma transport to the surface was stagnating. Too many open questions remained unsolved, such as the mostly unknown source mechanisms of volcanic signals, the influence of the topography of volcanoes, the problem of proper hypocenter determination, the relationship between the occurrence of seismic signals of different type and the associated surface activity of a volcano. Since the late 1980's to early 1990's the use of portable and robust broadband seismometers and newly developed low power consuming 24bit A/D converters as well as the extensive use of seismic array techniques opened new horizons and different views onto the source mechanisms and the importance of volcano-seismic signals in the framework of early warning.

This chapter should be seen as a guideline for establishing a seismic monitoring network or at least a temporary experiment at an active volcano. Because of the large number of different volcanoes and many different kinds of source mechanisms, which may produce seismic signals, a description of all aspects is not possible. Also, a comprehensive review of case studies, including the variety of volcanic earthquake sequences, is beyond the scope of this paper. Relevant references include the excellent text books *Encyclopedia of Volcanoes* (Sigurdsson, 2000), *Monitoring and Mitigation of Volcano Hazards* (Scarpa and Tilling, 1996) and the comprehensive article of McNutt (2005). Most of the relevant topics dealt with in these text books are summarized below.

13.1.1 Why a different chapter?

Volcano seismology uses many terms and methods known in earthquake seismology. This is no surprise as the same instruments and the same mechanism of elastic wave propagation through the Earth are used to investigate the subsurface structure and the activity state of a volcano. However, there are some deviations from conventional earthquake seismology, both in the physics of the signals and the methods of analyzing them. As outlined below, the signals vary from "earthquake-like" transients to long-lasting and continuous "tremor" signals. The most striking differences between earthquake and volcano seismology are the proposed source mechanisms and the related analysis techniques. In Section 13.2 and Section 13.4 we will discuss some of these aspects.

When setting up an earthquake monitoring network an optimal station coverage is needed in order to locate the events precisely. Depending on the tasks of the network, at least some stations should be located as close as possible to the active volcanic area in order to model the related seismic source with sufficient accuracy and determine the source depth. Hence, we are looking for a site-distribution which optimizes the station coverage and minimizes the influence of shallow structure and topography of the Earth. In contrast, in volcano-seismology we are left with sometimes very rough topography and nearly unknown propagation and site properties of the medium. Some of these aspects will be discussed in Section 13.3 and Section 13.4.

13.1.2 Why use seismology when forecasting volcanic eruptions?

The use of seismological observations in the monitoring and forecasting of volcanic eruptions is justified because nearly all seismically monitored volcanic eruptions have been accompanied by some sort of seismic anomaly. The Pinatubo 1991 (Pinatubo Volcano Observatory Team, 1991), the Hekla 2000 (http://hraun.vedur.is/ja/englishweb/heklanews.html#strain) and the 2010 Mt. Merapi eruption (http://www.merapi.bgl.esdm.go.id/aktivitas_merapi.php?page=aktivitas-merapi&subpage=seismisitas) are examples of successful long- and short-term eruption forecasts made by mainly seismic observations. For further case studies on volcanic "early warning" see the comprehensive articles by McNutt (1996, 2000a, 2000b).

While most of these "early warnings" were simply deduced by counting the number and type of volcanic events per hour or day or even better by monitoring their hypocenter distributions, the physical meaning of the different seismic events and their relationship to the fast ascending magma are not yet well understood. To give an example: increasing volcanic

tremor is always a sign of high volcanic activity, but although the occurrence of tremor will increase the alert level, its role for short-term prediction is still not known with sufficient precision because we do not know the related physical process of this signal (fluid flow; movement of magma, water and/or gas; crack extension etc.). Furthermore, how can we distinguish between an intrusion and a developing eruption, both of which generate a large number of seismic signals and often share similar characteristics?

The extensive use of seismic methods during the last decades also showed that using them alone will not help the improvement of our knowledge about the internal processes of rapid magma ascent. This will be discussed in more detail in subchapter Section 13.5. Planning a new monitoring network or a short-term seismic experiment, we must also keep in mind that every volcano has its own characteristics, both with respect to seismic signal generation and wave propagation effects.

13.1.3 Why is a revised version needed?

Since the writing of the first version of this chapter in 2002, much has changed both in the understanding of volcano-induced seismic signals as well as regarding technical aspects in recording the associated signals. The most dramatic changes appeared in the interpretation of the source mechanisms and the propagation of seismic waves at active volcanoes. This increased knowledge is mainly attributed to the availability of efficient numerical algorithms for simulating the signal generation as well as seismic wave propagation in complex media and by the increasing amount of high performance, parallel computing facilities. Another rising field in interpretation of volcanic unrest can be seen in the increasing number of applications in the field of remote sensing.

Both topics are far too large to be covered in detail in this manual. Especially the high performance computing part requires a lot of investment, which will not easily be covered especially in countries with multiple natural hazards and often small national budget. Therefore we will only briefly discuss the most important outcome of this expensive modeling.

While leaving the classification part nearly untouched, most of the changes in the revised version will be made in the source model part of Section 13.2 and some newly introduced analysis techniques in Section 13.4. Another major change is made in Section 13.5 where other monitoring techniques than seismology are briefly discussed. Here much more emphasize is given to new but already quite well established remote and ground based techniques (e.g., P-InSAR; SO_2 remote sensing; infra-sound measurement etc.). We finalize the revision by describing new technical developments in communication technology and software, i.e., database management systems, which are now thought to be “state of the art”.

13.2 Classification and source models of volcano-seismic signals

Most of the confusion in volcano seismology is caused by the huge number of different terms for classifying volcano-seismic events. While this is mainly caused by the imperfect knowledge about the source mechanisms, we will focus on the basic nomenclature widely used in the literature. Most of these terms simply describe the appearance and frequency content of the signal, while others imply a certain source mechanism. However, one should be

aware in both cases that the sources are often unknown and the propagation medium alters the shape and the spectral content of the signals significantly.

While pioneering work in classifying volcano-seismic signals was made by Shimozuru (1972) and Minakami (1974), most of the following discussion follows the work of McNutt (1996, 2000a) and Chouet (1996a). We will divide the known signals mainly into transient and continuous signals, even if some of these continuous signals reflect simply the superposition of discrete signals. We will also discuss, where appropriate and physically plausible, differences in the signal generation related to different types of magma (i.e., low/high viscous, gas rich/poor). In addition to the usual classification, "up-to-date" source models and interpretation of the occurrence of different signals will be given.

13.2.1 Transient volcano-seismic signals

13.2.1.1 Volcanic-Tectonic events (deep and shallow)

Deep (below about 2 km) Volcanic-Tectonic events (VT-A) manifest themselves by the clear onsets of P- and S-wave arrivals and their high frequency content (> 5Hz). This leads also to the class name *high-frequency* event (HF) (Fig. 13.1).

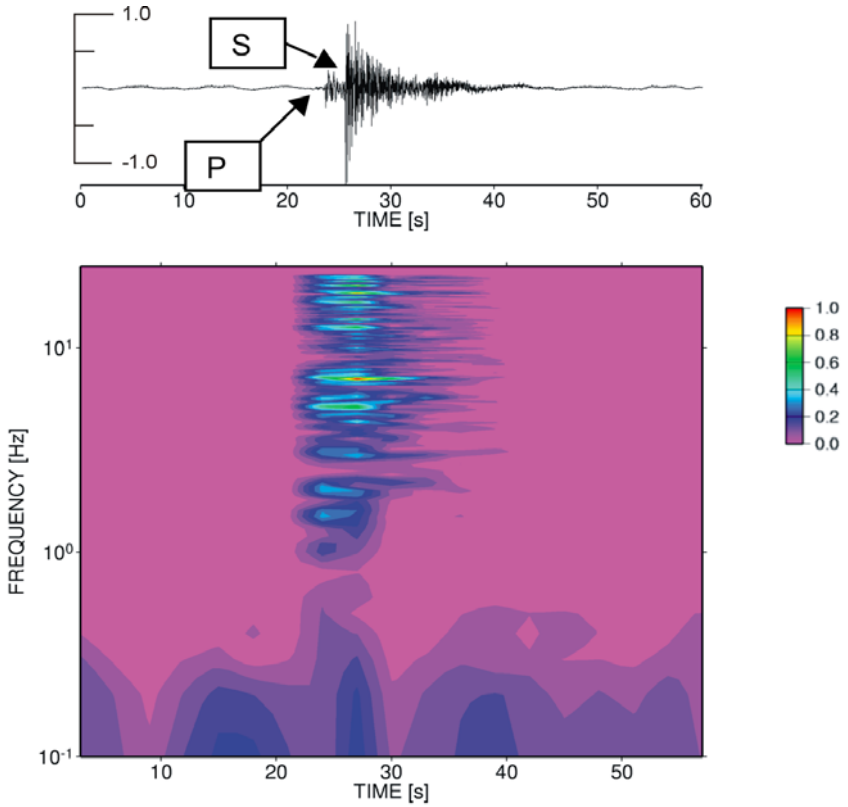

Fig. 13.1 VT-A type event recorded at Mt. Merapi, Indonesia. The impulsive P- and S-wave arrivals are clearly visible in this signal, as well as their high-frequency content and short signal duration. The given color coding, representing normalized amplitude spectral density, is valid for all following figures. Also the amplitudes of the corresponding amplitude-time representation are in arbitrary units and when given are normalized to the amplitude shown in this figure.

The name of this event type implies a well known source mechanism, namely a common shear failure caused by stress buildup and resulting in slip on a fault plane similar to a tectonic earthquake source. The only difference from the latter is the frequent occurrence of swarms of VT events, which do not follow the usual main-after-shock distribution (McNutt, 2000a) and are located within a volcanic edifice. An earthquake swarm is a sequence where the largest events are similar in size and not necessarily at the beginning of the sequence. The high frequencies and the impulsiveness of the P- and S-wave arrivals seems to be caused by low scattering due to the short travel path through high scattering regions and low attenuation.

In contrast, *shallow (above about 1-2 km) Volcanic-Tectonic* events (VT-B) show much more emergent P-wave onsets and sometimes it is even impossible to detect any clear S-wave arrival (Fig. 13.2). The spectral bands are shifted to lower frequencies (1-5 Hz). Both observations are thought to be caused by a shallow hypocenter location and therefore a larger amount of scattering during wave propagation, especially of higher frequencies.

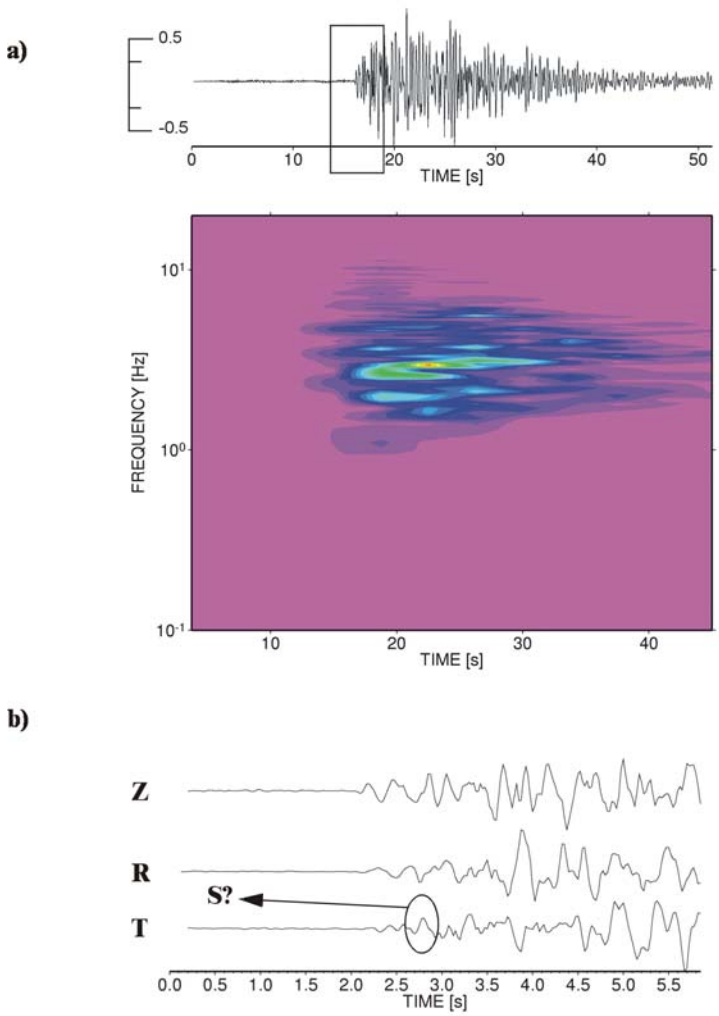

Fig. 13.2 a) Typical example of a VT-B type event recorded during a high activity phase at Mt. Merapi. Note that the overall frequency content is mainly between 1 – 10 Hz with a dominant frequency at roughly 3 Hz. **b)** zoomed-in version of all three components of the same event. Whereas the P-wave arrival is clearly visible, no clear S-wave arrival can be seen. The circle marks the wavelet that has the approximate S-wave travel time for the estimated source location.

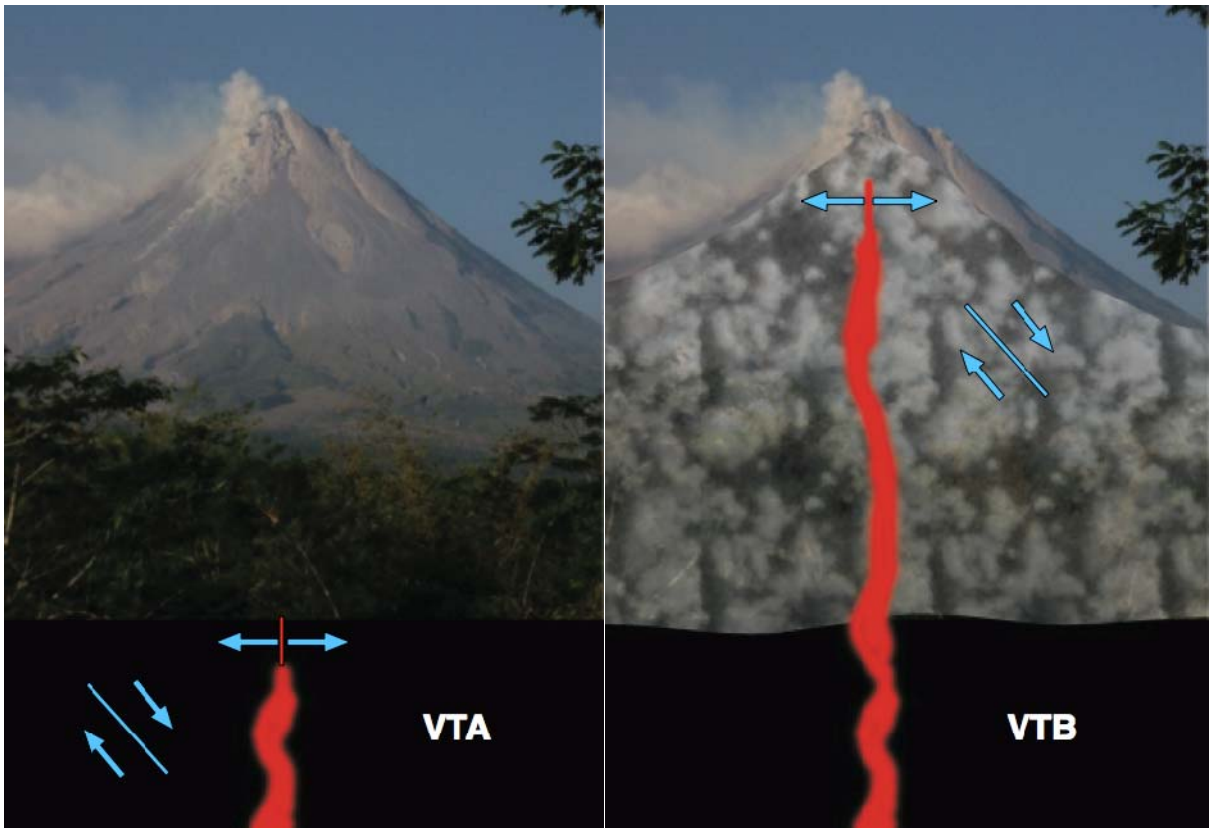

Fig. 13.3 Two different models describing the occurance of VT –A/B events when a volcanic crisis is emminent. While some VT events are simply caused by reactivation of existing faults by the increasing stress due to magma ascent, the other possible mechanism is directly linked to the enplacement of the magma in the feeder system and the associated tensile faulting. In this picture the difference between VT-A and VT-B is simply their location with respect to a high scattering region.

Source models and interpretation

Recently, detailed studies showed that the sources of some VT events deviate significantly from that of a pure shear failure, but show some similarities with the later described *Low-Frequency* events. An indication for location-dependent waveform changes is shown in Fig. 13.4. While the borehole station shows a seismogram which is typical for a common double couple source, the station at the surface within a volcanic caldera shows no visible S-wave onset, a lower dominant frequency but a very long coda. However, even using very sophisticated Moment-Tensor inversion techniques, which includes 3D Greens function computation (see Section 13.4.5) it is still not possible to resolve the ambiguity in estimating the "true" source mechanism of this class of signals. While there is a general agreement that the dominant part of the source process can be modeled by a double couple (DC), the role and amount of non-DC contributions remains debatable. Several papers on the inversion of the seismic moment tensor showed a significant contribution of non-double couple parts (Dahm and Brandsdottir, 1997; Saraò et al., 2001). The reason for the imperfect inversion will be discussed in more detail in Section 13.4.5.

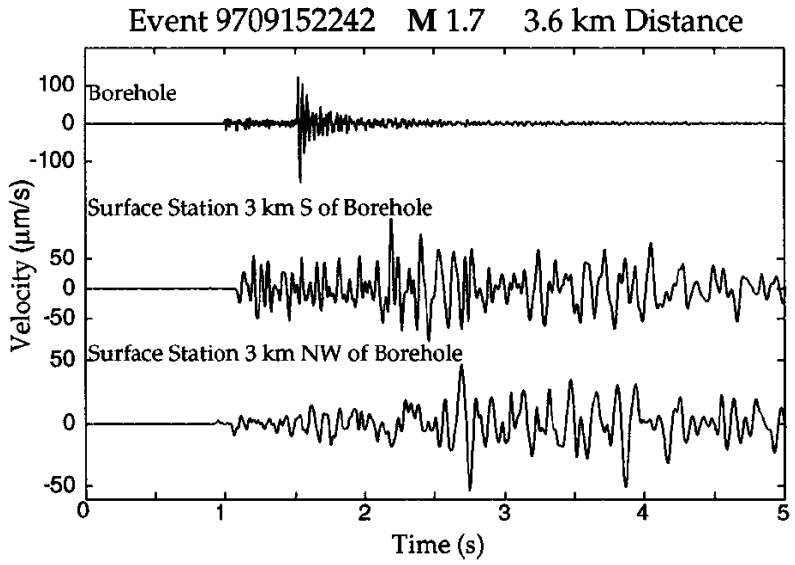

Fig. 13.4 Comparison of vertical component seismograms recorded in a borehole with records from the two surface stations nearest the borehole at the volcanic area of Long Valley Caldera , California. (from: Prejean and Ellsworth, 2001)

The main benefit in recording and analyzing VT-type earthquakes originates from the assumption that rising magma is acting as an additional stress source. This additional stress possibly superimposed by a regional stress field either leads to tensile faulting when magma is breaking the host rock or to earthquakes on preexisting faults in the country rock as a reaction to additional stress (see Fig. 13.3). While the first is directly linked to rising magma, the second possibility is a more passive and blurred image of magma inflation. Roman et al. (2006) showed that estimating fault plane solutions (see Section 3.4 in Chapter 3) gives important information of the current state of an active volcano and might, under certain conditions, serve as an important early warning tool. In their work Roman et al. (2006) showed that deep VT-A type events at Montserrat indicate a changing pattern of the P- and T-axis before a new eruption cycle starts. In their study the authors used a simple fault plane solution program (FPFIT, Reasenberg and Oppenheimer, 1985) and thus neglect a more realistic velocity and topography. The estimated pattern, however, is striking and while planning a surveillance procedure, fault plane solutions should be considered as an important indicator of changing volcanic activity.

Recently found evidence in laboratory experiments (Lavalee et al., 2008) and in field observations (Tuffen et al., 2003) point towards a source region, which lies in the rising magma itself. Depending on the applied strain rate viscous magma might change its rheologic behavior from visco-plastic to brittle. Within this model, tracking the sources of VT events makes a direct estimate of the fluid path and rate possible.

A very distinct feature of VT events is their swarm like occurrence. McNutt (2002) pointed out that the main duration of VT-swarms is about 5 days. At several volcanoes the VT-A and VT-B type events happen several days to weeks prior a volcanic eruption. Whatsoever, it must be emphasized that the majority of magma ascent events, which on one hand are accompanied also by VT events, results in intrusions and will, on the other hand, not be associated with any surface, i.e., eruptive activity. This ambiguity is one major source of mis-classification of the current state of a volcano.

13.2.1.2 Low-Frequency events

Low-Frequency events (LF or Long Period - LP) usually show no S-wave arrivals but a very emergent signal onset (Fig. 13.5). The frequency content is mostly restricted to a narrow band between 0.2-10 Hz. In the still rare cases in which the location of LF sources are determined, they are often situated in the shallow part of the volcano (< 2 km). Locations are deduced mainly by amplitude distance curves, from the rare hypocentral determinations using clear first onset recordings, and by semblance location techniques from particle motions recorded on a broad-band seismometer network (Kawakatsu et al., 2000). Some volcanoes (e.g., Kilauea) are known to produce deep (30-40 km) LF events (Aki and Koyanagi, 1981; Shaw and Chouet, 1991). Fig. 13.6 depicts different models to described two of the proposed source mechanisms of LP –events.

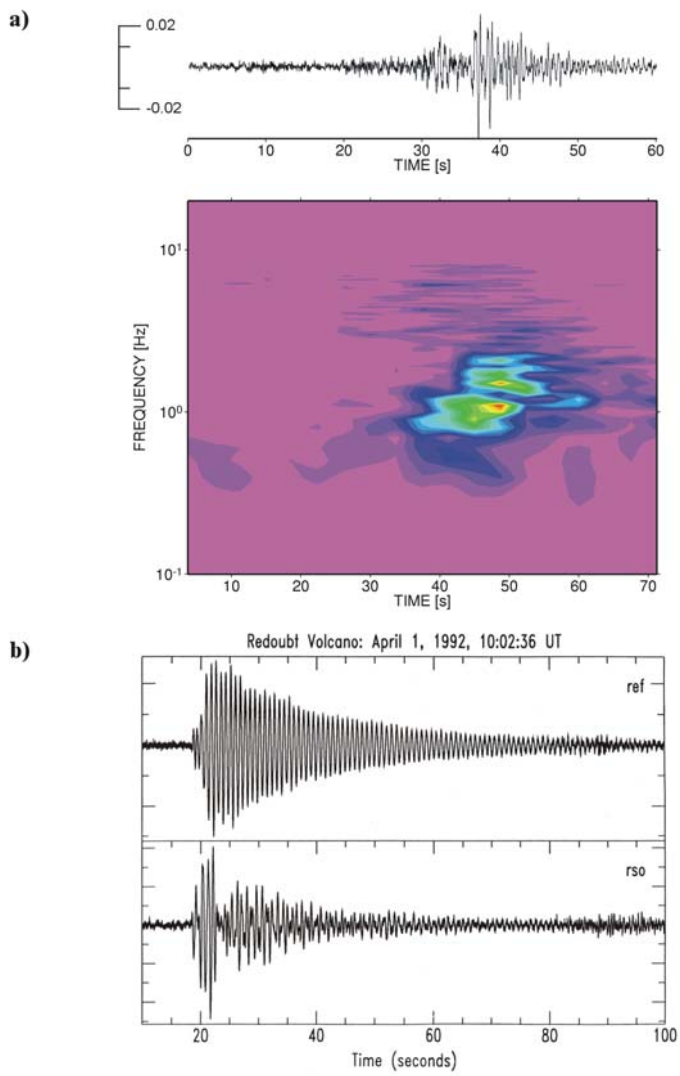

Fig. 13.5 **a)** example of a LF-wave group recorded at Mt. Merapi. Clearly the dominant frequency is around 1 Hz. **b)** shows an example of a LF event recorded at two different sites located at Redoubt volcano, Alaska (courtesy of S. McNutt, Alaska Volcano Observatory; AVO). The spindle shaped signal is also known as Tornillo.

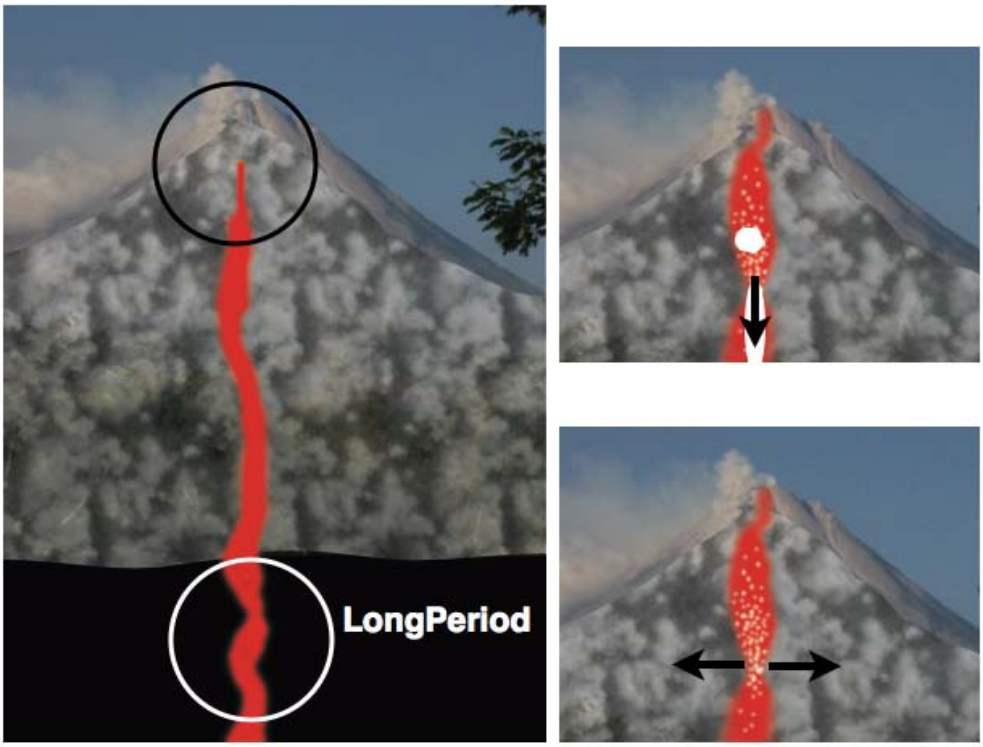

Fig. 13.6 Two different models to described two of the proposed source mechanisms of LP – events. While in deeper parts of the volcanic edifice an oscillating crack model is the most apropriate source model, the signature of LP events in shallower parts can be explained best by pressure disturbances, caused by an ascending gas bubble within a (moving) fluid.

Source models and interpretation

The associated source models of LP events range from an opening and resonating crack when the magma is ascending towards the surface (Chouet, 1996a) to the existence of pressure transients within the low viscous fluid-gas mixture causing resonance phenomena within the magma itself (Seidl et al., 1981 see Fig 13.6). Both models are able to explain large parts of the observed features in the time as well in the spectral domain but leave the physics and the trigger mechanism unresolved. Papers by James and others (2006, 2009) show that the source process of low frequency events within low viscous magma can be modeled by pressure transients within the magma caused by changing geometry of the dike system (Fig. 13.7). This pressure transient in turn can cause an oscillation in the fluid.

Neuberg et al. (2006) and Collier and Neuberg (2006) propose a very detailed source and trigger mechanism for low frequency events in a more viscous magma environment. These authors argue that most of the magma ascent happens aseismically up to a certain depth level is reached where large portions of gas bubbles are formed. Within the magma column a strong gradient of viscosity is assumed, caused by the cooling of the outer layer of magma at the conduit wall. At a certain depth the transition from no slip to friction controlled slip occurs when reaching the brittle failure condition (Dingwell and Webb, 1990). After cracks and veins are created, gas can now escape and the ascent is then dominated by friction controlled slip which is aseismic (Collier and Neuberg, 2006).

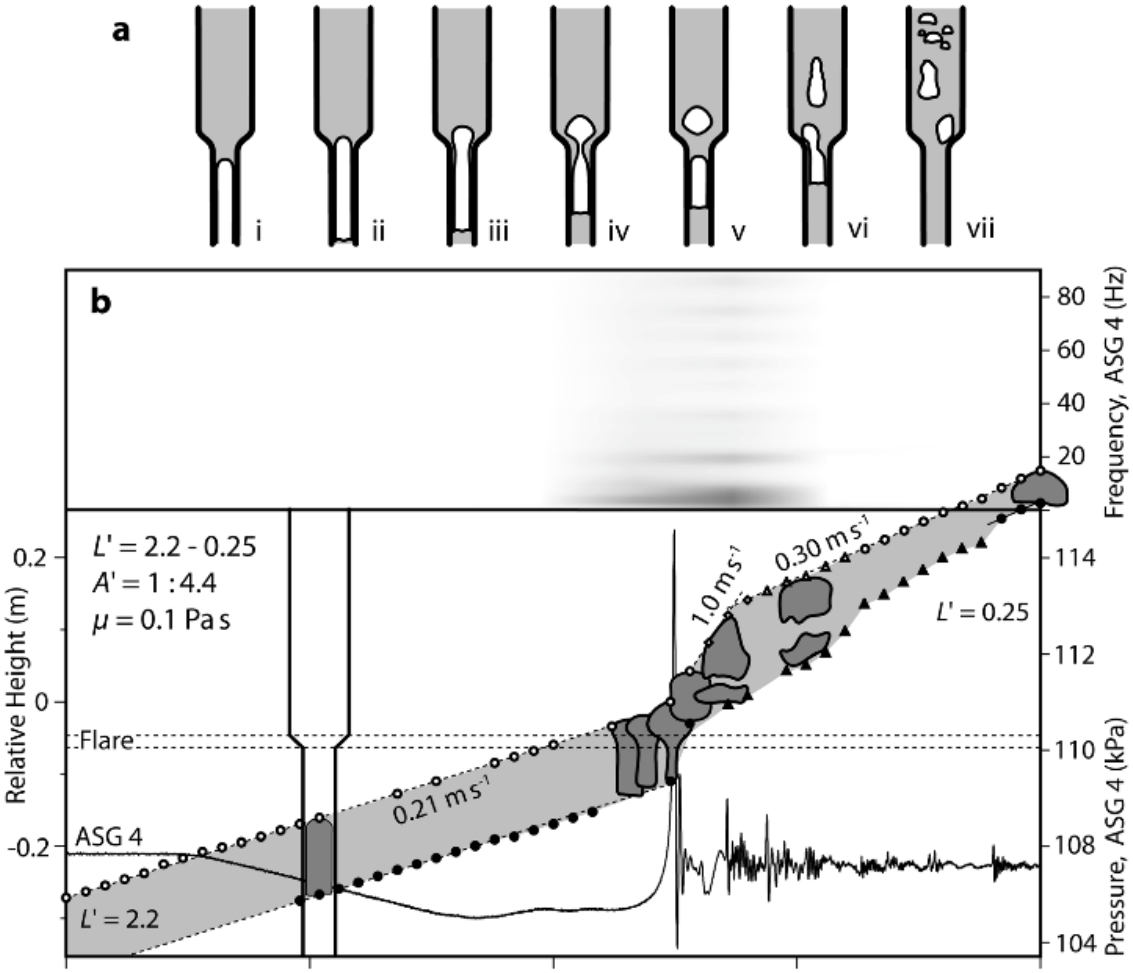

Fig. 13.7 Experimental setup and results of an ascending slug passing through a widening conduit. A clear pressure pertubation can be detected in the fluid and the acelerating slug may be also an effective mechanism for generating elastic waves in the surrounding subsurface structure (from: James et al., 2006).

An alternative mechanism for triggering LP or LF events is given by Denlinger and Hoblitt (1999). These authors favor a supply rate controlled stick-slip mechanism, which is deduced from observations of technical polymer melts. Both proposed trigger mechanisms are able to explain the frequently observed timely very regular repetition of LF events, which may lead even to a continuous signal (see Section 13.2.2.2). The model of Neuberg et al. (2006) and Collier and Neuberg (2006) is also able to explain the frequently observed similarity of waveforms in the recorded data. This is a surprising feature by its own as a volcano is a very heterogeneous geological structure making scattering distortion a very dominant feature. Numerical simulations by Sturton and Neuberg (2006) and Neuberg et al. (2000) show that the overall shape of the seismograms and their frequency content can simply be explained by the excitation of multiple reflected borehole (i.e., Stonely) waves at the magma-conduit interface.

In the context of using seismology as an early warning tool in volcanology the detection and analysis of LF/LP events is a very important tool, because of their direct connection to the ascending i.e. flowing magma within the subsurface. Monitoring fluid movement or pressure disturbance directly makes early warning much more successful and effective in both timing and size estimates of an eruption. However, there is still a large ambiguity caused by intrusion rather than extrusions, i.e. eruptions.

13.2.1.3 Hybrid events, Multi-Phases events

Some volcano-seismic signals share the signal and frequency characteristics of both LF and VT-(A,B) events. Signals of this class are usually labeled as *Hybrid* events, which may reflect a possible mixture of source mechanisms from both event types (see Fig. 13.8) and/or additionally reflect possible path effects (Harrington and Brodski, 2007). For example, a VT microearthquake may trigger a nearby LP event. Lahr et al. (1994) and Miller et al. (1998) detected swarms of *Hybrid* events during the high activity phase of Redoubt (Alaska) and Soufriere Hills volcano (Montserrat, West Indies), respectively. Miller et al. (1998) concluded that such events reflect very shallow activity associated with a growing dome.

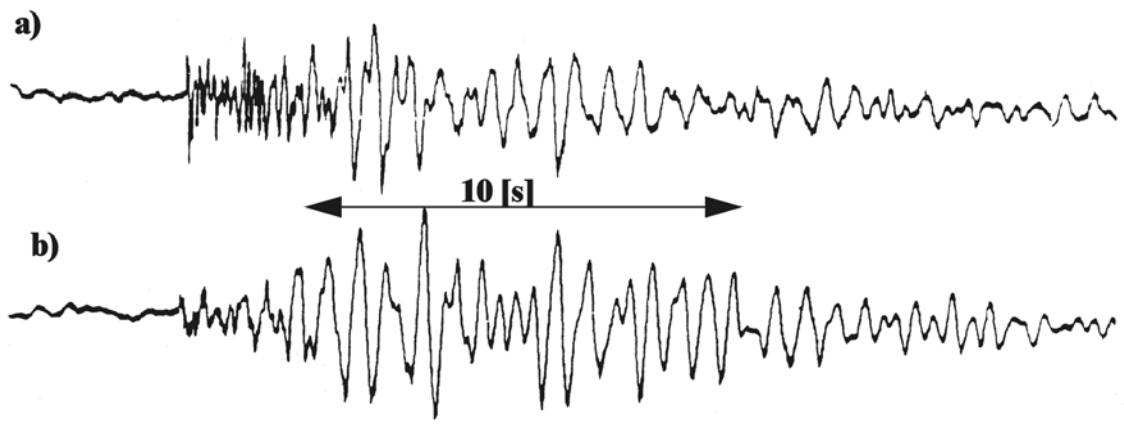

Fig. 13.8 **a)** shows a Hybrid event and **b)** a VT-B event for comparison. The higher frequencies at the beginning of the Hybrid event are an obvious feature, while the later part shows the similarity with the VT-B event (courtesy S. McNutt, AVO).

Multi-Phase events (MP also *Many-Phases* event; see Fig. 13.9; Shimozuru, 1972) are somewhat higher in their frequency content (3 to 8 Hz) than *Hybrid* events but are related as well to energetic dome growth at a very shallow level. The name reflect their complicated waveforms with seems to consist of multiple phases just after each other.

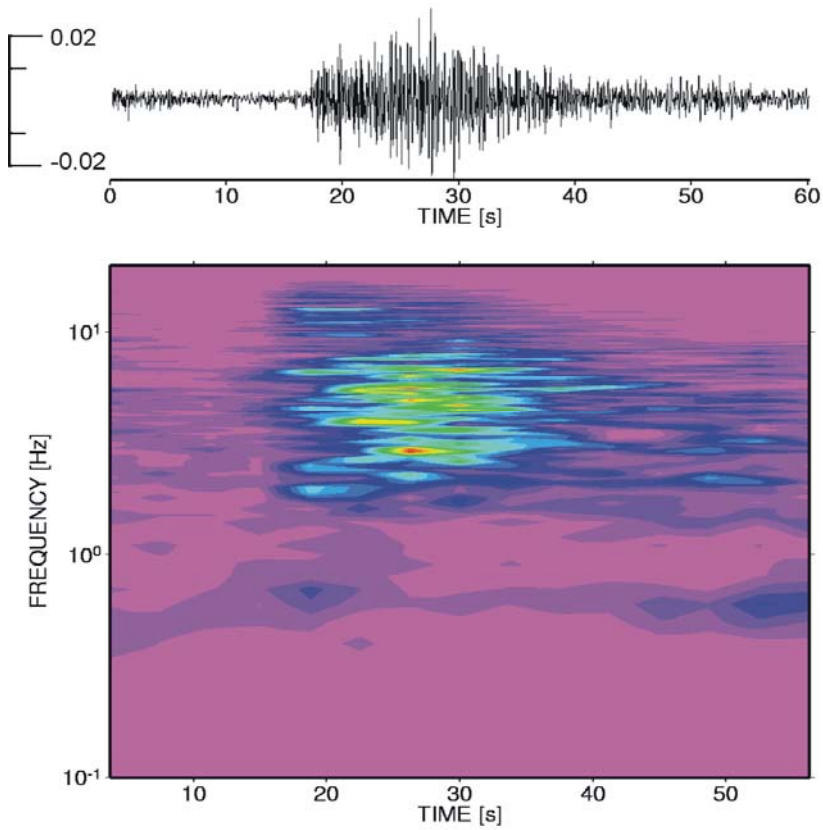

Fig. 13.9 MP-event recorded at Mt. Merapi during strong dome formation. The frequency is restricted between 3 - 10 Hz and resembles that of a VT-B type event at this volcano. Note the long duration of this event whilst its amplitude is much smaller than for the VT-B event shown in Fig. 13.2.

Source models and Interpretation

Both types of signals and their associated mechanisms are still a topic of research as their occurrence might be a good indicator for the instability and/or the growth rate of highly viscous lava domes. The trigger or source mechanism is likely the same for LP/LF events (see Section 13.2.1.2), while the source depth is significantly shallower at least in case of MP events. Recent advances in laboratory experiments, which investigate the plastic to brittle transition, point towards a source mechanism, which is located in the moving fluid itself (Lavallée et al., 2008).

13.2.1.4 Explosion quakes, very-low-frequency events, ultra-low-frequency events

Very pronounced *ultra long period* (ULP; f < 0.01Hz) and *very low frequency* (VLF; f ~ 0.01 - 0.1 Hz) signals are observed and are well documented at many volcanoes in Japan and on Hawaii (e.g., Aso: Kawakatsu et al., 2000; Iwate: Nishimura et al., 2000; Kilauea: Ohminato et al., 1998) using several broadband seismometers located in the near-field to intermediate-field distance from the source. To the same of class belong the *explosion quakes*, a signal that accompanies Strombolian or other (larger) explosive eruptions, showing clear waveform characteristics. Most of these signals can be identified by the occurrence of an air-wave which is caused by the sonic boom during an explosion, when the expanding gas is accelerated at the

vent exit (see Fig. 13.10, see also Section 13.5.1). This wave mainly travels through the air with the typical speed of sound (330 m/s at 20°C). While we do not discuss the explosive mechanism at the magma air interface in detail, the source, which leads to this explosion is not yet completely deciphered and several concurrent models will be discussed later. Some LF events show the same frequency-time behavior as the explosion quakes but lack an air phase (McNutt, 1986). This might reflect a common driving source of deeper LF-events and shallower explosion quakes.

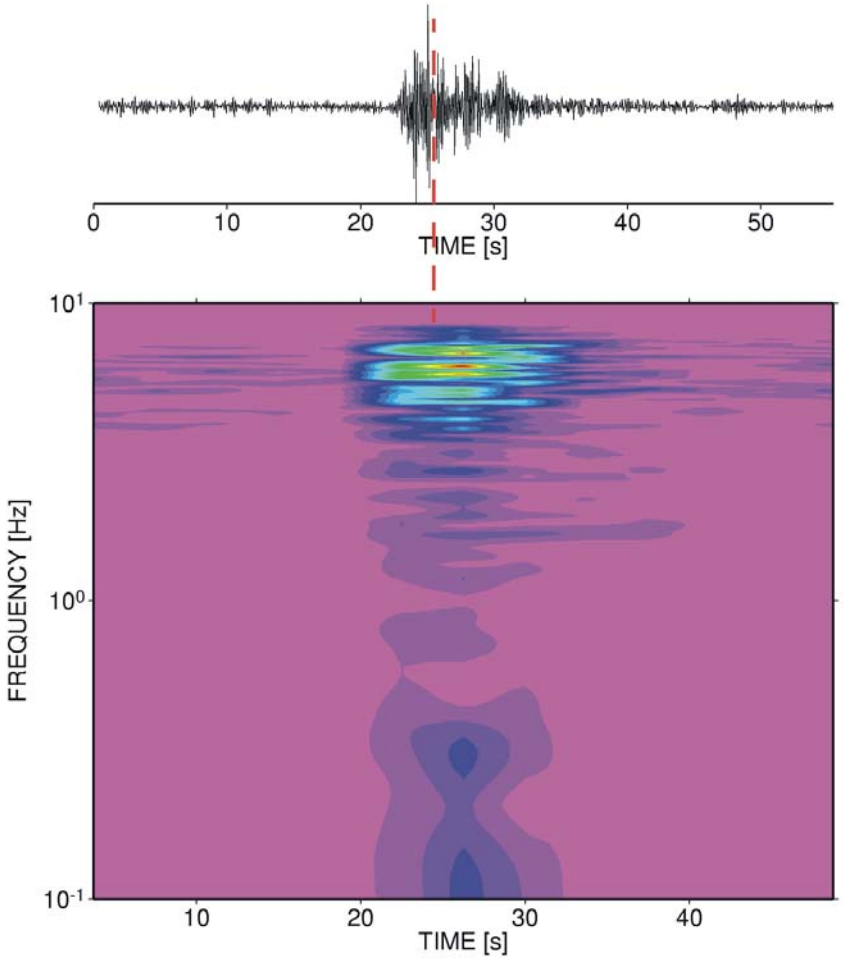

Fig. 13.10 An explosion signal recorded at Stromboli volcano, Italy. The seismic station was located just 400 m from the active vent. The dashed line gives a rough estimate of the onset of a sonic wave also visible as high (red) amplitudes in the time-frequency plot around 5 Hz.

Since the early 1990ies portable broadband seismometers with corner frequencies as low as 0.00833 Hz shed new light on this open question (see Fig. 13.11). It could be verified that at Stromboli volcano (Italy) ULF pressure buildup takes place several minutes before the onset of a Strombolian eruption (Dreier et al., 1994; Neuberg et al., 1994; Wassermann, 1997; Kirchdörfer, 1999). As this is only visible in the near-field of the seismic sources with a geometrical spreading factor proportional to r^{-2} (implying a simple volumenetric source), the seismic stations must be located close to the active vent of the volcano (see Fig. 13.11). Since the first near-field broadband observations of strombolian activity many examples at volcanoes around the globe exist nowadays, making ULP signals a common signal accompanying low to medium viscous volcanism.

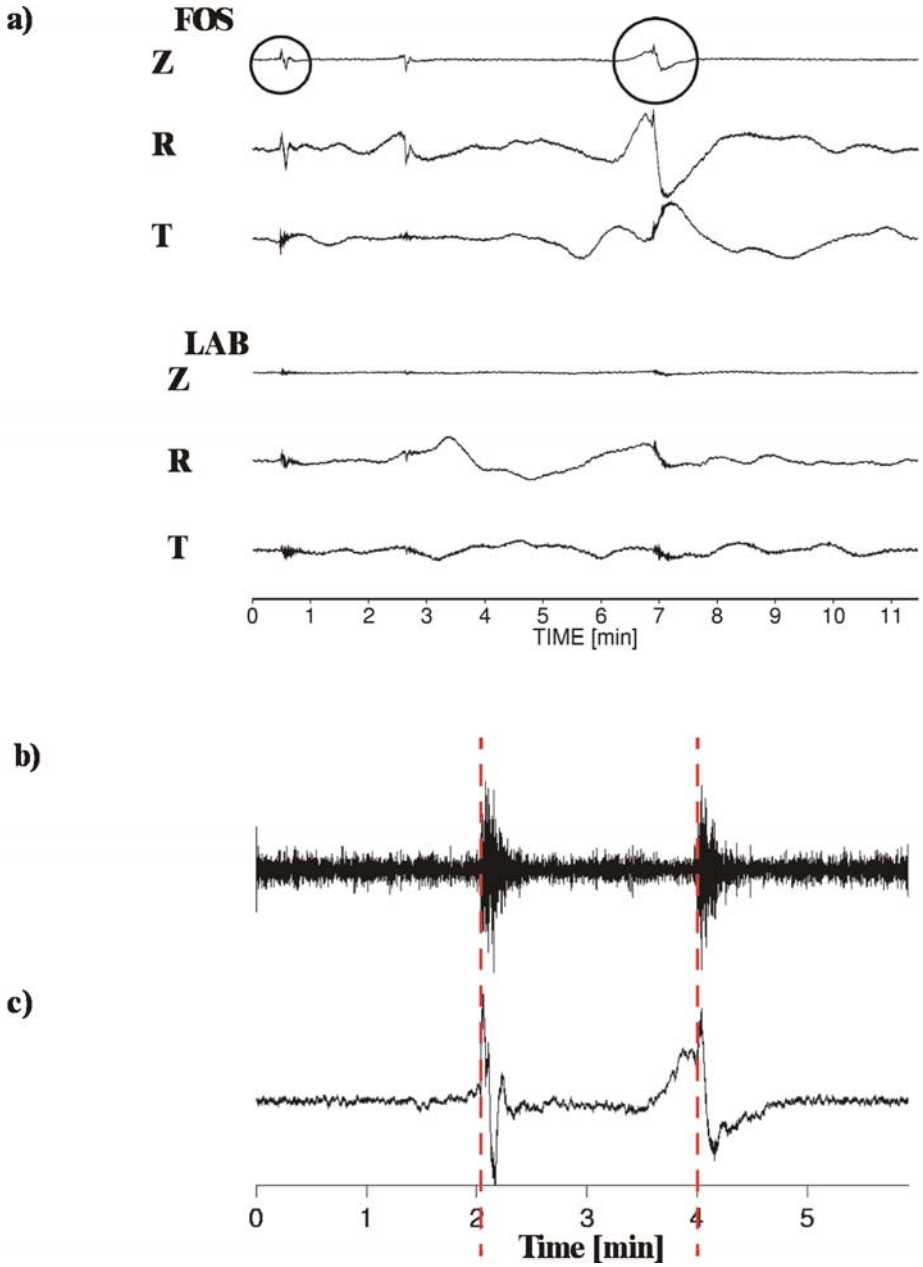

Fig. 13.11 **a)** ULP signal recorded with a Streckeisen STS2 broadband seismometer at Stromboli volcano. We removed the instrument response down to 300 s and the resulting traces are integrated to reflect ground displacement. The three uppermost traces show the three-component seismograms of a station located 400 m from the vent, whereas the lower three traces show the same but at a site located 1800 m from the active vent indicating a large signal only visible in the near-field. The two circles mark two different types of seismic signals caused by strombolian activity which were not linked to different active craters.
b) shows the seismogram of a 1 Hz seismometer during two different explosion quakes, the dashed lines mark the visible onset of strombolian eruptions. c) shows the displacement signal of two different explosion quakes. Note, not all explosion signals produce the same amount of long-period displacement signals.

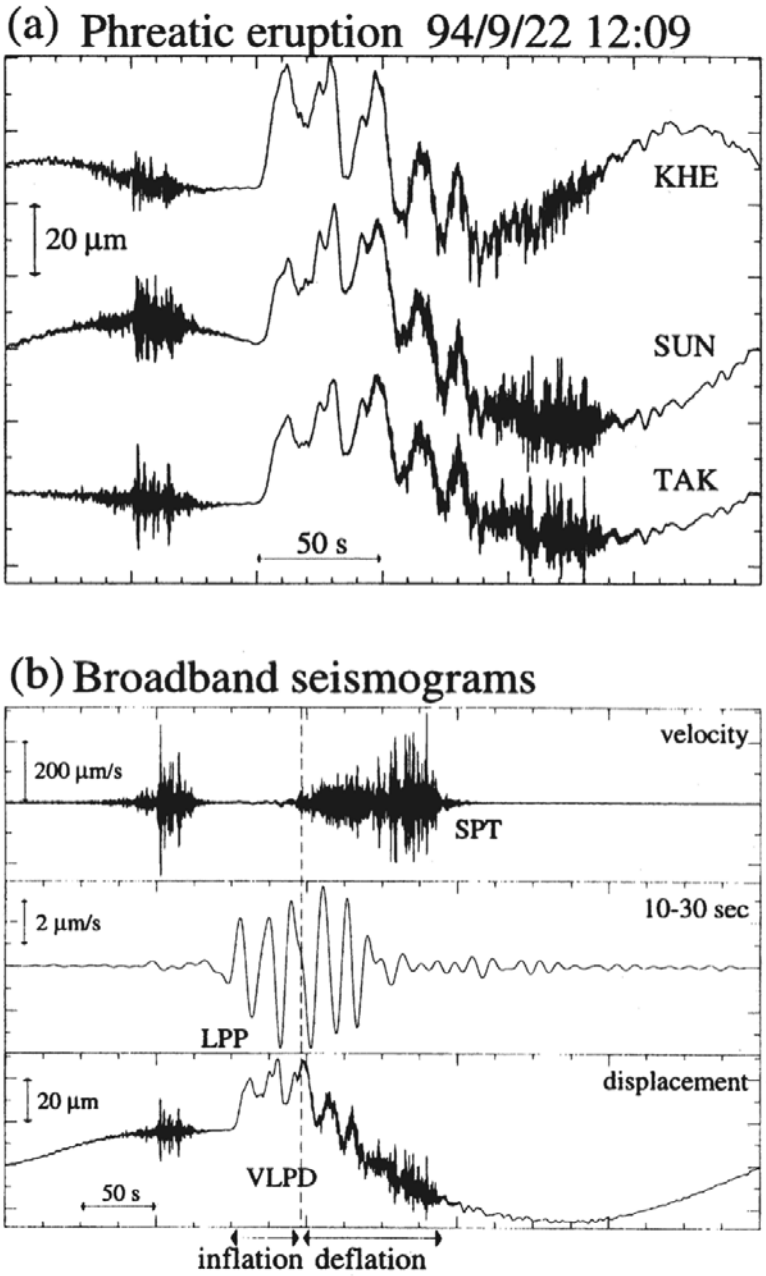

Fig. 13.12 a) ULP (or very long-period displacement) signal observed at three broadband stations during a phreatic eruption of Aso volcano. b) original velocity, band-pass filtered velocity and displacement seismogram of the same event observed at station TAK. The vertical line in b) indicates the onset of the eruption, all stations are located within 2 km from the volcanic centre (from: Kawakatsu et al., 2000).

ULF and VLF events are still unknown at most andesitic and rhyolitic volcanoes, which possibly implies that the described slug flow (Vergniolle and Jaupart, 1990, James et al. 2006) may be non-operative at this regime of viscosities. In contrast to this statement, the work of Hidayat et al. (2000) showed that there exists a moderate (0.25 Hz) VLF signal in the near-field of some MP events recorded at Mt. Merapi (Indonesia).

Source models and Interpretation

Since the late 1980's to early 1990's many of the ULP-VLP observations were interpreted as shallow (z < 1.5 km) phreatic eruptions with a strong low frequency pressure pulse (f ~ 0.01 Hz; see Fig. 13.12). At Aso volcano Kawakatsu et al. (2000) also detected a second signal with dominant frequencies roughly at 0.06 Hz at the same depth range as the modeled phreatic source. The authors classified this signal as *long period tremor* (LPT), which is seen to reflect the merging of isolated pulses into a nearly continuous signal (see Fig. 13.13 and Section 13.2.2.2: Fig. 13.17). Kawakatsu et al. (2000) interpret these signals as caused by the interaction of hot magma/fluid with an aquifer situated in 1 - 1.5 km depth below the craters of Aso volcano.

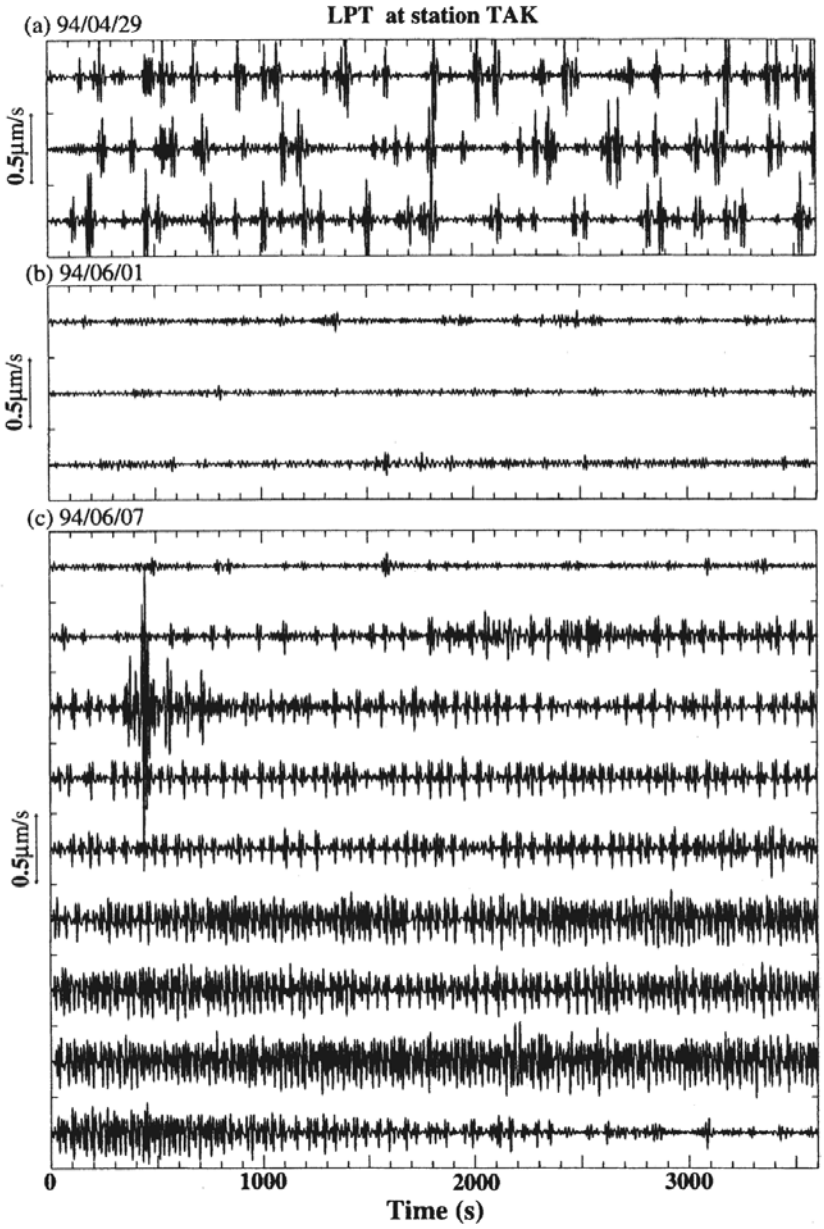

Fig. 13.13 Vertical component broadband seismograms band-pass filtered at 0.033 to 0.1 Hz at Aso volcano during three different days 1994. The isolated ULP pulses visible in a) and b) merge together in c) forming the continuous signal of *long period tremor* (from: Kawakatsu et al., 2000).

A different model of ULP/VLP generation, which fits the visual and seismological observations very well consists of a shallow magma chamber and a tiny feeder system to the surface, which may additionally vary in size and width. The accumulation of a gas pocket and the ascent of this pocket as a gas slug explain the observed pressure buildup up to a certain precision (Vergniolle and Jaupart, 1990). However, most of the strombolian eruptions at Stromboli and other volcanoes show only small over-pressure without any visible difference in the associated surface activity. Some more recent results of Gerst (2010) will be discussed in Section 13.5.1.

Results from still rare moment tensor inversion imply a rather complicated mixture of double couple (DC), compensated linear vector dipole (CLVD) and isotropic components (IC). In order to explain the recorded low frequency seismograms some authors combine a number of cracks, cylinders and additional single forces (Chouet et al., 2003; Cesca and Dahm, 2008; Aster et al., 2008; Chouet et al., 2010) for eruption at Kilauea (Hawaii) and Stromboli volcano or more violent explosions at Mt. Erebus (Antarctica). In Section 13.4.5 we will focus on the method of moment tensor inversion and its associated problems in much more detail.

A very comprehensive physical model for mild strombolian eruptions is given by a series of papers by James et al. (2006) and James et al. (2009). In these papers the physics of an ascending large gas pocket (slug) is experimentally and mathematically investigated.

The conceptional model of James et al. (2009) combines the viscous flow of the fluid film along the condutit wall and the pressure above in the fluid head (the nose) of a rising gas slug which is assending in a volcanoes conduit. This model is able to explain the change from gas puffing to strombolian eruption as well as the observed overpressures. The controlling factor between puffing and bursting is seen in the starting pressure, the length of the slug and therefore in the involved gas mass which is transported towards the surface (James et al., 2009). While this model can explain the observed infra-sound signals it will not explain the generation of LP/ /VLP/ULP signals during slug ascent.

In a different paper James et al. (2006) showed that changes in the condiut diameter can act as a very prominent source of pressure transients which then are able to couple into the surroundings and produce elastic deformation signals (Fig. 13.7). While models by Schick et al. (1982) and Seidl et al. (1981) in the early 80ies already describe similar mechanims, the paper of James et al. (2004, 2006, 2009) put these ideas in the context of a physically and mathematically more quantitative model.

13.2.2 Continuous volcanic-seismic signals

The appearance of continuous seismic signals at active volcanoes demonstrates the most profound difference between tectonic earthquake and volcano seismology. The suspected mechanisms range from obvious surface effects such as rockfall, landslide or pyroclastic density flow to internal ones such as volcanic tremor. Nearly every volcano world-wide shows the signal of volcanic tremor during different activity stages. Volcanic tremor is the most favored parameter in volcano early eruption warnings. Because of possibly differing source mechanisms we discuss tremor separately for the two flow regimes: high and low viscosity.

Recently the observation of so called non-volcanic tremor is attracting a lot attention in the seismologic community. This type of earth tremor is associated by slow, episodic slip in subduction zones, which makes it an important tool to understand the dynamical behavior of subduction related earthquakes. Sharing a lot of the signal characteristics with its volcanological counterpart, many of the methods developed in volcano-seismology are now further investigated in order to shed more light on this signal type.

13.2.2.1 Volcanic tremor (low-viscous two-phase flow and eruption tremor)

Most of the monitored basaltic volcanoes show some kind of cyclic appearance of *volcanic tremor*. The tremor signals can last between minutes and months in duration and, in most of the cases, their spectra are very narrow-band (1-5 Hz; Fig. 13.14).

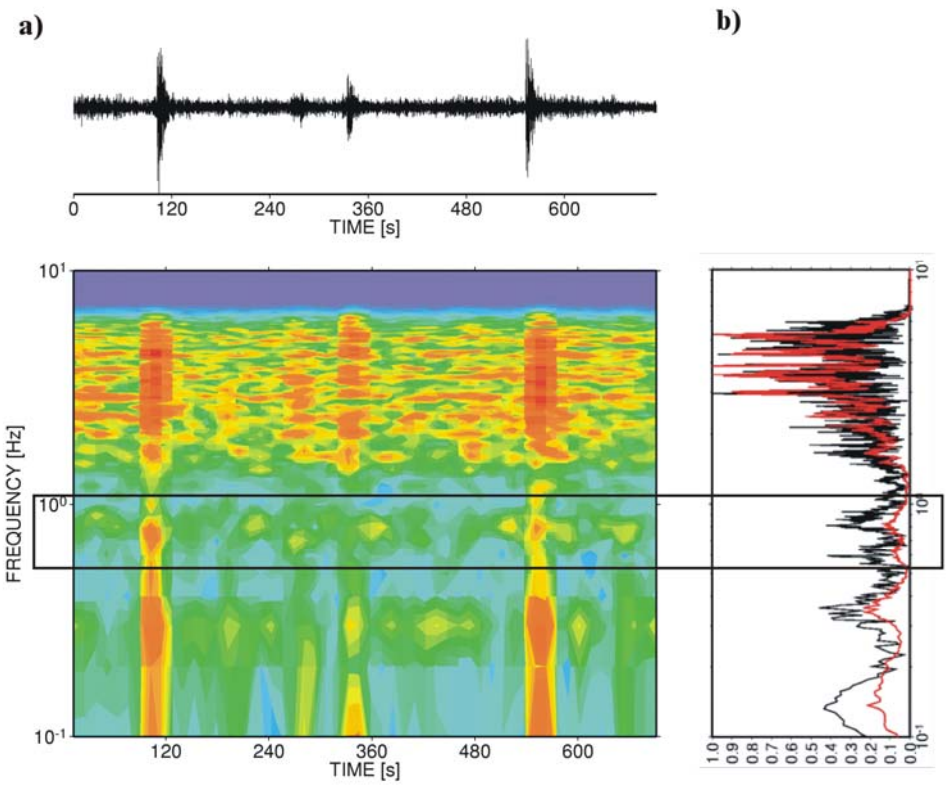

Fig. 13.14 a) explosion signals superimposed on the continuous signal of volcanic tremor at Stromboli volcano. The box marks the frequency band of a weak but typical volcanic tremor band at Stromboli volcano. Note that the explosion quake also excites the same frequency band whereas below this frequency band the spectral amplitude of the explosion quake type signals are somewhat smaller. The tremor band with frequencies above 2.0 Hz is partially distorted by the ejected volcanic debris falling back to the surface and tumbling down the slope of the volcanic edifice (see Section 13.2.2.3). **b)** the normalized Fourier transform of a explosion quake type signal (black) and of a normalized power spectrum of six hours of continuous recording (red). While the first reflects the typical spectrum of all explosion quakes, the overall behavior of the second spectrum is mainly due to volcanic tremor. The overall similarity between the explosion quake and tremor signal types is obvious.

Some tremor signals show strong and short-pulsed amplitude variations (termed *beating tremor*), while others are nearly stationary over several days or even months. The common similarities in the spectra of volcanic tremor and LF and even explosion quake events are another important observation which has to be explained when looking for the source mechanisms. At Mt. Etna volcano (Italy), strong fluctuations and changing signal characteristics of volcanic tremor amplitude are associated with lava fountaining at one of its summit craters or after the opening of a flank fissure (Cosentino et al., 1989, Langer et al., 2011). Gottschämmer (1999) described a tremor cycle at Bromo volcano (Indonesia) where the tremor amplitude fluctuation could be visually correlated with heavy ash plumes (large amplitude - *eruption tremor*) or white steam (small tremor amplitude) episodes (see Fig. 13.15).

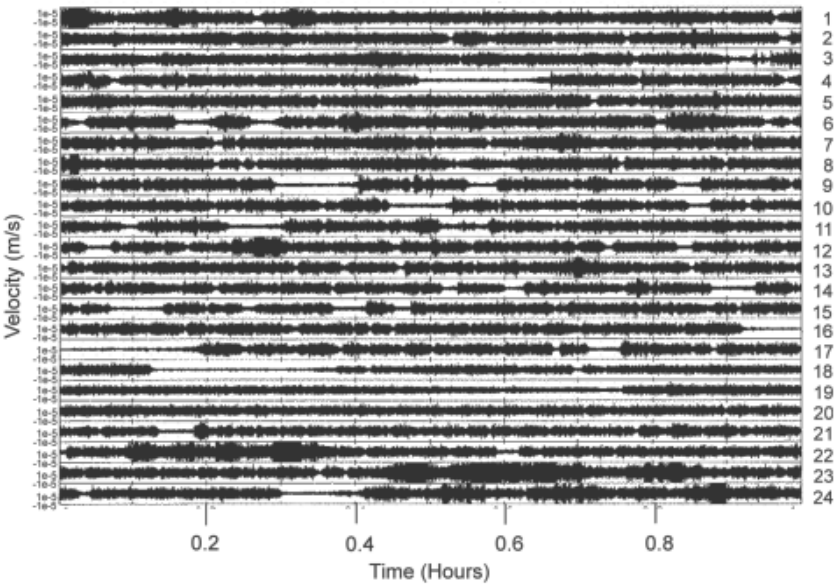

Fig. 13.15 Volcanic tremor at Bromo volcano (Indonesia) during a high activity phase at the end of 1995 (courtesy of E. Gottschämmer, University of Karlsruhe). Large tremor amplitudes correlate with the eruption of heavy ash plumes while small tremor amplitudes appear during quiet steam emissions (Gottschämmer, 1999).

These observations made at different volcanoes with either low viscosity magma or a huge amount of volatiles (free or after the fragmentation of high viscosity magma; steam) suggest the involvement of gas/fluid interaction in generation of volcanic tremor. In general it must be stated that the appearance of volcanic tremor is always a sign of high volcanic unrest, which might lead to an eruption. Whether this eruption may follow or the activity terminates by an intrusion cannot be decided without other geophysical/geodetical/geological evidences. Whatsoever, even in the cases where a well established and "complete" monitoring system exist signs of unrest or precursors may still carry significant ambiguities caused by the complexity of magma flow and the physics of volcanic eruptions.

Source models and Interpretation

The similarities in the overall spectral content of LF/LP events and volcanic tremor are reflected in similarities of the proposed source mechanism or of the source region (resonating fluid). Flow instability is thought to play an important role in the excitation of volcanic tremor

in multiple phase flow pattern (Seidl et al., 1981; Schick, 1988; James et al., 2004, 2006) and the associated LF events are seen as a transient within the same physical system. On the other hand, Chouet (1987) and Chouet (1986) state that a repeated excitation of a connected crack system could cause a harmonic and long-lasting signal, where the fluid is only passively reacting to the crack oscillations. James et al. (2006) could show, that under certain circumstances the pressure transients produced by changing geometry of the feeder system can couple into the elastic solid surrounding of the feeder system (Fig. 13.7).

The spectral content observations support both the low viscosity magma and volatile interpretations. Explosions at Stromboli volcano excite the same frequency band as volcanic tremor does, which supports the idea of a common resonating system (Fig. 13.14). However, care must be taken when interpreting the frequency spectra of volcanic tremor. Detailed studies on the spatial frequency distributions at Stromboli showed that single frequency peaks are possibly influenced, to still an unknown amount, by the propagation medium (Mohnen and Schick, 1996).

13.2.2.2 Volcanic tremor (high-viscous - resonating gas phase)

During the last decade, many observations were made of the occurrence and characteristics of volcanic tremor at volcanoes with high-viscosity lava. At Semeru volcano (Indonesia) the spectra of volcanic tremor contained up to 12 overtones. This supports the assumption of a resonating medium with a high quality factor (Q) as well as a precisely working feedback mechanism (Hellweg et al., 1994; Schlindwein et al., 1995) (Fig. 13.16). Similar observations were also made at Lascar volcano (Chile), where up to 30 overtones could be identified in the seismic signals (Hellweg, 1999).

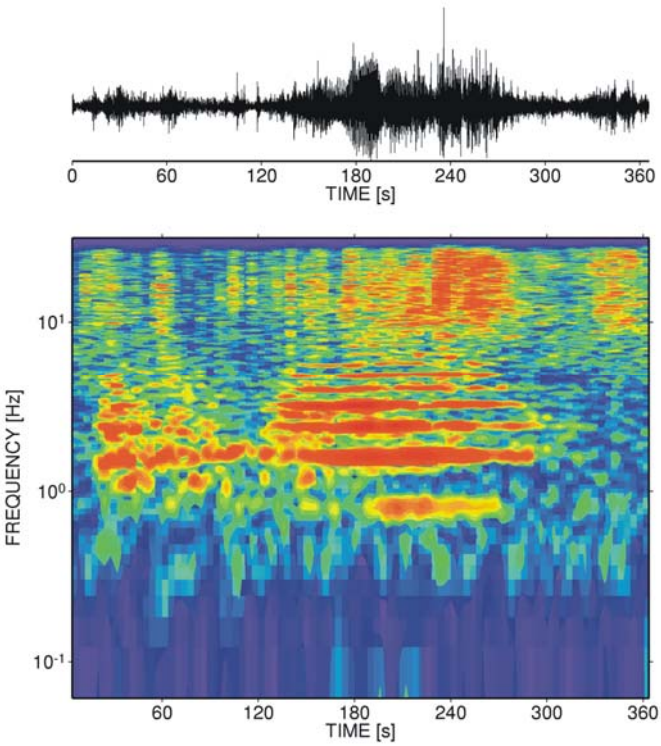

Fig. 13.16 Harmonic tremor signal recorded at Mt. Semeru, Indonesia. Up to six overtones can be recognized starting with a fundamental mode located at roughly 0.8 Hz.

Source models and Interpretation

Schlindwein et al. (1995) proposed a feedback mechanism similar to that of sound generation in a recorder, and also discussed a repeating source with precise repetition time as a possible mechanism. This model was refined by Johnson and Lees (2000) and Neuberg et al. (2000). In the feedback mechanism case, the resonating body must consist of a pure gas phase as the lava at Mt. Semeru is too viscous for resonance at the observed frequencies. The second mechanism requires a very precise timing mechanism for producing the highly stable overtones. Observations at Montserrat volcano (Neuberg et al., 2000) and Mt. Merapi volcano (Indonesia) support the hypothesis of a repeating source (Fig. 13.17). During several cycles of increased volcano-seismic activity we recognized the transition from closely timed MP/Hybrid events into the continuous signal of volcanic tremor and vice versa. As the source mechanisms of both types of signals are still unknown, the driving force behind these mechanisms is also not known. Also the type of feedback mechanism, which needs to be involved in this model could not yet be identified.

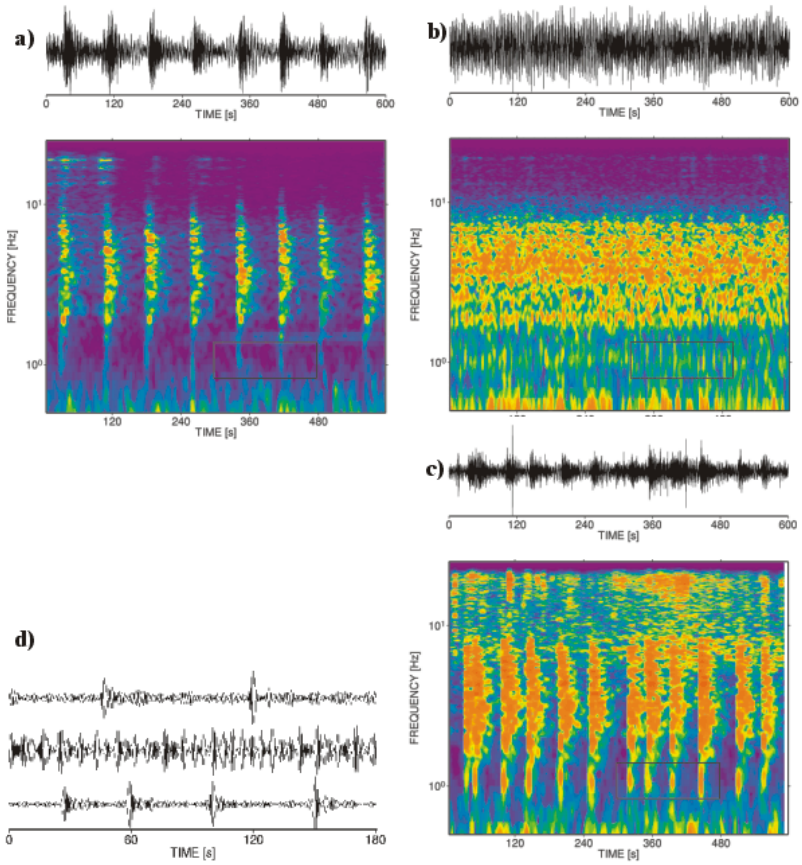

Fig. 13.17 Sequence of repeating seismic signals at Mt. Merapi volcano in 1996. a) very regularly timed MP-events before they merge together to form volcanic tremor (see b). c) after some hours the tremor is replaced by a sequence of discrete events with slightly higher amplitudes than before. Note: in contrast to the classification given in Fig. 13.5, the frequency content of these signals is lower (0.7 - 10 Hz) and might not resemble "pure" MP-events. In d) the marked time-frequency region of plots a)-c) are plotted in time domain. A band-pass between 0.8 - 1.3 Hz was applied before zooming. The individual wavegroups seen in the filtered continuous signal also supports the idea of the merged events causing the volcanic tremor.

Volcanic tremor is, as previously noted, always a sign of high activity. However, since the exact mechanisms are still unknown, the importance of and timing between the first appearance of tremor and possible eruptive activity is still a matter of discussion (McNutt, 2000a). The review papers by Konstantinou and Schlindwein (2002) and Kawakatsu and Yamamoto (2007) may give further information about the types and proposed source mechanisms of volcanic tremor.

13.2.2.3 Surface processes

Substantial release of seismic energy at active volcanoes is related to surface processes acting directly on the volcanoes edifice. For example, pyroclastic flows, lahars (volcanic debris flows) and rockfalls from unstable domes or crater walls can generate seismic signals with amplitudes exceeding several times those of the typical volcano-seismic signals. The most important signals for monitoring purposes are those associated with pyroclastic flows and lahars. The monitoring of lahars, which includes also acoustic and visual monitoring, is especially important when monitoring a volcano which is capped by a glacier or which is located in a tropical area. Melting the snow during an eruption or heavy rainfall during the rainy season will occasionally mobilize a huge amount of volcanic debris. The signals of all this activity are mostly high-frequency (>5 Hz), show spindle (cigar) shaped seismogram envelopes that can last several minutes (Fig. 13.18).

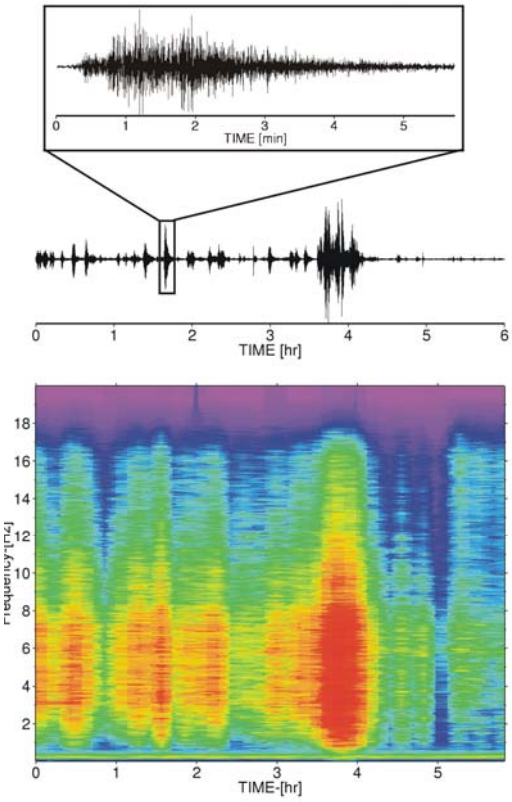

Fig. 13.18 Sequence of medium to larger pyroclastic flows recorded at Mt. Merapi volcano during the 1998 dome collapse. Note the 6-hour time scale and that individual events last many minutes, longer than the seismograms of typical earthquakes. Just before 4 hours the largest pyroclastic flow in the whole eruption sequence takes place and lasts for about 30 minutes.

13.2.3 Special note on noise

Most of the extensively monitored volcanoes lie in densely populated areas with strong human activity (that is why they are monitored). Hence, care must be taken when interpreting the signals usually classified as volcanic tremor. In some cases, human activity excites signals occupying the narrow spectral band between 1-4 Hz (big machines etc.). Also a distinct 24 h rhythm is very likely caused by increasing human activity during daylight time and should therefore be analyzed with special care (Fig. 13.19). Even when using three-component seismometers it is not easy to discriminate for sure between volcano-seismic and man-made noise. The topography at active volcanoes is very often radially shaped and the propagation paths to the seismic stations are shared by ambient seismic noise and volcanic signals.

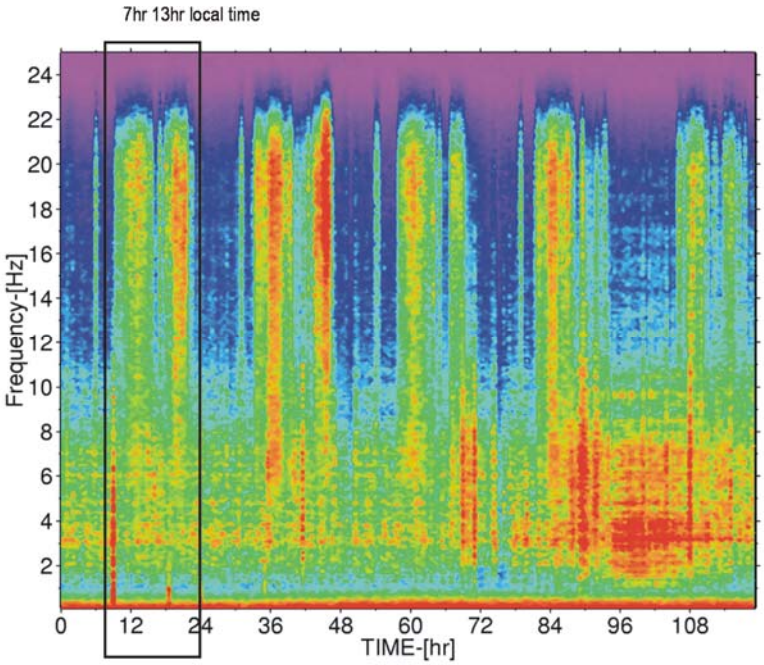

Fig. 13.19 Spectrogram of background noise recorded at a seismic station at Mt. Merapi. As the station is located in farming area, the human daylight activity can be clearly recognized by its distinct 24 hour periodicity. Furthermore, it is possible to see that there are two main working periods during daytime (marked by a box). Large spectral amplitudes are visible around 7 hrs local time and a second peak is located around 15 hrs after a time of quiescence during noon.

In conclusion, we note that most of the above classifications and proposed source mechanisms are deduced from simple observations of spectral content and overall shape of the associated seismograms rather than by physically verified constraints. Care must be taken when interpreting the occurrence of one of these signals during increasing volcanic activity. There are many examples of increasing numbers of VT events and increasing volcanic tremor amplitude without any surface activity at volcanoes. Thus, to be truly effective and diagnostic, seismic monitoring should be complemented, whereever possible, by other instrumental monitoring techniques (e.g., geodetic, geochemical) and regularly made visual observations of the volcanoes being monitored remotely (see Section 13.5).

13.3 Design of a monitoring network

One of the most important decisions to be made, when establishing a seismic monitoring network, is the design of the station distribution. In most cases, volcanoes are monitored with at least four to six seismic stations, which are distributed around the volcanic center. Newer deployments try to setup arrays of sensors or, even better, a network of different arrays (also named "Array of Arrays"). However, some of the design criteria deviate from the usual earthquake monitoring networks and are discussed in the following sections.

13.3.1 Station site selection

Considering a location as a possible site for a seismic station is always a compromise between noise considerations and accessibility. Of course, it would be best to place the seismic station far away from any human activity (see Fig. 13.19), away from big trees or sharp cliffs and ridges. However, the accessibility is very important, especially at the beginning of a surveillance campaign at a volcano. Also, the rough and harsh environment typical of many volcanoes usually requires frequent station visits for maintenance. Valleys, which generally are accessible places for seismic stations rather than ridges or cliffs, are often flooded during winter or the rainy season (not to mention the higher exposure to possible pyroclastic flows).

A second important decision must be made when choosing on "what" the station should be placed. Usually, seismologists prefer hard rock to unconsolidated sediments. At many active volcanoes, hard-rock sites are rare and, even if they exist, they are not necessarily good choices. Hard-rock sites often are small lava tongues or big blocks of lava buried in ash or soil, causing waveguide effects or even block rotation to an unknown degree. This is especially important when installing broadband seismic stations, which are very sensitive to tilt (see Chapter 5 and Fig. 13.20).

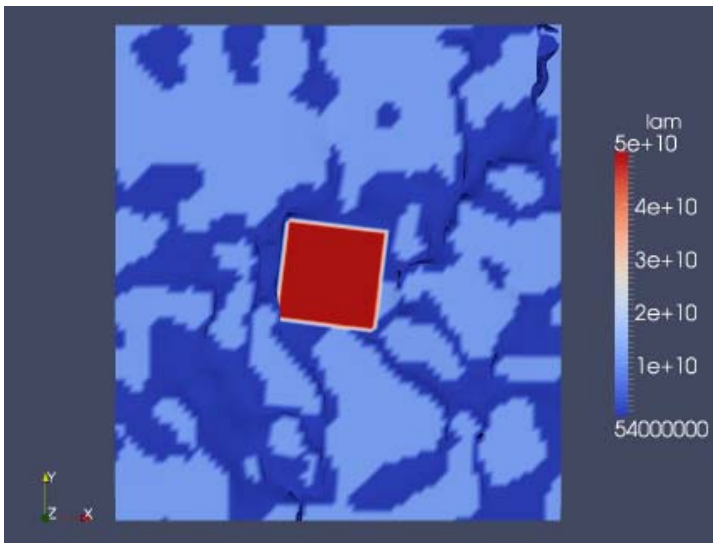

Fig. 13.20 Simulated effect of strain-tilt coupling. The uniform input strain acts on the y-direction. As a consequence of medium inhomogenuity an assumed rigid plate (which is a placeholder for the seismometer monument) is rotated and tilted considerably. The inhomogenity is caused by the modelled random (gaussian) medium which is represented by alternating values of Lame`s parameter λ. (courtesy M. v. Driel).

A network-wide homogeneous installation with good temperature isolation is preferable to apparent “hard-rock” installations (see Section 13.6 for a more detailed description). Sites near singular obstacles should be avoided such as high trees, cliffs, big towers etc., as they are likely sources of wind-generated noise. While wind noise is usually high in a frequency range > 5 Hz, wind pressure is a very strong source of tilt-noise in the low frequency part (< 0.1 Hz). Hence, special care must be taken when installing a broadband seismic instrument.

13.3.2 Station distribution

Good station coverage is crucial for nearly all monitoring efforts as well as for successful scientific research. A good choice is to install a network at two scales - one large scale network extending into non volcanic regions ($\Delta < 20$ km) and one network with stations concentrated on the flanks and on the top of the volcano ($\Delta \sim 0$ - 2 km). The large-scale seismic networks are very useful to distinguish between volcano-seismic signals and regional or local earthquake activity. Also the larger dimension improves the localization accuracy for deep-seated sources of magmatic activity. On the other hand, most of the seismic signals at active volcanoes are very shallow, usually small in amplitude and additionally influenced by strong scattering and high attenuation path effects. For detailed studies of the volcano-induced seismic signals, most of the stations need to be placed close to the activity center(s). One or two stations should be placed as near as possible (without danger to researchers and instruments) to the active volcanic region. Other stations should be placed such as to ensure a good overall azimuthal coverage. If possible, the station spacing should be comparable to the source depth to insure good depth control. It is good to have all parts of the focal sphere surrounding a source to be sampled by seismic stations. Best results are expected when the source is located within the station network, both lateral and vertical.

If a broadband seismometer is available, best results are achieved if it is installed as close as possible to the active area, provided that the safety of operating personnel is assured. Most of the recorded ULF and LF signals at volcanoes are detectable only in the near-field distance range (see Fig. 13.10) as well as the effect of scattering is lower as closer the station is located to the active source region (Section 13.4.5). For the best characterization of shallow low and utlra low frequency event source mechanisms, at least a few seismic stations should be placed as close to the crater or source region as possible. If an on-line radio link is desired, the station site must additionally be chosen such as to guarantee an undisturbed direct line-of-sight to repeaters or receivers (see Section 13.6 and Chapter 7, Section 7.3).

13.3.3 Seismic arrays in volcano monitoring

Modern approaches in volcano seismology are based on deploying seismic antennas (arrays) at active volcanic areas. Stations in an array should be spaced close enough to sample a wavefield several times in a wavelength, often requiring a spacing of about 100 m. The main advantage of such antennas and the application of array techniques is the improvement in evaluating the radiated wave-field properties, velocity structure and the source location (see Chapter 9). A comprehensive review paper dealing with standard seismic array techniques at volcanoes has been published by Chouet (1996b).

Most of the problems in operating a seismic array at an active volcano are of a technical

nature. The requirements on array site conditions are demanding, the cost of array components are rather high, and the installation and maintenance of an array during different activity stages and weather conditions require significant economic and human resources. Such requirements generally preclude the long-term use of arrays in volcano monitoring. Therefore, most of the work done so far in using array techniques at active volcanoes were short-term deployments of occasionally large arrays. Despite the mostly short duration of deployment, however, much information was gathered during these experiments. The results range from a more comprehensive description of the wave-field properties (Saccorotti et al., 1998; Chouet et al., 1997) to tracking the source volume of volcanic tremor signals (Almendros et al., 1997; Furumoto et al., 1990).

13.3.4 Array of seismic arrays

In attempting to achieve both monitoring and research objectives, a good compromise is to establish a network of small-aperture seismic arrays. The advantage compared to single (dense) array applications is the better spatial evaluation of the wave-field properties as well as the better azimuthal coverage when focusing on the location of the different seismic signals. In any event one has to compromise between aperture, number of instruments, spatial sampling and station accessibility. In 1997, a network of small-aperture arrays was established at the Merapi volcano, Indonesia (see Fig. 13.21). This network consists of three different array sites distributed around the volcano. The main objective of this array configuration is to attempt the automatic classification of the volcano-seismic events on the basis of the wave-field properties and an automatic hypocenter determination of the classified volcano-seismic events (Wassermann and Ohrnberger, 2001).

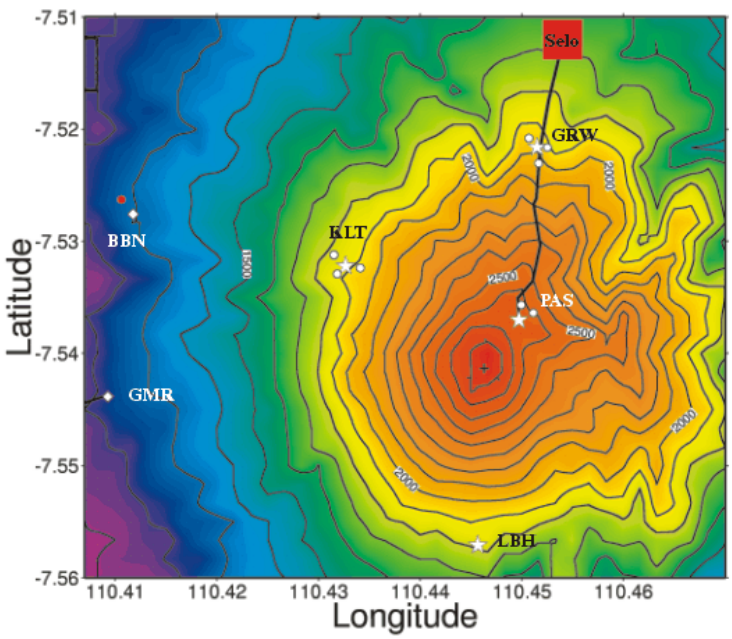

Fig. 13.21 Example of a combined seismic array/network approach at Mt. Merapi volcano. The stars show the location of broadband seismometers, whereas the circles mark the position of three-component short-period seismometers, in total forming three small-aperture arrays. The diamond symbols show the location of seismic acoustic stations (short-period sensors with a microphone array).

Before installing a network of arrays, a detailed plan of features to be investigated and criteria to be met should be made, e.g., required spatial coverage and resolution, accuracy of hypocenter determination, shallow and/or deep seismicity, broadband signals etc. A good choice is a network with at least four different array sites. Each array should consist of one three-component broadband seismometer as central station surrounded by three to six short-period, vertical-component seismometers deployed in a configuration which fits best the number of seismic stations (see Chapter 9). The most suitable distance between related seismometers must be carefully evaluated during the initial stage of the setup. Decisions must be made between the peak values in the spectral domain and the desired coherence band of the signals recorded. Ideally, the stations should be roughly 100 to 200 m apart from each other (Fig. 13.21). Reducing the inter-station distances with the same number of seismometers will cause an undesired loss of resolution in slowness due to the smaller aperture and also increase the noise coherence (see Fig. 13.22).

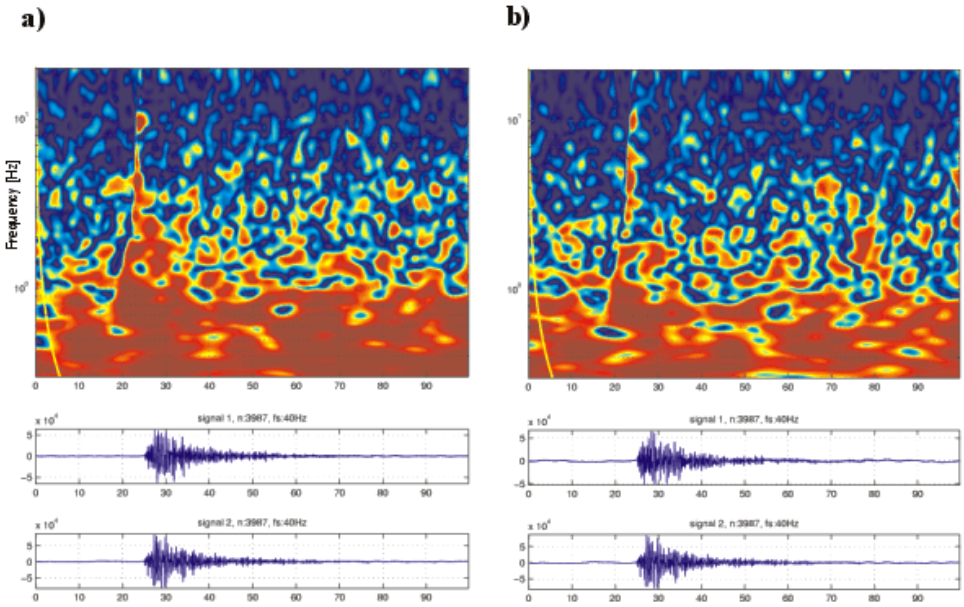

Fig. 13.22 Time-frequency coherence plot of a) the station combinations GRW0- GRW1 and b) GRW1-GRW2 (see Fig. 13.21). The seismometers in a) are deployed 170 m from each other, whereas in b) GRW1 and GRW2 are separated by roughly 300 m. Note: the signal coherence is computed in a sliding window with the time axis centered at the middle of the sliding window. High coherence above 2 Hz is only visible in the very beginning of a seismic event, indicating an array wide coherent phase arrival. It is also obvious that the overall coherence is somewhat lower in b) than in a) indicating the reduced signal coherence at more separated stations. On the other hand the noise coherence is also reduced in b) which improves the signal to noise ratio of the semblance estimation significantly.

13.4 Analysis and interpretation

In this chapter, we will briefly review the basic techniques of analyzing volcano-seismic signals. Most of the described concepts are based simply on visual pattern recognition abilities of the responsible interpreter. The last two sections will discuss more recent and objective approaches that attempt to automate these tasks.

13.4.1 One-component single station

Most of the observations made in the 60's and 70's were obtained by using only a few instruments located at most active volcanoes. Since then, nearly all well-monitored volcanoes are equipped with at least four to six instruments and, for a number of volcanoes, dozens of instruments. However, the basics of the classification scheme discussed in Section 13.2 is deduced by the single station approach and even today the statement "better one than nothing" holds regarding the number of deployed instruments. This is especially true when initiating short-term projects or monitoring very remote volcanoes.

13.4.1.1 Spectral analysis

With the advent of inexpensive, portable and efficient computers, spectral analysis became an increasingly important tool for monitoring the activity of an active volcano. As mentioned already in Section 13.2, most of the classification is based on the time-frequency characteristics of seismic signals. Volcanic tremor episodes were distinguished by their spectral shape and appearance. There are many different techniques for computing the spectral seismic amplitude such as *Seismic Spectral Amplitude Measurement* (SSAM; Rogers and Stephens, 1991), short-term Fourier transform or power spectral density estimates, which provide the observer with signal information in the spectral domain (e.g., Qian and Chen, 1996). An important feature of volcano-seismic signals is their narrow-band spectra. In particular, volcanic tremor sometimes shows just one dominant spectral band with a bandwidth as small as 0.2 Hz. This is the reason why it is often called "harmonic tremor". Monitoring the changes of spectral properties is a useful tool not only for signal discrimination but also for characterizing the state of volcanic activity. An example is given in Fig. 13.23. In Fig. 13.23a the total power in the frequency range between 0.6 and 3.0 Hz is plotted as a function of time. This frequency range was chosen because of its importance in discriminating between rockfall and pyroclastic flow signals (see Section 13.2.2.3). Three pronounced peaks are obvious with amplitudes well above the average value. The peaks at day 9 and day 18 are associated also with a significant increase of the power density between 2 to 10 Hz (Fig. 13.23b). On the other hand, the sharp peak in day 14 in Fig. 13.23a seems to be of a different nature and might be caused by a regional or teleseismic earthquake. The remaining times with high power density amplitudes in b) might be due to small pyroclastic flows or rockfall.

At Mt. Etna (Italy), Cosentino et al. (1989) reported a significant frequency shift in the volcanic tremor spectra prior to a flank fissure eruption. The authors detected a significant shift to lower frequency values of the dominant spectral peaks of volcanic tremor just several hours before the opening of flank fissures.

Because the efficiency of today's computers is rapidly increasing, a good choice would be to calculate complete spectrograms (or periodograms) first and decimate the amount of data only in a later step (e.g., to SSAM). This would allow the extraction of any hidden information in a later "off-line" step of the analysis without any redundant work load. Crucial in this context is a good knowledge of the possible features of different signals and their relationship to the state of volcanic activity at a specific site. It must be emphasized that stations of monitoring networks at volcanoes should be maintained for years (even decades) without any changes in the system (gain, position etc.). When upgrading an old station to new "up-to-date" technology, a sufficient overlap of both systems should be guaranteed. This precaution cannot

be overemphasized.

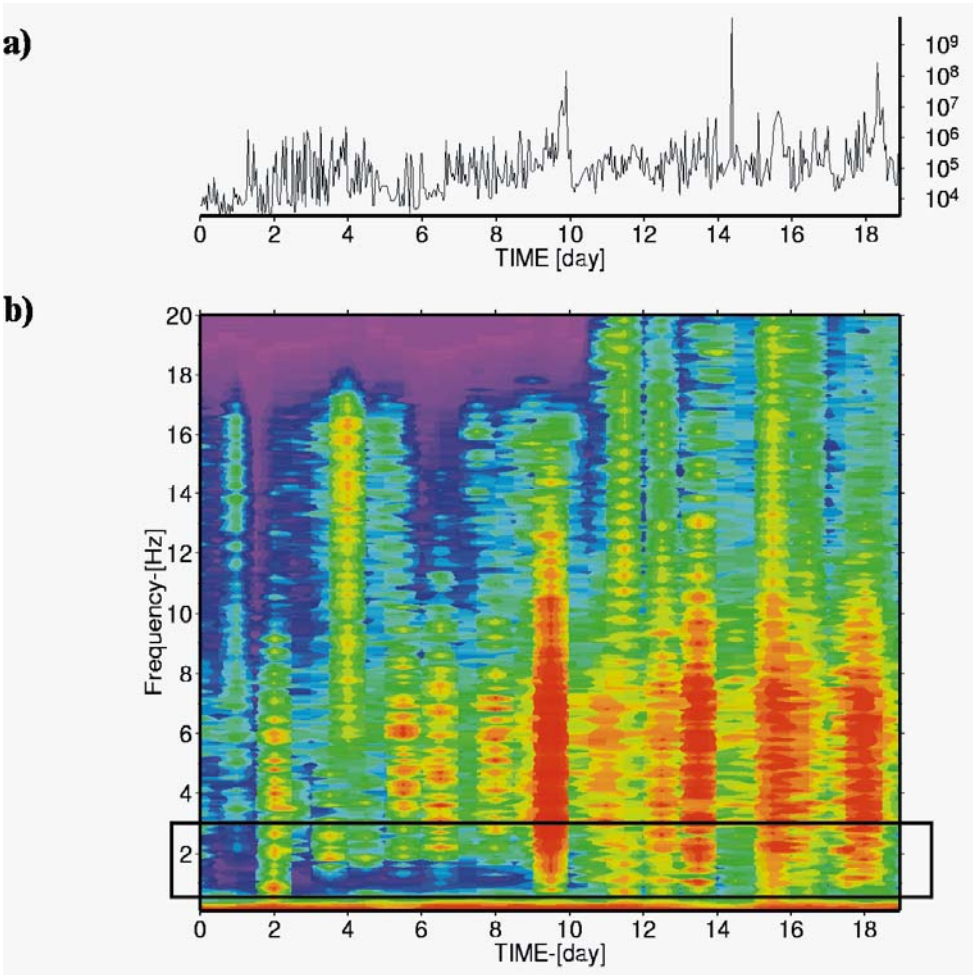

Fig. 13.23 a) shows the the total power (per 60 minutes) calculated in the frequency band between 0.6 - 3.0 Hz from 01 - 19th July 1998 at Mt. Merapi, displayed on a logarithmic scale. Two of the visible peaks (i.e., day 9 and day 18) are associated with pyroclastic flows, while the sharp peak visible at day 14 is caused by a regional earthquake. b) the power spectral density vs. time in the same time range, where the box shows the frequencies used for total power plotted in a).

13.4.1.2 Envelope, RSAM and cumulative amplitude measurements

An important source of information which can be deduced by small networks is the overall appearance of the signal shape in the time domain. This is important both for event classification (e.g., volcanic tremor, rockfall etc.) as well as for monitoring changes in the seismic activity of a volcano. A very efficient tool for visualizing increasing seismic activity is the *Real-Time Seismic Amplitude Measurement* (RSAM) technique proposed by Endo and Murray (1991). In its original form, RSAM was designed for analog telemetry and consisted of an A/D converter, averaging of the seismic signal in 1 min or 10 min intervals and storing of the reduced data on the computer:

$$RSAM(iT) = \frac{1}{T} \sum_{t = iT - \frac{T}{2}}^{iT + \frac{T}{2}} |s(t)|$$

Here T is the averaging interval (originally 1 or 10 min) and $s(t)$ the sampled seismic trace. Various examples for successful applications of this technique are given by McNutt (2000b).

Some applications try to normalize the records from several seismic sensors located at different distances from the volcanic center by correcting the measured seismic amplitude for the assumed source distance (McNutt, 2000b):

$$D^b{}_R = \frac{Ar}{2\sqrt{2}G}, \text{ and } D^s{}_R = \frac{A\sqrt{\lambda r}}{2\sqrt{2}G}$$

where D^b and D^s are the reduced amplitude for body and surface waves, respectively. A is the peak to peak amplitude in centimeters, r the distance to the source, λ the seismic wavelength in cm and G the gain factor (magnification) of the seismic sensor. The main difference between these two equations are the different correction terms for the geometrical spreading and the effective wavelength. The reduced amplitude measurements should be considered as a pure observation parameter without any physical meaning. It should definitely not be used for the physical interpretation of an ongoing eruption. The reduction of the seismic amplitude assumes specific modes of wave propagation, i.e., body wave and surface waves, respectively. As there is no reliable estimate of the wave-field properties, it is possible with just one or a few seismometers that the assumption of the degree of geometrical spreading is highly speculative. Also the effect of site amplification and the strong scattering observed frequently at volcanoes (Wegler and Lühr, 2001), which depend in general on the source location, structure and topography of the volcano, may alter the amplitude-distance relationship significantly. They are neglected in this approach.

Another way of displaying changes in the radiated seismic wave-field is based on the computation of the de-trended cumulative radiated power of the seismograms at a single station (see Fig. 13.20):

$$P_{cum}(f_{1-2}, t) = \sum_t \left(\sum_{f = f_1}^{f_2} P_t(f) - trend \right)$$

with $P_t(t)$ being the power spectral density during the time interval t and f_1, f_2 the lower and upper frequency for computing the cumulative power. *trend* is the slope of the cumulative power, calculated during a quite time period, i.e., baseline activity of the volcano (Fig. 13.24).

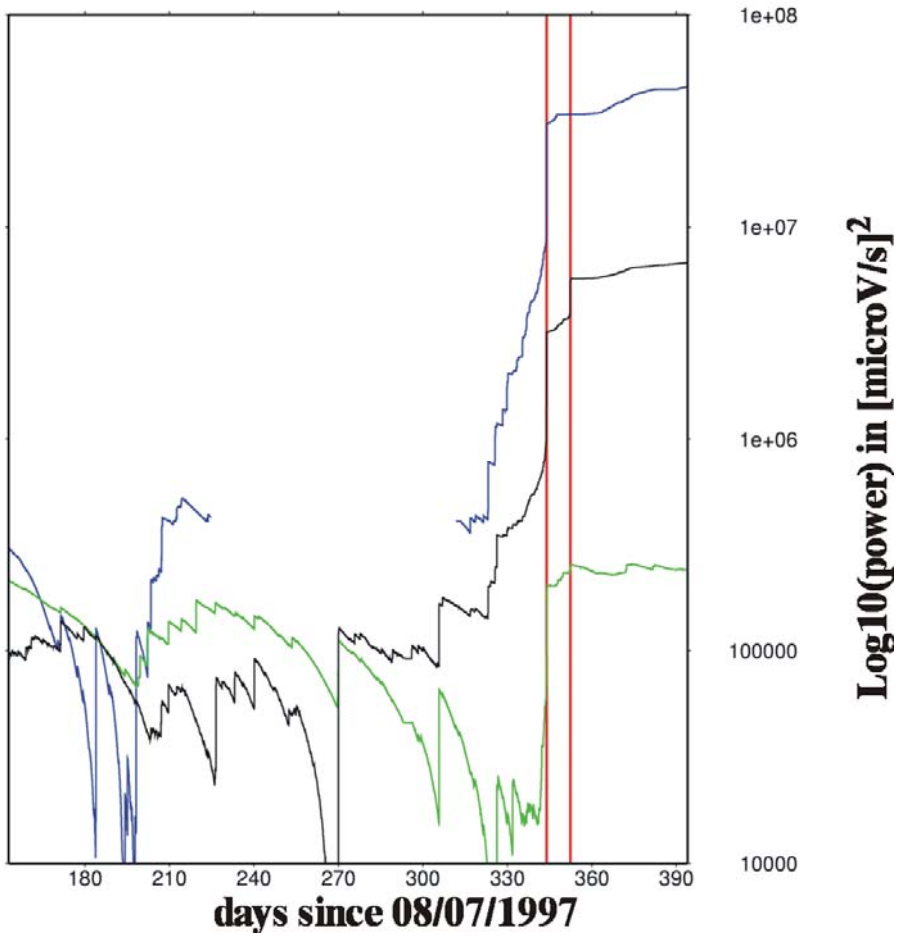

Fig. 13.24 De-trended cumulative power of the vertical components of all broadband seismometers at Mt. Merapi during 1998 activity. The red lines mark the occurrence of two pyroclastic flows. A steep increase of the total cumulative power 10 days before the onset of the first pyroclastic flow is visible, following a period with very low seismicity. Also the second eruption is preceeded by an increase of cumulative power at two stations, while one station (blue) was out of operation. The background trend was estimated during a low activity phase in 1997.

To avoid a fast saturation of the cumulative power values, a good way is to estimate the slope of the cumulative power when the activity of the volcano is on its baseline. This estimated trend can be removed for each time step resulting in a de-trended cumulative power plot, which shows strong deviation from the "normal" background seismicity. Furthermore, cumulative power can be used to analyze certain frequency bands (see Fig. 13.23a), unlike the power change in time, which resembles the method of RSAM. In Fig. 13.24, the de-trended cumulative power of three broadband stations at Mt. Merapi is shown. Note the steep increase of seismic power roughly ten days prior to the first eruption. A further increase in cumulative power is obvious for two stations preceding the second large pyroclastic flow. The third station was out of operation caused by ash fall on the solar panels.

A common way to display information on the current status of a volcano is to count the different seismic event types in a hourly or daily manner (Fig. 13.25). While the physical interpretation of the type of event is sometimes impossible when using only one station, such event/time plot is an excellent tool for displaying all information (objective and subjective)

within one single plot. There are many papers, which rely strongly on this kind of activity measurements. Most of the observations are summarized by McNutt (1996, 2000b). Also in this case, we must emphasize that, without a complementary detailed seismological study, this is just a visualization of observed patterns with, strictly speaking, unknown physical meaning.

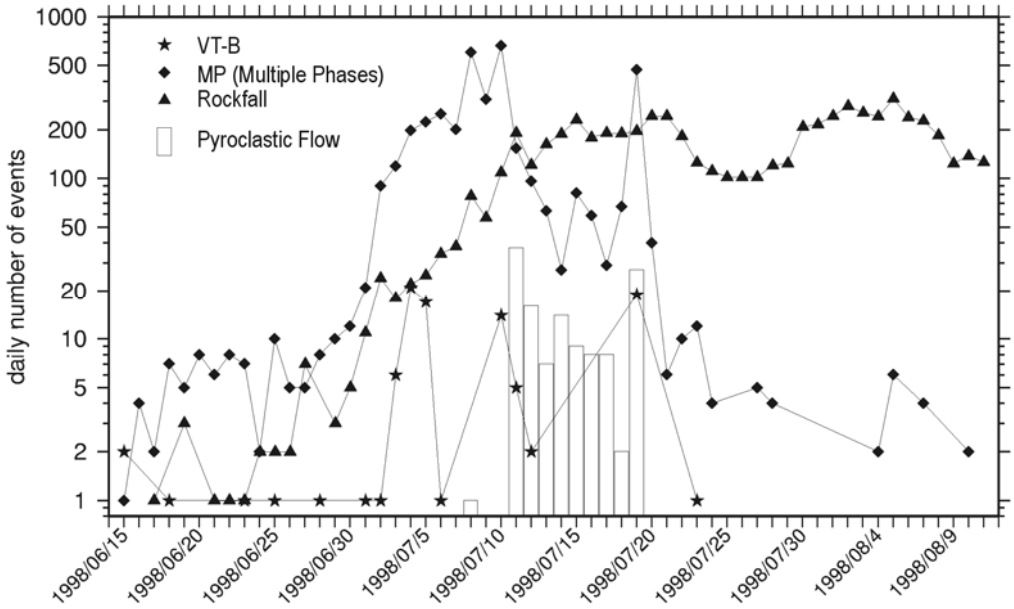

Fig. 13.25 Event-type per day plot during the high activity of Mt. Merapi during July 1998. Note the increase of the three event classes before the onset of the first pyroclastic flow. Also note the similarity of the VT-B type event curve to the occurrence of pyroclastic flows (courtesy of VSI- BPPTK, Yogyakarta).

Whatsoever, if knowledge about the hypocenters (see Section 13.4.3.1) and even source mechanism is available these event-time plots are very valuable in order to evaluate the activity state of a volcano. At Soufriere Hills volcano (Montserrat island) it was possible to distinguish different activity phases with the help of these seismicity plots (Miller et al., 1998). Just before the surface activity starts to develop a swarm of VT-A earthquakes appeared. During cycles of inflation in the upper part of the growing dome a large number of Hybrid and LP events were detected. Finally, a large number of surface events, mainly rockfall signals, were recorded as the dome became more and more unstable. While this pattern of seismic signals is very important during a high activity phase of a volcano, it must be emphasized that every volcano and every eruption has its own unique pattern.

13.4.1.3 Failure Forecast Method (FFM)

While the FFM originates from material sciences and relates the rate of precursory signs of failure to the likeliness of failure, Voight (1989), Cornelius and Voight (1995) and Kilburn (2003) introduced an early warning method, which is based on the rate of precursory signs (e.g., number of a certain type of seismic signal, RSAM, cumulative tilt etc.) and correlates their accelerations to the onset time of an eruption. The governing equation is given by:

$$\partial^2\Omega/\partial t^2 = A(\partial\Omega/\partial t)^{\alpha}$$

where $\partial^2\Omega/\partial t^2$ and $\partial\Omega/\partial t$ are the acceleration and rate of the monitored parameter. A and α are empirically determined parameters. Cornelius and Voight (1995) pointed out that α evolve from 1 to 2 before an eruption. Kilburn (2003) pointed out that the peak of event rates are better suited to forecast the timing of a failure (i.e. eruption) and that α = 2 should be used. With this assumption the equation can be simplified to:

$$1/(\partial\Omega/\partial t) = A(t_f - t)$$

where t_f is the time of failure. Fig. 13.26 gives an example of a successful application of FFM.

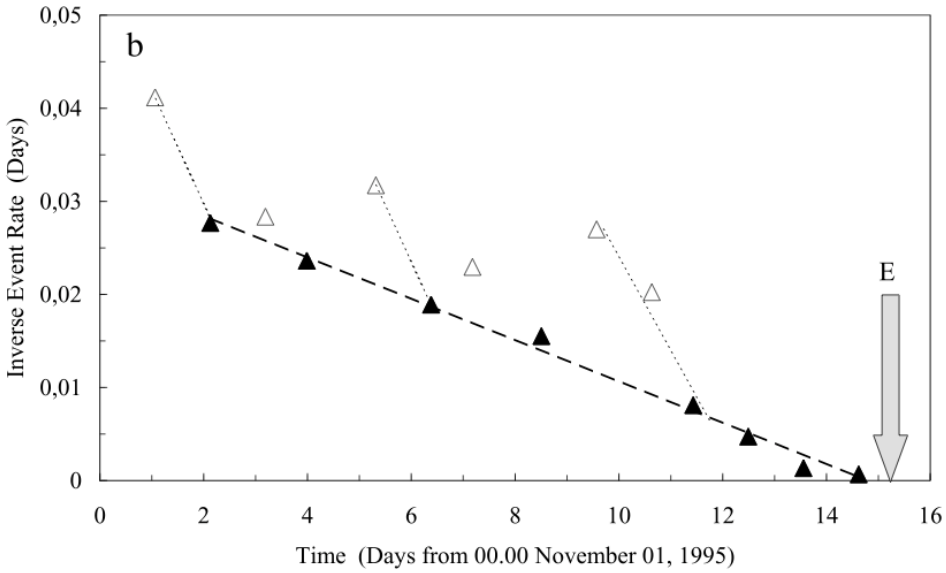

Fig.13.26 Change in recorded seismicity before the 1995 eruption of Soufriere Hills on Montserrat. Arrow E marks onset of magmatic activity. On an inverse-rate diagram, the filled triangles, which correspond to inverse-rate minima, lie along a linear trend (large dashed line). Such a trend possibly could be recognized by Day 8, which results in a maximum 6-day warning of eruption. Note that peak values are more readily identified from the inverse-rate minima than the actual event-rate maxima, and that steeper linear trends occur among individual sequences (small dashed lines) (from: Kilburn, 2003).

13.4.2 Three-component single station

Most modern seismometers are three-component sensors, which record the vector of ground motion produced by seismic waves. Observation of the particle motion will not help to precisely determine source locations and their variations without a detailed knowledge of the wave-field properties (e.g., Rayleigh waves, Love-waves, P- or SH and SV-waves). In some cases it might be possible to “steer” or point towards the active source region by estimating the particle motion of the very first wavelets of LF or ULF events. As this is possible mainly in the near field there might be an unknown degree of distortion. Changing patterns of particle motion may help estimate the activity changes of a volcanic system in a qualitative way, however.

13.4.2.1 Polarization

Seidl and Hellweg (1991) showed results from analyzing the 3D-trajectories of a single seismic broadband station at Mt. Etna volcano (Italy) using very narrow bandpass filters. They argued that the occasional strong variations in the azimuth and incidence angles of the trajectories may reflect sudden changes of the active source location. Recent experiments using array techniques showed, however, that the wave field radiated from a volcanic source is a combination of complex source mechanisms and strong path influences (e.g., Chouet et al., 1997). Hence, the wave-field consists of a mixture of many wave types and care must be taken when only polarization information is available. On the other hand, carefully extracted information and the associated changes of polarization pattern during different cycles of volcanic activity may help to identify changes in the state of the volcanic system (see Fig. 13.27 below).

The use of a broadband seismic station located close to an active vent, i.e., in the near-field, improves the quality of source estimations based on simple polarization analysis. This is because of the small influence of the propagation path in the near-field. Unfortunately, complicated source mechanisms, i.e., when the usual assumption of a point source is no longer valid, will complicate the interpretation of the observed polarization pattern to an unknown degree (Neuberg and Pointer, 2000). Also, the nearly unknown influence of the topography of the volcano on signals with a wavelength comparable to the topographic obstacle will make interpretation difficult. Near-field measurements at Stromboli volcano (Italy) showed, that in some cases, a fairly good estimation of the source region could be made using just a single three-component broadband station (Kirchdörfer, 1999; Hidayat et al., 2000) under the assumption of a simple source mechanism.

13.4.2.2 Polarization filters

When evaluating the polarization properties of volcano-seismic signals as part of a monitoring system, an automatic estimation of parameters is needed. Best results will be obtained when focusing on the basic parameters, i.e., the azimuth, incidence angle and a measure of the rectilinearity of the signals. Various approaches will extract this information from a continuous data stream. Most of them are based on a least-square fit of the 3D-trajectory of the seismic vector to a 3D-ellipsoid. Typical algorithms consist of solving the eigenequation and simultaneously searching for the orientation of the eigenvector corresponding to the largest eigenvalue (e.g., Flinn, 1965, Montalbetti and Kanasewich, 1970):

$$\begin{vmatrix} x_i \\ y_i \\ z_i \end{vmatrix} \left| C - \lambda_i I \right| = 0$$

where x_i, y_i, z_i represent the components of the i-th eigenvector, $\underline{I}$ is the identity matrix and λ_1 is the eigenvalue according to the i-th eigenvector. $\underline{C}$ represents the covariance matrix of the 3D signal recorded:

$$C_{ij} = \sum (u_i - u_i)(u_j - u_j)$$

where u_i, u_j are the i-th and j-th component of the seismic sensor and $\bar{u}_i$, $\bar{u}_j$.represents the mean values of the data traces within the analyzed time window. A possible way to display the polarization properties vs. time is to plot the orientation of the eigenvector associated with the largest eigenvalue (corresponding to the major axis of the ellipsiod) in the coordinate system of the sensor, i.e., its azimuth Φ_{az} and incidence angle Θ_{inc}:

$$\Phi_{az}(t) = \operatorname{atan}\left(\frac{y_1(t)}{x_1(t)}\right), \text{ and } \Theta_{inc}(t) = \operatorname{atan}\left(\frac{z_1(t)}{\sqrt{x_1^2(t) + y_1^2(t)}}\right)$$

with x_1, y_1, z_1 representing the eigenvector components of the largest eigenvalue $\lambda_1(>\lambda_2>\lambda_3)$. Note: without any further assumption about the analyzed wave-type, i.e., P-, SH- or SV-wave etc., the computed azimuth has an ambiguity of 180 degrees, whereas the incidence angle varies between 0 - 90 degrees. Typically, a measure of the rectilinearity of the signal's polarization (i.e., the relative elongation of the ellipsoid in one direction) is computed (e.g., Vidale, 1986):

$$L(t) = 1 - \left(\frac{\lambda_2(t) + \lambda_3(t)}{\lambda_1(t)}\right)$$

L(t) is only larger than 0 if λ_1 is bigger than the combination of the other two. Fig. 13.27 gives an example of the variation of the parameters Φ_{az} and Θ_{inc} over a long time period at Stromboli volcano.

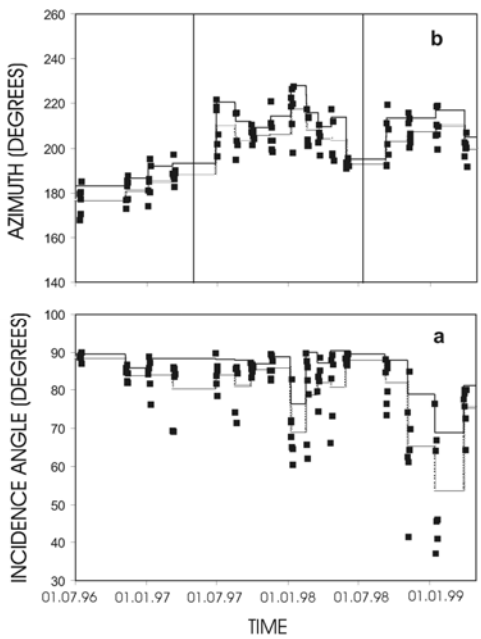

Fig. 13.27 Long-term variations of incidence angle (a) and azimuth (b) in the 115 time windows selected from July 1996 to April 1999 at Stromboli volcano. In both panels, solid and dotted line depict mean value and standard deviation, respectively, computed over 5 to 7 consecutive days in the 17 time windows selected from July 1996 to April 1999. The polarization parameters were estimated using the technique of Montalbetti and Kanasewich (1970). The variation of this waveform information seems to match changes in the activity states of the volcano (courtesy of S. Falsaperla, Istituto Nazionale di Geofisica e Vulcanologia).

Because we have no knowledge of the wave type represented by the computed polarization parameters, they must be seen as varying activity parameters rather than interpreting them as part of a technique for hypocenter determination.

13.4.3 Network

13.4.3.1 Hypocenter determination by travel-time differences

Modern seismic monitoring networks at active volcanoes usually consist of at least four to six seismic sensors distributed in various azimuths and distances from the volcanic center. While continuous signals such as volcanic tremor or transients like LF-events often lack any clear phase arrival, some signals (VT, explosion quake) with clear onsets can be located using standard seismological techniques.

Usually, events with clear P- and/or S-wave onsets are selected visually and the first breaks are picked interactively. The inversion for the source location is frequently done using algorithms such as HYPO71 (Lee and Lahr, 1975) or HYPOELLIPSE (Lahr, 1989) or HYP2000 (Klein, 2002). Note, however, that most of the standard hypocenter determination programs are based on the assumption of a horizontally layered half-space and/or models with linear gradients with no topography. Also new approaches exist, which are not restricted to 1D or 2D velocity models and which try to locate the sources in a non-linear, probability based manner (e.g., Lomax et al., 2000). However, in most cases no good velocity models for the monitored volcanoes exist and the computed source coordinates, especially when focusing on shallow events, must be seen just as an approximation to the true hypocenter. Relative earthquake locations of multiplets with similar waveforms can greatly improve the resolution of volcanic structures (Rubin et al, 1998; Waldhauser and Ellsworth, 2000; Ratdomopurbo and Poupinet, 1995). De Barros et al (2009) showed that when the network is dense enough such that events correlate at different station very good and reliable locations are possible using a grid search method.

There are many papers on the topic of imaging the hypocenter distribution during or before a volcanic eruption (e.g., Newhall and Punongbayan, 1996; Power et al., 1994; Chouet et al., 1994). Very useful information about the geometry of the plumbing system as well as the physical properties of the host rocks can be deduced by analyzing the time-space pattern of frequently occurring swarms of deeper earthquakes (Power et al., 1994).

Also the migration of hypocenters during a high activity phase of a volcano is important in forecasting the subsequent volcanic eruption. In Fig. 13.28 an example of the 1991 Mt. Pinatubo eruption is shown. The migration of the seismic events from a cluster at 5 km depth north-west of the volcano in A) to a very shallow location directly underneath the erupting vent in B) is very obvious and possibly marks the ascending magma.

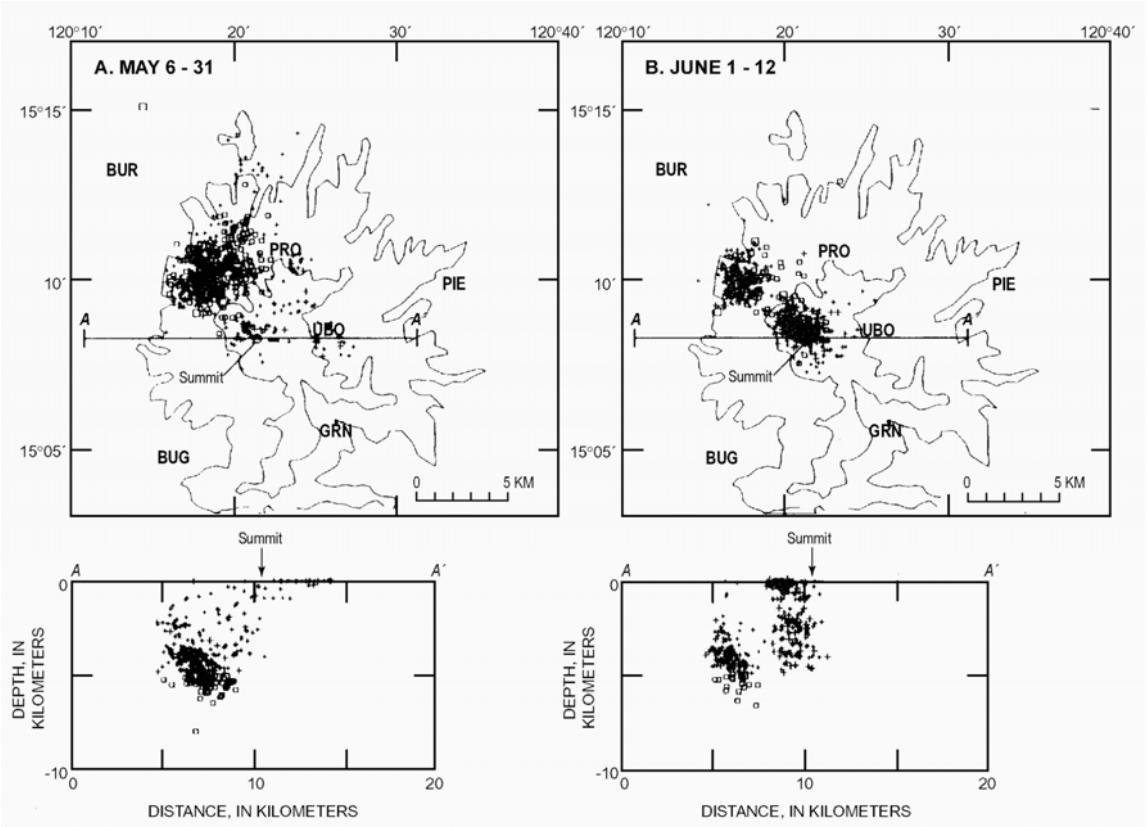

Fig. 13.28 A) Mt. Pinatubo seismicity during May 6 to May 31. The seismic events are clearly clustering northwest of the volcanic center. B) shows the seismicity between June 1 to June 12 indicating a shift of the hypocenters to shallow depths and closer to the summit of Mt. Pinatubo (courtesy of Pinatubo Observatory Team (1991), EOS Trans. Am. Geophys Union, 72, 545, 552-553, 555)

13.4.3.2 Cross correlation of diffusive wavefields

Weaver and Lobkis (2001a), Campillo and Paul, (2003) and Wapenaar et al. (2006) showed that correlating the coda of earthquakes which are azimuthally well distributed around a seismic station pair will result in an estimate of the Greens function of the subsurface structure between these two stations. Shapiro and Campillo (2004) also showed that the Greens function, or at least parts of it can also be retrieved when using the diffusive wavefield of noise. Sens-Schönfelder and Wegler (2006) used this property to monitor the seasonal changes at shallow depth on a volcanoes flank which is thought to represent different ground water saturation. Brenguier et al. (2008) showed, that monitoring the changes of the Green's function can be interpred as a change in the velocity field at a volcano. This change is caused by the deformation of the volcanoes edifice caused by inflating or deflating magma. Fig 13.29 gives an example.

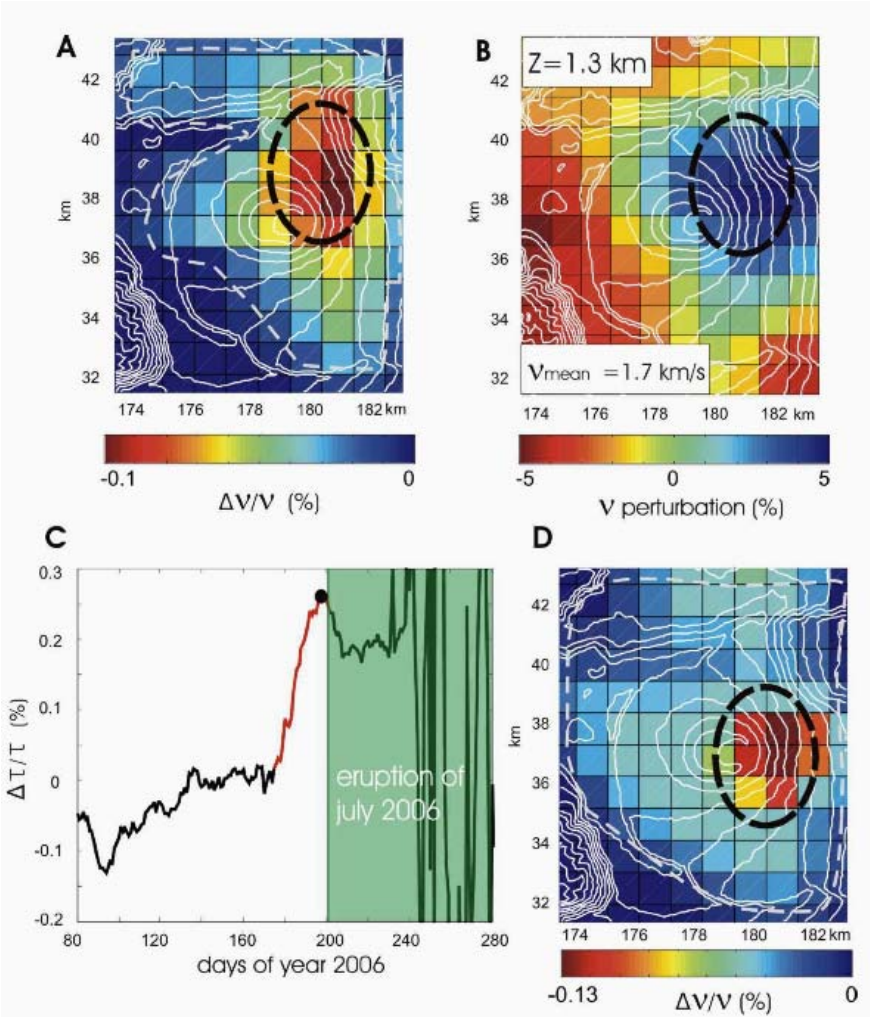

Fig. 13.29 (A) Relative velocity perturbations associated with the second eruption precursor (day 85, Sept. 1999) at Piton de la Fournaise volcano (Reunion island). The gray dashed line represents the limits of ray coverage. **(B)** Fast shear velocity anomaly imaged by passive surface wave tomography (and interpreted as an effect of solidified dykes associated with the zone of magma injection. **(C)** Relative time perturbations before the eruption of July 2006. **(D)** Associated regionalized relative velocity perturbations one day before the beginning of the eruption (from: Brenguier et al., 2008)

While in praxis the technique is rather complex and sophisticated, parts of it are already included in daily monitoring routines (e.g., EARTHWORM, see Section 13.4.6).

13.4.3.3 Amplitude - distance based hypocenter determination algorithms

Even in the case of no clear P- or S-wave arrival, it is sometimes possible to estimate an approximate source area. Assuming a certain wave type (body or surface wave), neglecting an uneven radiation pattern of the source, and assuming a simplified propagation path, it is possible to compute amplitude-distance curves and model the source region. This can be seen as an iterative approach of fitting or contouring the amplitudes or radiated energy measured in the whole network. Successful applications of this technique were reported for locating volcanic tremor at Bromo volcano, Indonesia (Gottschämmer and Surono, 2000) and Mt.

Etna, Italy (Cosentino et al., 1984). However, care must be taken in the a priori assumption of the wave-type, i.e., body or surface waves. When locating the paths of pyroclastic density at Soufriere Hills volcano (Mountserrat), Jolly et al. (2002) were using a surface wave relationship. Battaglia et al. (2005) showed that volcanic tremor can be successfully located (see Fig. 13.30) by applying a rather simple amplitude-distance relationship. However, Battaglia et al. (2005) clearly pointed out that before applying this technique to the data a so called coda normalization has to be done in order to remove station-site dependent amplifications (Battaglia et al., 2005).

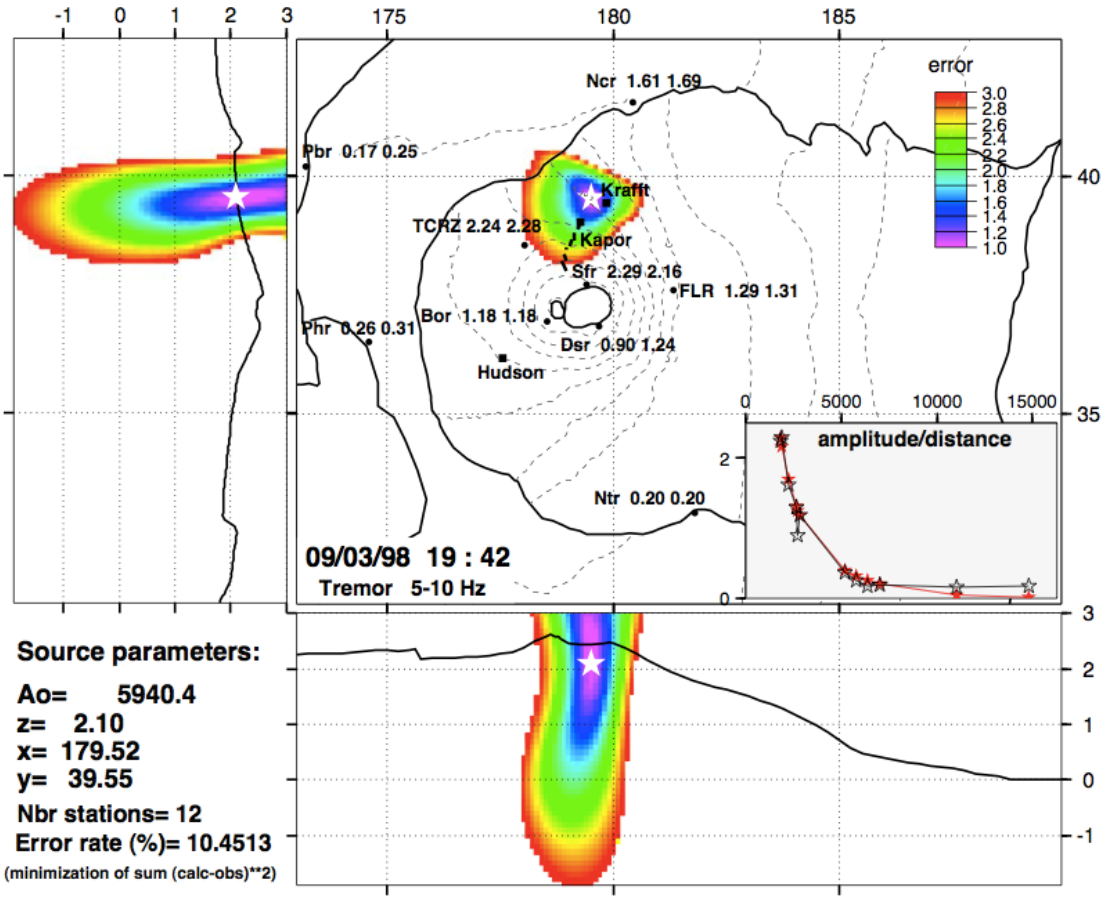

Fig. 13.30 Example of an individual location in the 5–10 Hz frequency band for a tremor sample collected during the 1998 eruption of Piton de la Fournaise volcano (Reunion island). Map view and NS and EW cross-sections are shown. The result of the location is plotted as a white star, which is superposed on the normalized error contours. (from: Battaglia et al., 2005)

Wegler and Lühr (2001) and Friedrich and Wegler (2005) showed that the largest amplitudes visible in the seismograms recorded at the Mt. Merapi volcano are fitted best by assuming a strong scattering regime (see Fig. 13.31), which also alters the amplitude-distance relationship.

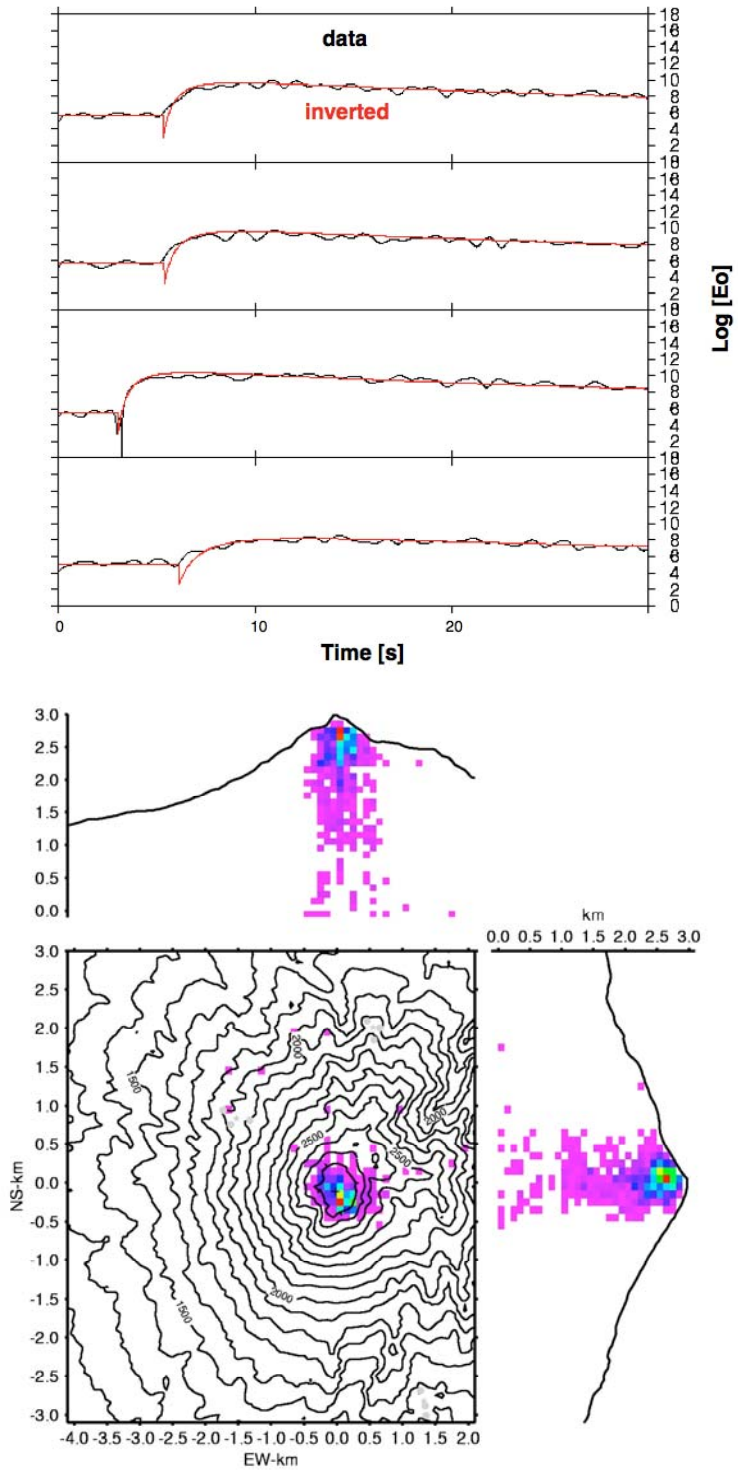

Fig. 13.31 a) Envelope of MP event measured at different stations around Mt. Merapi and the result of fitting the scattering relationship of Wegler and Lühr (2001) to the data. **b)** shows the stack of locations of several hundreds of MP events using this amplitude distance relationship.

Also the influence of near-field effects may influence the amplitude-distance curve significantly (see Fig. 13.32).

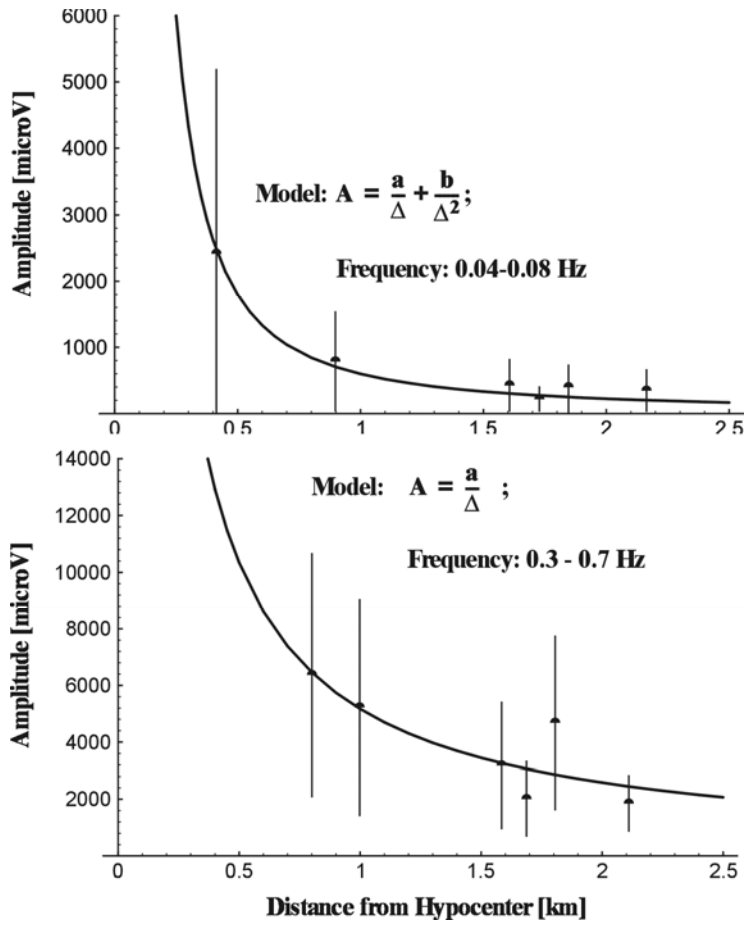

Fig. 13.32 Top: Amplitude-distance relationship at Stromboli volcano. The amplitudes were measured in the frequency range 0.04 - 0.08 Hz. The best fit of the amplitudes at different distances from the active vent was obtained when an additional near-field term was added ($A \sim 1/\Delta^2$). **Bottom:** Same as top diagram but in the frequency range 0.3 - 0.7 Hz. In this case the best fitting curve follow the usual factor of geometrical spreading $1/\Delta$ for body waves. It is also obvious that in b) site effects are more pronounced than in a).

Amongst others the following relationships have been proposed:

- body waves (Battaglia et al., 2005): $A^2 \sim A_o^2/r^2$;
- surface waves: $A^2 \sim A_o^2/r$ (Jolly et al., 2002);
- near field: $A^2 \sim (A_o/r + B_o/r^2)^2$ (Wassermann, 1997);
- scattering: $A^2 \sim A_o^2 (1/(2\pi\, d\, t))^{3/2} \exp\{-bt - r^2/4dt\}$ (Wegler and Lühr, 2001)

13.4.4 Seismic arrays

The analysis of seismic signals using array techniques is seen as the most prominent and emerging modern tool for locating volcano-seismic signals and evaluating the seismic wave-

field properties (e.g., Chouet, 1996b). While most of the array techniques are discussed in Chapter 9, we will focus on some results obtained when applying them in volcano monitoring and signal analysis.

The main deviation from typical array techniques in earthquake seismology is that the height differences between the array stations can not be neglected when the array is deployed on the flanks of a volcano. The effect of a 3D-distribution of stations can be minimized by fitting a plane to the station locations which dips according to the topography. One then transforms all auxiliary information (i.e., station coordinates) and refers all estimated parameters (incidence, azimuth and horizontal slowness) to this "best fitting plane".

13.4.4.1 f-k beamforming

One of the most useful properties of a seismic array is its capability for suppressing undesired signals by filtering the incoming wave-field in the spatial as well as in the frequency domain. Thus, we can estimate the coherence, the signal power, the azimuth and the apparent velocity of an incoming wave. Because most seismic signals map into different regions of the frequency-wave number plane (see, e.g., Fig. 9.28, 9.38 and 9.40), f-k beamforming is an excellent tool to distinguish between the different wave-types. Beamforming can be thought of as delaying each seismic trace in time such that waves will add constructively when summed. The delay times necessary to obtain maximum "beam-power" is used to determine the direction of wave propagation through the array. Beams "aimed" in a direction, which is different than the true source direction will add destructively and produce a low signal. If the seismic array is located several wavelength from the assumed source area and the spatial extend of the array is small compared to the distance towards the source, we can also assume plane-wave propagation. Under these assumptions it is possible to estimate the backazimuth towards the source and, if the velocity model directly below the array is known, we can also estimate the incidence of the incoming plane wave. We can then invert for the source area of the signal (see Chapter 9, Sections 9.4.2 - 9.4.4).

Fig. 13.33a-e) gives an example of a broadband f-k analysis with data recorded at Mt. Merapi. Obviously only the very first part of the signal shows a phase with high coherence b), which additionally shows a small slowness c) (high apparent velocity). In contrast, later arrivals have randomly fluctuating backazimuth and slowness values. A possible interpretation of this pattern is that the recorded event consists of an array-wide coherent body phase (indicated by the high coherence and red color coding), which could be used for locating the event combining the backazimuth information and, if the velocity model just beneath the array is known, the incidence angle is estimated from the slowness. This coherent phase is followed by randomly incident waves.

Thus, the potential of a seismic array to discriminate between various types of incoming seismic waves and to quantify their properties makes the f-k beamforming perhaps the most powerful tool for investigation of continuous signals (i.e., volcanic tremor). Furumoto et al. (1990) and Almendros et al. (1997) showed the results of tracking a volcanic tremor source in space and time using seismic array beamforming. Other applications of large seismic arrays have been reported by Saccorotti et al. (1998), Chouet et al. (1997) and La Rocca et al. (2000), to name a few.

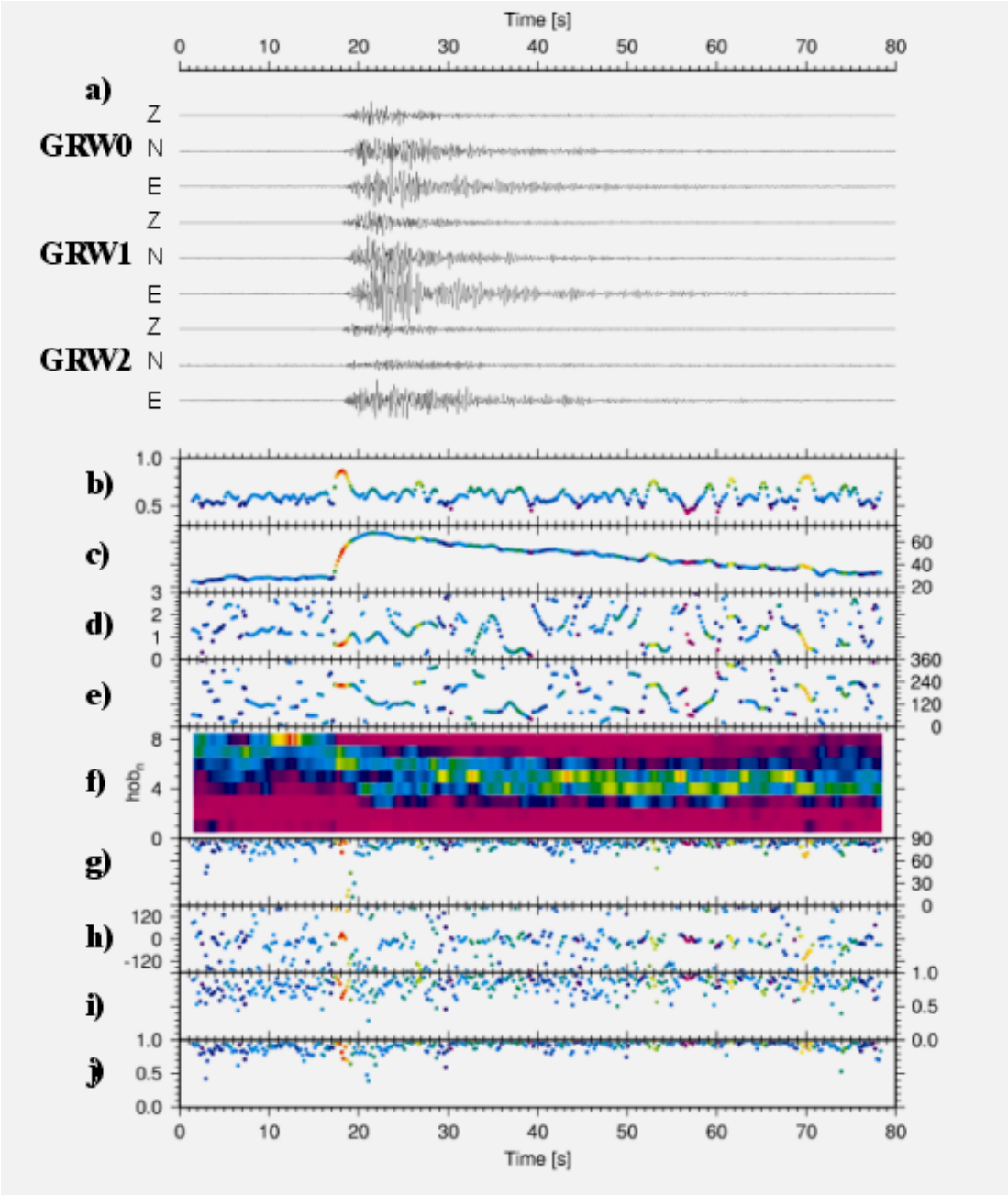

Fig. 13.33 Output of a continuous array analysis of a small three station seismic array with three component seismometers. a) shows the waveforms of a VT-B type event at the different seismometers. b) is the relative power (semblance) obtained by the f-k analysis, c) shows the overall power in the array in a dB scale, while d) and e) gives the slowness in s/km and the backazimuth in degree of the incoming waves, respectively. f) shows the array-wide averaged time-frequency pattern in 8 half octave bands. g) and h) show the incidence and azimuth of the array wide averaged polarization pattern (in degrees), while i) is a measure of rectilinearity and j) is the planarity of the analyzed signal. The color coding of b) to e) and g) to j) is proportional to the highest semblance value obtained in this signal. The high coherency phase at the beginning of the signal can be used for beam steering towards the source location (courtesy of M. Ohrnberger, University of Potsdam).

However, the application of beamforming techniques in volcano monitoring requires high computer power, rarely available during a volcanic crisis. In order to reduce it, one can use the spatial filter properties of seismic arrays and apply the f-k beamforming to steer in one or several directions of special interest (similar to beamsteering used to detect underground nuclear explosions; see Chapter 9, Section 9.6 and Section 9.7.7). Another way to reduce computational processing includes optimization of estimating the maximum of the beam in the f-k plane (i.e., highest coherence value) by using simulated annealing and/or simplex techniques (Ohrnberger, 2001).

13.4.4.2 Array polarization

As three-component seismometers are becoming the standard instrument nowadays and seismic arrays consist frequently of large numbers of three axial sensors, it is also possible to evaluate the polarization properties of the whole array. While there is no straight-forward method to include the polarization properties directly into the f-k-algorithm, it is possible to estimate array-averaged parameters of the 3D-trajectories. Jurkevics (1988) showed that array-wide averaging of the covariance matrices (see Section 13.4.2.2) results in a more stable estimate of the seismic wave vector (Fig. 13.27). Jurkevics (1988) also demonstrated the insensitivity of this estimate to alignment problems within the array. With this algorithm it is also possible to average the polarization properties over certain frequency bands which is a further link to the averaging properties of the broadband f-k-analysis (see Chapter 9, Section 9.7).

A further method to in-cooperate three-component seismic recordings of an array is to compute the “waveform” semblance (e.g., Ohminato et al., 1998; Kawakatsu et al., 2000). This approach consists of a grid search over possible source locations and the simultaneous rotation of the 3D ground motion vector towards these hypothetical sources. The semblance value of the L direction (L-Q-T system defining the direction from the source to the station L, the plane Q perpendicular to L including the source and receiver and the plane T perpendicular to Q) is computed. Assuming a source which generates solely a compressional wave in L direction the energy-density on the orthogonal components should be zero. Finally the “waveform” semblance should be 1 if the signal is coherent on all array stations and if no energy is left on the two directions perpendicular to L. The “waveform” semblance should be zero if there exists only incoherent wave-groups and/or there is still signal on the components different to L. It must be emphasized that this approach is restricted to cases where path effects and the influence of the free surface has no or vanishing influence on the orientation of the particle motion, i.e., low-frequency near-field observations.

13.4.4.3 Hypocenter determination using seismic arrays

As described in the Section 13.4.4.1 it is possible to track seismic sources in space and time using seismic arrays. Unfortunately, the exact seismic velocity distribution of a volcano is unknown. This results in large uncertainties in estimating the location of volcanic-seismic sources. One possible solution is to use not only one array but a network of arrays distributed around the volcano to compute the backazimuth of the coherent arrivals for each array separately and to invert them for the epicenter of the signal. Applications of this technique can be found in La Rocca et al. (2000).

Another difficulty arises when the seismic array is located close to the source and/or the height differences between the array stations are not negligibly. In this case the usually assumed plane wave propagation is no longer a good approximation and therefore the results are biased to an unknown extent, because neither the influence of the topography nor the deviation of the wave front from a plane wave is exactly known. In this case, a better way to localize the seismic source is to apply a more complicated approach, which first uses f-k beamforming to detect coherent phases within the continuous seismic data records and then apply two station generalized cross-correlation techniques in order to estimate the time difference of arrivals between the two stations. Wassermann and Ohrnberger (2001) successfully applied this technique to localize VT and strong MP events recorded at Mt. Merapi without the need for interactively determined onsets.

While this algorithm is only applicable to coherent and transient signals, algorithms exist which are based on the migration of coherent phases back to the source region (Almendros et al., 1999; Ohminato et al., 1998; Wassermann, 1997). Unfortunately, the computational load of these algorithms is high and their application is restricted to the "off-line" analysis of selected signals of special interest.

13.4.5 Automatic classification/detection

When establishing a seismic network at an active volcano it is also possible to revise the classification scheme used (it would be possible even with a single station, but not very reliable). Besides the usually semi-automatic trigger and (visually) applied time-frequency analysis (see Section 13.4.1.1), we can also use wave-field properties obtained from the array analysis to enhance our discrimination quality significantly.
The advances in performing an automatic classification during the last 10 years are tremendous and can be separated in two major groups. Group one uses pre-triggered data, which are than classified by a combination of Self-Organizing-Maps (SOM) and Neurnal Networks (NN). See Scarpetta et al. (2005) and Espositio et al. (2008) for further information. The drawback of these methods is that the detection problem, i.e. to separate signal from noise, has to be solved in advance at least for the currently available algorithms.

Ohrnberger (2001) was the first who applied Hidden Markov Model (HMM) based speech recognition techniques on parameters deduced from a continuous array analysis using data recorded at the Mt. Merapi volcano. Fig. 13.25 from Ohrnberger (2001) gives an example of the output of the continuous parameterization using seismic array techniques. The HMM approach solves the detection/classification problem in one single step by applying the double stochastic model which connects a Markov chain with the probability of observation parameters. Meanwhile a couple of applications exist (Beyreuther et al., 2008; Ibanez et al. 2009) where both groups are using the HTK-Toolkit for efficient computation of the classification probabilities. Fig. 13.34 gives an example of manual vs. automatic, HMM based detection and classification with data recorded in 1998 at Mt. Merapi volcano. Beyreuther and Wassermann (2011), also point out how the application of a slightly different stochastic model can improve the result significantly. In order to speed up the training and to ensure the flexibility of the classification, a guided training algorithm was developed as part of the EXUPERY project (see Section 13.6.5) by C. Hammer. This software is based on the python package ObsPy (www.obspy.org, Beyreuther et al., 2010), can be incorporated into the EARTHWORM system (see Chapter 13.4.7**)** and is available via the project webside www.exupery-vfrs.de.

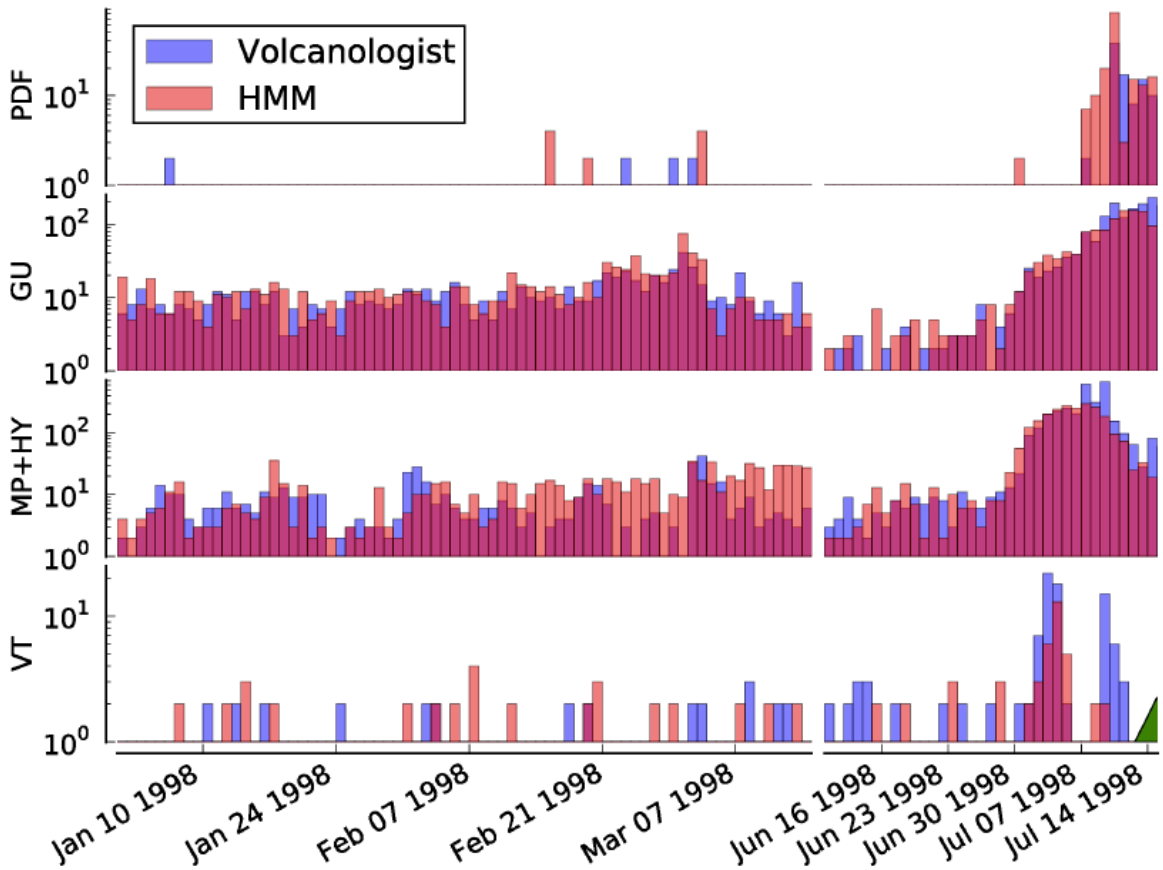

Fig. 13.34 Continuous classification using an automatic HMM based algorithm vs. human interpreter for seismic events from Mt. Merapi in 1998. The light red bars correspond to the classification results of the HMM classification, the blue bars correspond to the classifications of the local expert. The green triangle marks the onset of an eruption. The bars are transparent, thus a blue bar overlaid with a light red bar results in a purple bar (courtesy: M. Beyreuther).

13.4.6 Moment tensor inversion

In the recent years various approaches where made to investigate the dynamics of the different sources of the VLF and ULF signals using moment tensor analysis. While the estimation of the centroid moment tensor became a standard technique in earthquake seismology (e.g., NEIC and Harvard rapid moment tensor solutions), the application of this technique in volcano seismology is still restricted to specific applications or frequency ranges. The difficulties are manifold. First of all the influence of topography is neglected in the standard approaches, which results in large misfits of the computed synthetic Green's functions. Moreover, Ohminato et al. (1998) show that even when assuming a horizontal layered medium, the knowledge of the source location and velocity model with a high confidence is needed in order to apply this technique.

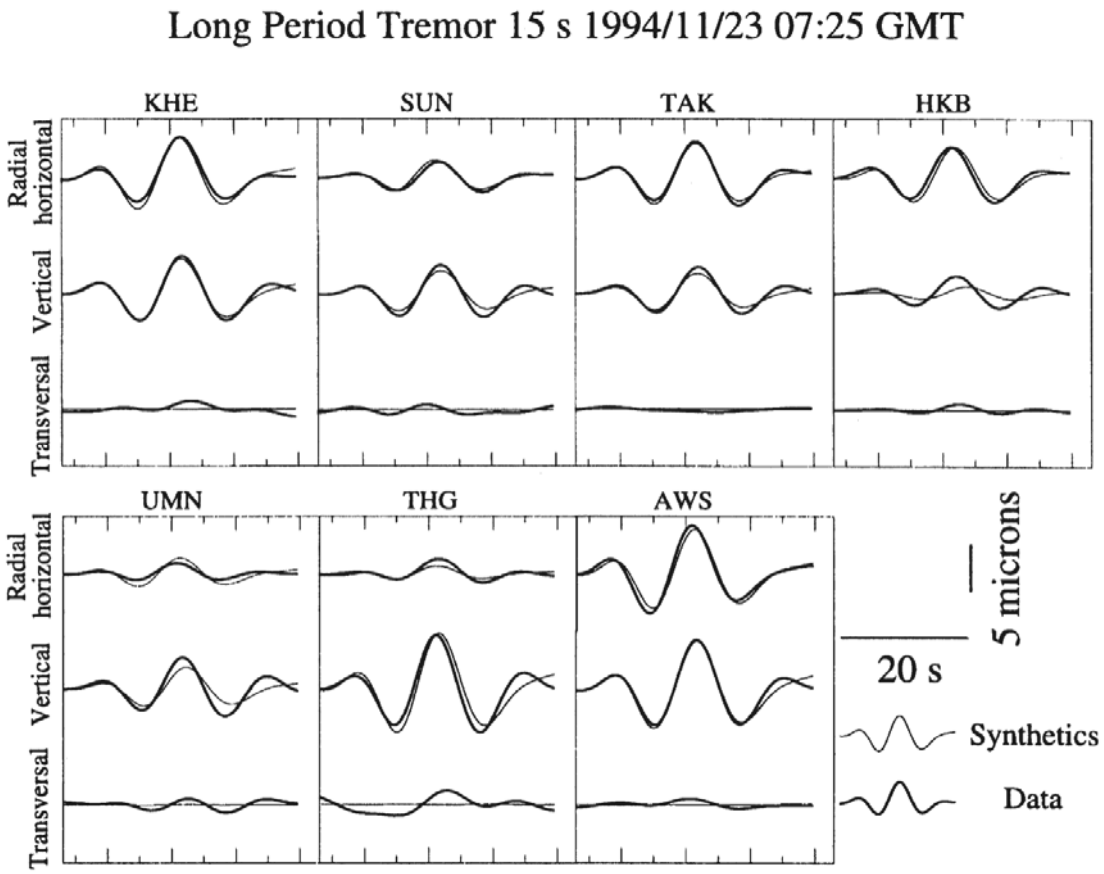

Fig. 13.35 Data (thick) and synthetic (thin) seismograms calculated from a inversion of the seismic moment tensor for a single pulse of *long period tremor* at Aso volcano. The corresponding source mechanism consists of a large isotropic component (97%) in addition to a small deviatoric part (Legrand et al., 2000).

Compensated linear vector dipole solutions (CLVD) are often biased by the uncertainty of the assumed simplified velocity structure. However, there are some applications of moment tensor estimations with VLF and ULF signals which gave reliable results, indicating source mechanisms which deviate significantly from a pure double-couple solution commonly known of tectonic earthquake mechanisms (e.g., Fig. 13.35 from Legrand et al., 2000; Ohminato et al., 1998; Aoyama and Takeo, 2001; Saraò et al. (2001).

13.4.6.1 Computation of Green's functions in 3D

The "day-to-day" increasing computer power combined with recent advances in computing synthetic seismograms (particle based methods: O'Brien and Bean, 2004; ADER-DG: Dumbser and Käser, 2006; Käser and Dumbser, 2006) makes it now possible to estimate Green's function in 3D up to high frequencies for medium sized problems. Due to the still enormous computer cost, the application of these techniques is restricted to institutions with

sophisticated (parallel) computational infrastructure. One of the first attempts to include the topography of a volcano into the simulation process or Green's function calculation was published by Ripperger et al. (2003). In their simple stair case model the authors already showed the importance of topography as a prominent scatterer in the higher frequency parts of the spectra. For the definition of the Greens function please see Chapter 3 of this manual and the paper by Graves and Wald (2001).

In a series of papers Bean et al. (2008), O'Brien and Bean (2004, 2009), Lokmer et al. (2007) and De Barros et al. (2011) impressively demonstrate the severe effects of topography, unknown velocity structure and source location on the inverted source mechanism. When not properly tested this will lead to completely wrong results where much of the error is projected in non-"double couple" parts of the inverted moment tensor. De Barros et al. (2011) also showed that the misfit or in other words "misleading forces" (see Section 13.4.5.2) can be reduced when observing volcanic signals in their near field and in a reduced frequency range. While scattering plays no important role for frequencies below, e.g., 0.2 Hz, the topography significantly change the Green's function and therefore, when not corrected for, causes severe errors in the resulting moment tensor. Additional sources of errors are uncorrected tilt signals especially when horizontal components of recorded seismograms are used and the unknown amount of strain-tilt coupling which is caused by local heterogeneities directly at the installation site of the deployed sensor (see Section 13.3.1)

13.4.6.2 Source modeling of complex processes

In theory nearly every seismic source known in earthquake seismology or related fields can successfully be modeled by an arbitrary moment tensor or by a combination of several moment tensors. However, when interpreting seismic signals of volcanic origin sometimes additional forces are needed in order to explain the recorded seismograms. Cesca and Dahm (2008) showed, that the 2005 paroxysmal eruption of Stromboli volcano can be modeled best by a combination of a moment tensor representing a CLVD (see chapter 3 for nomenclature) and a vertical orientated single force. The latter is often thought to represent the acceleration of the slug towards the surface. James et al. (2009) however show, that the single force is modeled best by a down flowing and thus accelerating viscous fluid.

A complete different explanation is given by De Barros et al. (2011). In numerical studies they can show, that the modeled single force often represent a sort of "trash can", which includes all unknowns of the source process itself, the propagation media or instrumental problems.

Chouet et al. (2010), Chouet et al. (2008), Aster et al (2008) and De Barros et al. (2011) show that the combination of different geometrical bodies (cracks, cylinders, spheres), may lead to a successful minimized least squares representation of the seismic source (see Fig. 13.36). However, we should keep in mind that this representation only models the seismic part and may not explain the physics leading to a volcanic eruption correctly. Only few percent of the momentum during the ascent of magma or a volcanic eruption is transferred into elastic momentum, i.e., seismic waves. In order to shed more light into the process of volcanic eruption different measurements representing different physical aspects must be taken into account (see Section 13.5).

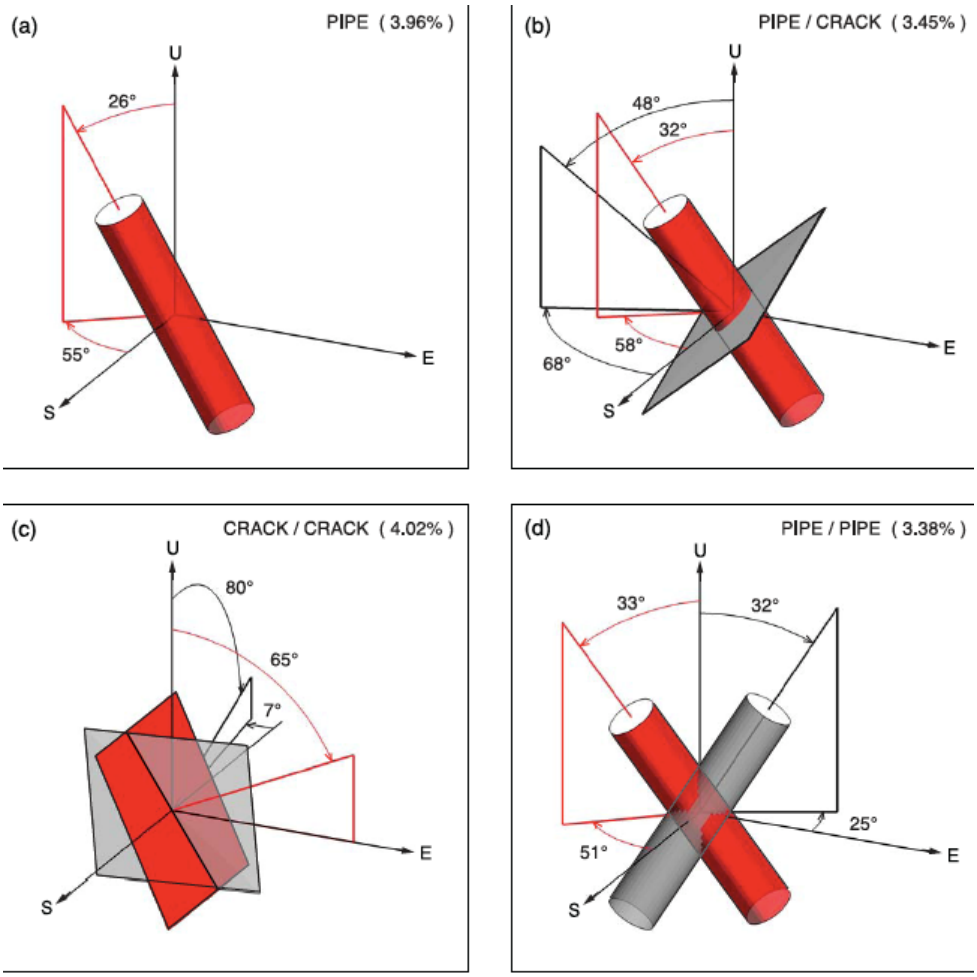

Fig. 13.36 Dominant source component (red) and sub-dominant source component (grey) of a degassing burst at Kilauea volcano (Hawaii, USA). Different geometries are compared and the residual errors are shown in parentheses at the upper right (from Chouet et al., 2010)

13.4.6.3 Limitations of Moment Tensor Inversion

Many limitations were already mentioned while discussing the computation of Green's function and source modeling. Unknown velocity model, source time function, tilt motions on the horizontal components and/or tilt-strain coupling and our limited knowledge about the physics of ascending magmatic material will naturally lead to a rather blurred view of the source processes in a volcanic conduit.

Still unknown are also the influences of scattering and the violation of the commonly used point source assumption. While the latter may lead to a wrong representation of the forces involved, the scattering of the wavefield will gain more importance when the focus is put on the observation, processing and thus detailed modeling of higher frequencies. Possible ways out of this dilemma will lead to even more complex and costly (i.e., computational time) simulations and modeling of the recorded wavefield. The strong scattering usually present at active volcanoes, however, may form a natural frequency limit of interpreting the seismo-volcanic sources.

13.4.7 Automatic analysis and databases

During a seismic crisis or in the framework of a long-term seismic surveillance, it is not possible to apply all the analysis tools described above in a visually controlled, interactive manner. During the October 1996 volcanic crisis at Mt. Merapi nearly 5000 events/day occurred. This large number of events obviously precludes any on-line, interactive analysis of the seismic data.

There are various approaches to automate at least some parts of the routine analysis in a volcanic observatory (e.g., Patanè and Ferrari, 1999). The most prominent software package is called EARTHWORM (Johnson et al., 1995), developed mainly under the auspices of the U.S.G.S. Many of the techniques described above are implemented in this "real-time" environment, e.g., continuous spectral analysis, RSAM, SSAM, automatic event associations, hypocenter location and magnitude. Mainly designed for monitoring local earthquakes, its widespread use at volcano observatories has led to the development of new, volcano related modules and promises new tools in the future. The EARTHWORM system appears to be very flexible and capable of being adapted to special requirements at different volcanoes. However, the great flexibility of this software package entails rather complex and unwieldy setup procedures when establishing the system the first time.

Also quite widely used is the system SEISAN (Ottemöller et al., 2011, for the latest release: http://seis.geus.net/software/seisan/). In strict sense not an on-line system, SEISAN combines flexibility, open source character and a stable but simple interactive environment, which altogether form an attractive tool for the global volcanic community.

While writing the revised chapter of this manual, several new developments were made in the framework of automatic, near-realtime analysis of seismic signals at active volcanoes. Next to now established LINUX/UNIX/MAC and WINDOWS versions of EARTHWORM (Johnson et al. 1995, www.isti.com) new systems are now available which may in future replace parts or the whole systems now currently running at volcanic observatories. E.g., seiscomp3, originally developed in the aftermath of the fatal 2004 Sumatra tsunami, is finding increasing applications within the global seismological and volcanological community (www.seiscomp3.org). While the majority of the routines, especially the data retrieval (seedlink protocol: http://geofon.gfz-potsdam.de/geofon//seiscomp/) is under GNU license, parts of the GUI, i.e., interactive parts are under binary license only. Currently seiscomp3 focuses on real-time analysis of seismic signals and thus needs a volcanological extension.

A volcanogical extension of EARTHWORM and seiscomp3 offers the newly developed geophysical database SeisHub (www.seishub.org), which was partly developed during the Exupery-project (see Section 13.6.5). Using a combination of a SQL-database (incl. the command set) together with XML structured documents it forms a very flexible way to store and retrieve information with geophysical content. It is especially able to store all parameters and data described in Section 13.5, regardless of whether the data consists of time-amplitude values or sequences of 2D images. The SeisHub database extensively uses a package named ObsPy (www.obspy.org), a python based library for unified input/output and analysis techniques. With its possibilities to connect or include parameters from seiscomp3 and EARTHWORM as well the possibility to connect to data centers via arclink/fissures/seishub, ObsPy closes the gap between real-time algorithms and more specialized application needed in volcanology.

Also the World Organization of Volcano Observatories (WOVO; www.wovo.org) is currently developing a SQL/XML database hybrid (WOVOdat; www.wovodat.org) able to store different parameters estimated or recorded at volcanic observatories around the world. The main focus of this data collection is to provide local observers with observations made at different volcanoes in order to enable a reliable estimation of unrest at "her/his local" volcano by comparing the surveillance parameters with that made at similar volcanoes.

13.5 Other monitoring techniques

As described at the beginning of this chapter, seismology is generally seen as the most reliable and diagnostic tool for monitoring a restless or erupting volcano. However, data from seismological surveillance alone are inadequate to understand and forecast eruptions. Modern monitoring systems will therefore combine seismology with other geophysical, geochemical, geodetic and geological techniques. In this section we focus on just a few of the various ground-based monitoring techniques which are closely related to seismology. We will not discuss the wide and fast-developing field of remote sensing in a volcanological context.

13.5.1 Infra sound

A method closely related to seismology consists in recording the infra sound produced by shallow volcanic processes. While the idea of recording infra sound is relatively old (e.g., Ripepe et al., 1996; Reed, 1987), the fields of application, instrumentation and theory is fast expanding. Most of the infra sound measurements are performed at volcanoes which show strombolian or hawaiianian activity. In this case the burst of large gas pockets (slug or annular flow) will produce large sonic signals which are recorded best in the infra sound range (Fig. 13.37).

Johnson et al. (2008) and Gerst (2010) show how the recordings of infra sound can help to estimate the overpressures of the bursting gas slug. Gerst (2010) however, pointed out that infra sound recordings alone will give wrong estimates of overpressures and bubble burst dynamics. Using additional measures taken by a Doppler radar instrument Gerst (2010) was able to develop a physical model how the bubble is bursting at the magma air interface. While the dynamics of the bursting bubble in this model is controlled by the kinetic and potential energy of the expanding bubble shell, the overall budged is dominated by the thermal energy of hot lava ejecta (Gerst,2010). The overpressures at Mt. Erebus volcano (Antarctica) remain small (3-7 bar) in relation to the violence of the eruptions. This is of great importance also for seismology at this type of volcano as it is then possible to better model the seismic coupling of the volcanic (fluid-gas) source to the elastic earth.

Also eruptions of more viscous volcanoes have been monitored using infra sound sensors. Caused by the different acting physics of ash jets and their associated sound the results are far less convincing than for their low viscous counterpart. Nonetheless, as a diagnostic of whether a volcano is erupting or the seismic signals are just reflecting an intrusion, infra sound recordings might help to discriminate and thus help to improve the early warning especially during bad whether conditions. Care should be taken, however, when installing an infra sound sensor (or sensor array). The reduction of wind noise or other unwanted signals is a difficult task, which might even act in favor of the installation of seismic broad band sensors instead. For details the reader is referred to Arrowsmith et al. (2010) for a very good overview of state

of the art research on seismo-acoustic wavefield and instrumentation.

a)

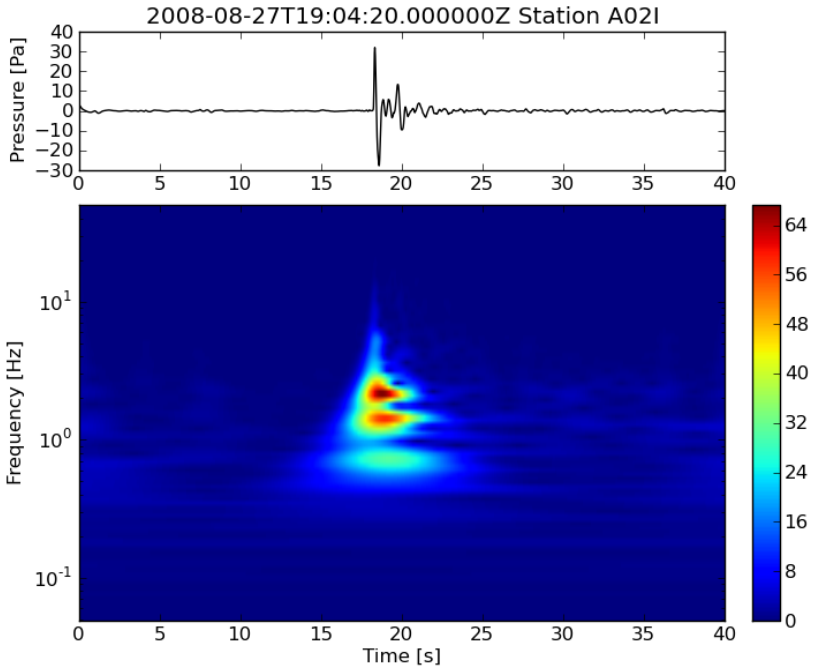

b)

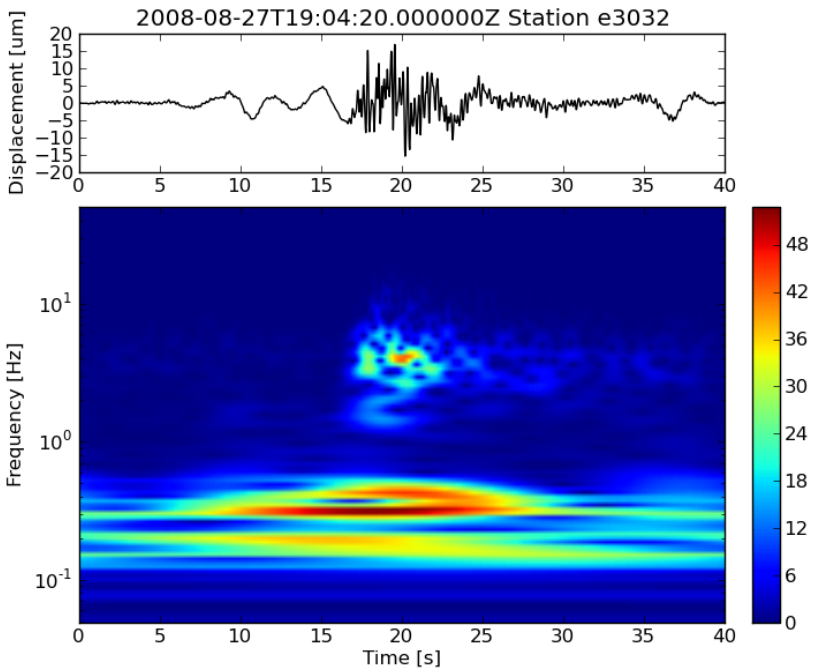

Fig. 13.37 Example of a strombolian type explosion recorded with **a)** an infra sound sensor and **b)** a seismometer at Mt. Yasur volcano (Vanuatu). The clear waveform of the infra sound signal is striking and supports the use and model of infra sound signals. However, the comparison with the seismic signal shows that, in this case, the latter already shows a significant amplitude at least 10 s before the onset of the acoustic signal.

13.5.2 Ground deformation (D-GPS, P-InSAR, strain, tilt)

Closely related to seismology is the monitoring of the deformation field caused by magma injection and/or hydrothermal pressurization within the volcanoes shallow or deep edifice. Deformation can be considered as an extension of seismology to lower, quasi-static frequencies, closing the gap of observed ground displacement to zero frequency. Modern techniques of monitoring the deformation signals of a restless volcano include borehole tiltmeters and/or strainmeters, electronic distance meter (EDM) and Global Positioning System (GPS) networks as well as airborne or ground based D-InSAR (Differential Synthetic Aperture Radar – Interferometry) measurements. Due to the increasing amount of positioning satellites (GPS, GLONAS) and accuracy, GPS will play an important role in the field of ground deformation monitoring over the coming decades. A relatively novel technique, which promises to have a large impact on the surveillance of active volcanoes are the airborne (airplane or satellite) or ground based differential InSAR measurements (Alba et al., 2008). While the airborne D-InSAR can cover a wide area with just one flight (see Fig. 13.38), the ground based D-InSAR has high repetition rate which makes the application of this technique very attractive during strong changes of the volcanoes edifice (Fig 13.39 for a non-volcanic example). For further reading on this exiting technique the reader is referred to text books of Hein (2004) or Hanssen (2001) and review articles by Bamler et al. 2009) and Bamler and Hartl (1998).

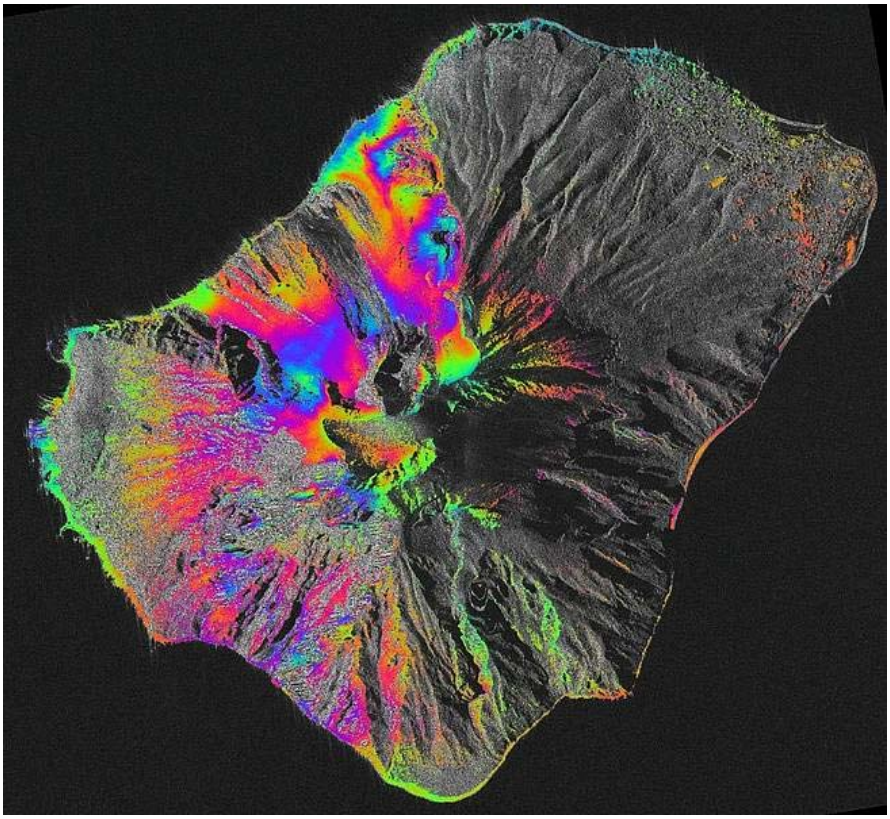

Fig. 13.38 Composition of differential interferogram and the amplitude image from Stromboli volcano (Italy). The differential interferogram was calculated from the same pair of satellites and an additional SRTM based DEM. Differential phase with the coherence bigger than 0.72 are shown (courtesy: DLR Oberpfaffenhofen, Germany; from: www.exupery-vfrs.de).

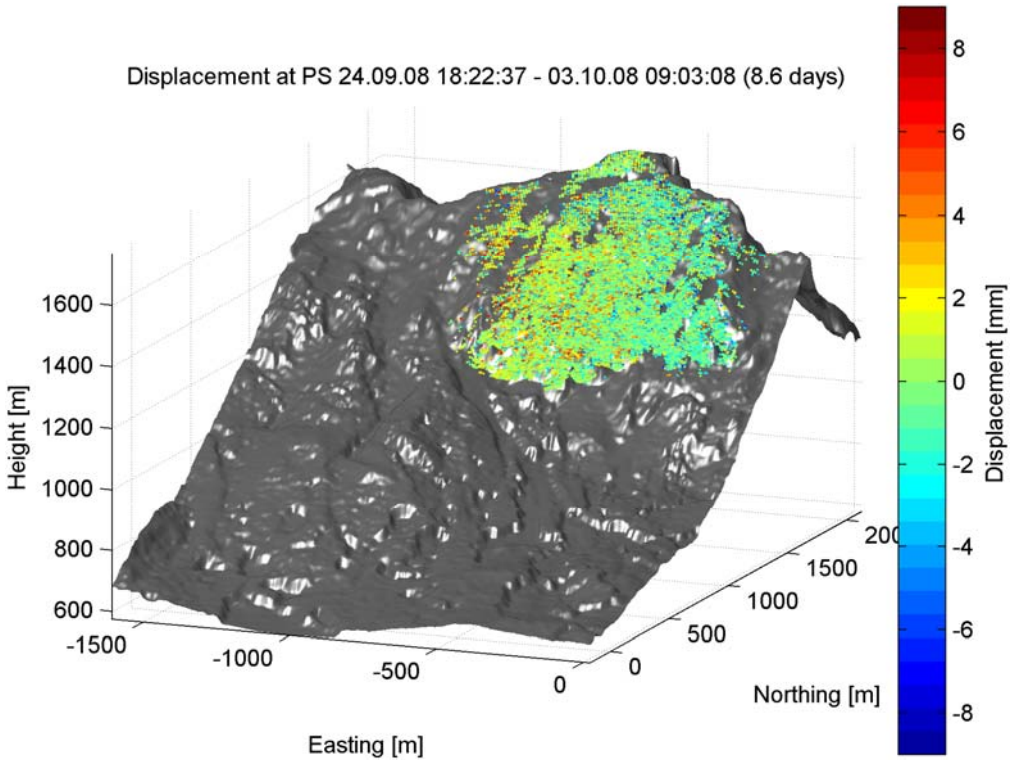

Fig. 13.39 Non-volcanic example of ground based D-InSAR measurement (Hochstaufen massif, Germany). While the covered area is small in comparison to flight based InSAR, the resolution and repetition frequency can be very high (courtesy: S. Rödelsperger TU Darmstadt, Germany).

A technique which is able to scan fast growing parts of the volcanoes edifice with even higher rates and precision, was originally designed to estimate the speed of particles expelled during strombolian eruptions (e.g. Hort and Seyfried, 1998; Hort et al., 2003). Vöge and Hort (2007) and Vöge et al. (2007) showed how this device, which consists mainly of a modified rain sensor commonly used in meteorology, could be adapted to monitor dome instabilities, which may lead to block and ash flows when this dome collapses. Recently Hort et al (2010) extended this method to also observe slow deformation processes by extracting specific phase information prior to eruptions at Stromboli and Santiaguito volcano.

Regardless what technique is used, the key point of monitoring ground deformation is the assumption that shallow or deep injection of large volumes of magma below a volcano will cause significant deformation of its surface. There were several successful approaches to forecast the 1980 eruption of Mt. St. Helens using deformation information (Murray et al., 2000) and at Hekla volcano, Iceland (Linde et al., 1993). The most recent 2000 eruption of Hekla volcano was accompanied by significant signals recorded by a cluster of strain meters located around the volcano (http://hraun.vedur.is/ja/englishweb/heklanews.html#strain). In addition, shortly before the eruption, increasing seismicity and volcanic tremor led to a precise forecast of the eruption (see Fig. 13.40). This can be seen as a perfect example of the complementarity of two different monitoring techniques. In addition there are many papers dealing with correlation between seismic signals and ground deformation at Kilauea volcano (Hawaii; e.g., Tilling et al., 1987)

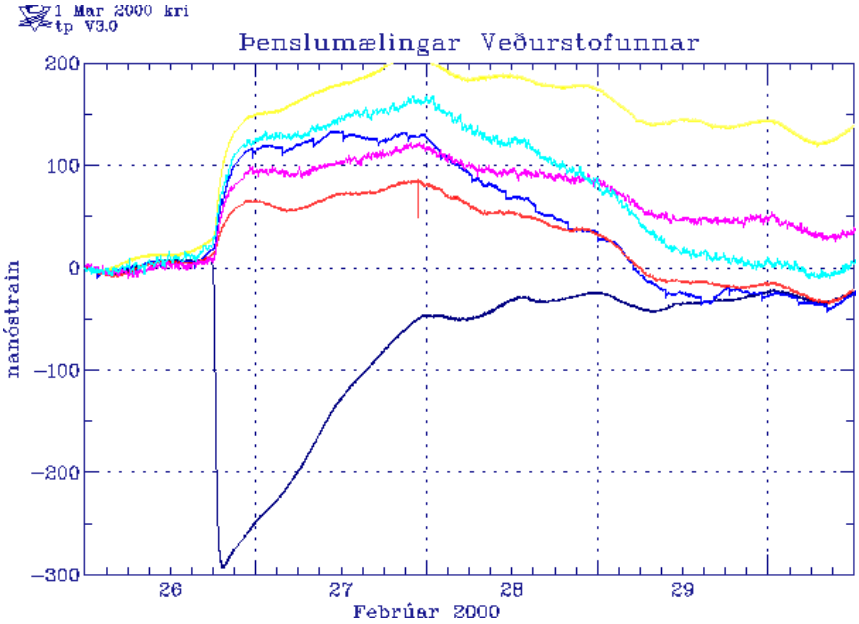

Fig. 13.40 The strainmeter data preceding the Hekla 2000 eruption are shown. As a result, three different phases could be defined. Firstly, a conduit was opened between 17:45 to 18: 17. Secondly, a reduced rate of expansion of the same conduit at 19:20 could be detected and finally all stations showed an increase when the conduit was fully opened and magma was flowing directly beneath the volcano (courtesy of Icelandic Meteorological Office, http://hraun.vedur.is/ja/englishweb/heklanews.html#strain).

A further example of good correlation between measurable deformation and the appearance of seismic signals is known from Suffriere Hill volcano, Montserrat island, West Indies, where Voight et al. (1998) observed a coincidence between several swarms of Hybrid events with cyclic changes in the deformation signals. This coincidence is very important regarding the inversion of source mechanisms of this class of signals. This kind of deformation signal, in conjunction with magma intrusion into the volcanic edifice, is known to be very small and mainly related to the active part of the volcanic dome. At Mt. Merapi several clusters of borehole tiltmeters are installed at the flanks, but only very weak signals have been recorded (Rebscher et al., 2000). In contrast, strong deformation signals are visible at the volcanoes' summit stations (Voight et al., 2000). This might indicate that at Mt. Merapi no large-sized and shallow-situated magma chamber exists and that the volume of ascending magma during typical eruptive phases is small. However, tilt stations at the flanks of Mt. Merapi and other volcanoes with apparently small magmatic activity would be very useful for discrimination between the usual small magma intrusions and possible larger ascending volumes of magma (as in 2010), which will then produce a much more pronounced tilt signal at the flanks of the volcano.

This points to a dilemma of the surveillance of active volcanoes. Some measurement techniques will produce years of just baseline data, which might lead to a reduction of attention (e.g., in equipment maintenance, new investment, number of staff etc.) and instruments. However, if a larger, more threatening eruption is imminent these long-term measurements might be of crucial importance for reliable hazard assessment and risk mitigation.

13.5.3 Micro-Gravimetry

The appearance of gravity changes at an active volcano also reflects possible inflation/ deflation cycles of magmatic material. There is a complicated interaction between physical and geometric properties (i.e., density, volume, location) of the moving material and height changes caused by the deformation of the surface of a volcano. Therefore, the monitoring of gravity changes is a challenging task that should be carried out with great care. As height changes are a significant component of gravity changes, gravity monitoring should always be combined with high precision leveling (e.g., total stations -electronic distance meters attached to an optical theodolite- or GPS measurements). For a reliable and less ambiguous inversion of the gravity data, a good knowledge of the velocity/density structure of the volcano is needed. Models of the magmatic system from gravity data should be regarded with caution, unless the conclusions are also supported by other independent observations.

13.5.4 Gas monitoring

Another important parameter preceding a volcanic eruption is the volume, velocity, temperature and composition of the emitted gas from a volcanic vent or fumarole. Volatiles and released gases are seen as the most important driving forces for both an eruption and the source of volcanic signals (e.g., explosion quakes, LF, MP, volcanic tremor; Schick, 1988; Vergniolle and Jaupart, 1990). Different techniques of gas sampling are in use, ranging from routinely collected gas samples in a weekly or monthly manner to a continuous analysis (every 20 - 30 min) of the emitted gas using a gas-chromatograph (Zimmer and Erzinger, 2003). For example high sampling rate in continuous data at Mt. Merapi revealed surprisingly short period pulsations (with a duration of 3-5 hours, see Fig. 13.41) in the water to carbon-dioxide ratio as well as in the temperature of a fumarole (Zimmer and Erzinger, 2003).

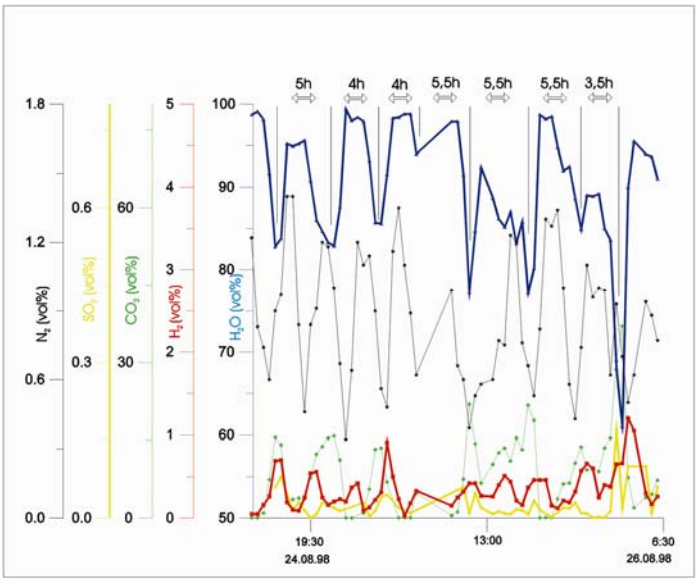

Fig. 13.41 Variation of the gas composition at one of Mt. Merapi's fumaroles. The gas is automatically analyzed approximately every 30 min using a gas-chromatograph. The analysis shows a fast changing composition of the gas with a period of roughly 5 hr. This special fumarol field (Woro) was altered/destroyed during the 2006 and 2010 eruptions of Mt. Merapi (courtesy of M. Zimmer, GFZ-Potsdam).

However, no significant correlation between this pulsation and the related seismicity could be found. The rhythms in this pulsating gas source only changed when the number of very shallow MP-events also increased. This lack of correlation between fast sampled gas data and seismic signals at Mt. Merapi might be caused by the our imperfect knowledge of how to parameterize the seismicity and the gas composition, respectively. Several case studies of changes in the chemical composition of fumarolic gases including descriptions of the accompanying seismicity and ground deformation is given by Martini (1996).

Many other papers deal with the long-term variations of gas prior to a volcanic eruption, which makes this technique a useful tool for long term monitoring (e.g., Stix and Gaonac'h, 2000).

Sulfur dioxide measurements from satellites make it possible to monitor volcanic activity and eruptions on much lager, even global scales. E.g., the Global Ozone Monitoring Experiment (GOME-2; carried by the MetOp-A satellite launched in 2006) provides, next to other gases, SO_2 columns with a global coverage within 1.5 days and a spatial resolution of 40 x 80 km (Fig. 13.42)

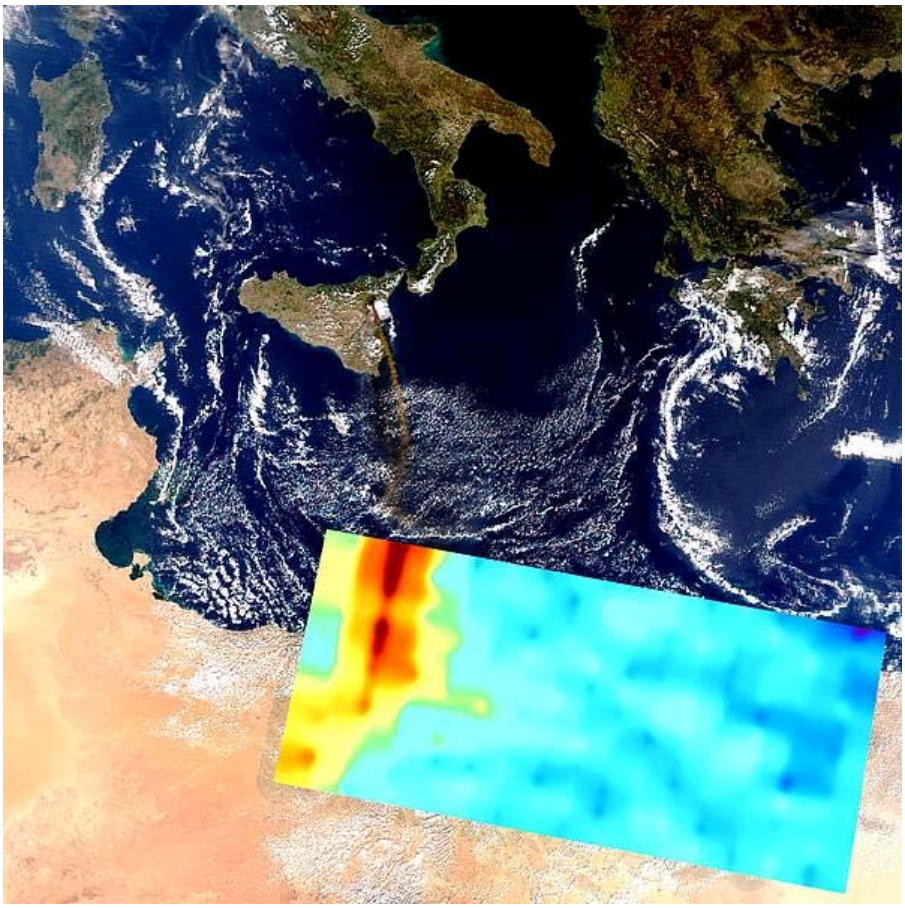

Fig. 13.42 Space-based observations allow near-real time detection of volcanic activity: SO_2 columns from GOME-2 as overlay on a MODIS (Moderate Resolution Imaging Spectroradiometer) imagery of Mt. Etna volcano, Italy (courtesy: DLR Oberpfaffenhofen; from: www.exupery-vfrs.de).

The satellite based volcanic SO_2 emissions are determined from solar backscatter measurements in the ultra-violet spectral range. In so doing, the Differential Optical Absorption Spectroscopy (DOAS) is applied, a technique, which may also be used as a ground based installation. The ground based counterpart has again much higher repeat rates and is thus a very valuable technique when a volcano shows first signs of unrest. The main goal of the satellite based technique is to monitor and forecast the dispersion of volcanic plumes up to 3 days and to attribute the detected SO_2 to a particular volcano. The final goal is than to facilitate a global warning service using SO_2 data. Over the past couple of years DOAS measurements are starting to be replaced by so called SO2 cameras (see e.g. Bluth et al, 2007; Mori and Burton, 2006), at least for the determination of the SO2 concentrations. They allow a 2D measurement at a rather high temporal resolution (up to 10Hz).

13.5.5 Thermal and video recordings

Monitoring of volcanic activity using radiometer or other imaging systems has been increasingly used over at least the last 25 years from space-borne or ground based remote sensing infrared sensors. The primary goal is the detection and analysis of volcanic hot spots and plumes at remote volcanoes. Modern sensors are now capable of resolving thermal anomalies even allowing the detection and monitoring of smaller effusive events. Over the last decade most observation from space of volcanic eruptions were carried out using data from AVHRR, GOES, MODIS, ASTER, BIRD, and Landsat-7 / ETM system. The different systems differ mainly in their spatial resolution ranging from 8×8 km for 6.47–7.02 µm band on GOES down to 15×15 m pixels for the VNIR bands on ASTER. Also the repeat times varies also strongly, with geostationary systems sending images every 15–30 min in contrast to the ASTER/MODIS system with repeat cycles of 16.5 days. At some volcanoes stationary, ground based infrared cameras proved to be useful to monitor changes in the volcanic system. Meanwhile cheap(er) and less sensitive devices are on the market which makes a remote installation at a sight with visibility to active vents possible (e.g., Stromboli, Popocatepetel etc.).

A lot more material can be found on the web page www.exupery-vfrs.de.

13.5.6 Meteorological parameters

While not directly linked to the eruptive behavior of a volcano, monitoring meteorological conditions is important for the proper interpretation of observed parameters as well as for the anticipation of possible triggering of volcanic activity. Lahars, i.e., volcanic debris flow, are often triggered by heavy rainfall, which additionally weakens the unconsolidated volcanic material. At Mt. Merapi, small-size gravitational dome collapses take place more frequently during the tropical rainy season.

The influence of meteorological conditions on the installed monitoring equipment is manifold. Barometric pressure and temperature changes could cause severe disturbances on installed broadband seismometers and tiltmeters, respectively. While these influences can be reduced by proper installation of the sensors (see Section 13.6), it is never completely removed. Spectral analysis of both meteorological and surveillance parameters may help to identify possible disturbances of the installed sensors. As mentioned before, rainfall may trigger volcanic as well as seismic activity. A good monitoring station will therefore also have

a continuously recording rain gauge.

In order to better judge the influence of meteorological (and also tidal) effects on the sensors and/or the volcanic activity, continuous long-term meteorological recordings are needed. Frankly speaking this is a difficult and sometimes impossible task because of the harsh environments at many active volcanoes. However, the continuity of such measurement are among the most important functions of a volcano observatory.

13.6 Technical considerations

In this chapter, some baseline information regarding the technical design of seismic surveillance network is given.

13.6.1 Site and vault

After selecting a possible site (see Section 3.1) for a seismic station or a seismic array, siginifcant care should be taken to protect the sensor from meteorological and other external effects. In Fig. 13.43a, a sketch of a possible installation scheme is shown. If a broadband sensor is to be deployed, even more care must be taken to protect this sensitive sensor from temperature and barometric pressure influences (see Chapter 5, Section 5.5 and Chapter 7, Section 7.4). Installations cover the sensor completely in sand in order to avoid instrument near air convection, which may lead to long period noise. Please inspect your instrument manual if this method will work for your instrument.

The weather conditions at volcanoes at even moderate altitudes can be very rough and rapidly changing. Protection against rain and lightning is the most important task when constructing a seismic station. All equipment should be placed in water tight casings, however, a water outlet should always be present. Most of the time it is harder to remove the water condensate from the vault than protect it against meteoric water.

Lightning protection is the most important and, unfortunately, the most difficult problem to solve (see Chapter 7, Section 7.4.2.5). Commonly, volcanoes have high resistivity surface layers (ash, lapilli etc.), making a proper grounding of the instruments nearly impossible. One of the optimal techniques to protect the equipment against lightning damage is to install a tower at the vicinity of the station with a mounted copper spire on top. The tower should be grounded as much as possible and be connected entirely with the ground of power-sensitive equipment. Furthermore, lightning protectors should be placed in front of any equipment to reduce the effect of high-voltage bursts (see Fig. 13.43b-c). Long cable runs should be avoided or changed to fibre optics. Using fibre optic cables for signal transmission has also the advantage that they are in-sensitive to electro-magnetic effects, which sometimes cause spike bursts on the transmitted signals.

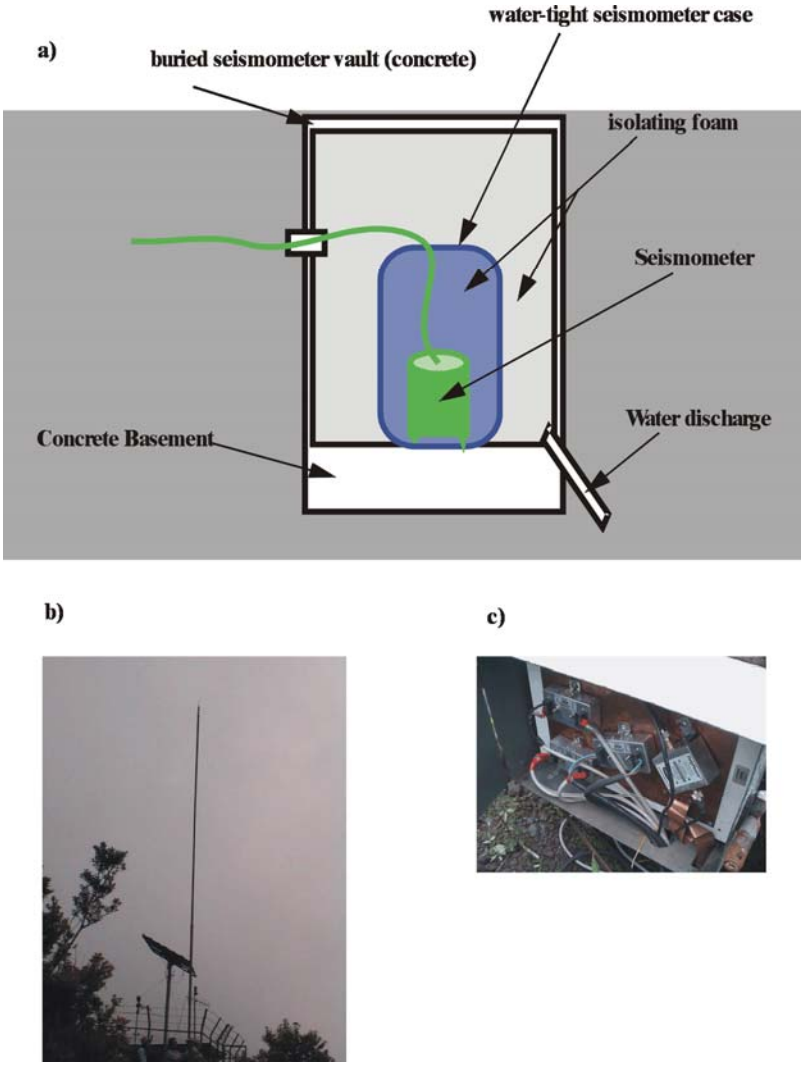

Fig. 13.43 **a)** sketch of a seismometer vault. The sensor should be placed in a water tight casing which is placed firmly on a concrete basement. In order to isolate the sensor from temperature and pressure changes due to air turbulences, the void space should be completely filled with insulating rubber foam or similar (see Chapter 7, Section 7.4.2). **b)** shows a lightning tower installed at Mt. Merapi, while **c)** shows additional lightning protectors for all sensitive equipment. The copper plate and all external devices (photo-voltaic modules) should be connected to the lightning tower.

13.6.2 Sensors and digitizers

Because the seismic signals produced by an active volcano cover a wide dynamic range the choice of the digitizer, i.e., the required dynamic range, should be carefully evaluated. Modern digitizers will sample the analog seismometer output with 24 bit resolution which results in a dynamic range of roughly 136 dB (depending on the sampling rate). A 16 bit A/D converter would usually be sufficient, but eruptive phases with various large amplitude signals will then saturate the digitizers' dynamic range (e.g., pyroclastic density flows, big explosions etc.). So called "gain-ranging" (i.e., the pre-amplification will be lowered if the signal is getting stronger) should be avoided because it will result in lower resolution and might mask small but important signals. Best suited are digitizers which sample with 24 bit

resolution but store the data depending on the recorded peak amplitude (i.e., 8 bits are stored if the signals are small and the activity is low, 16 bits when the activity is increasing and 32 bits if high activity occurs and the full 24 bit range is used).

If a network of seismic sensors is planned, several three-component short-period instruments (i.e., with 1 Hz corner frequency) will be sufficient (see Section 13.3.2). If the near-crater range is accessible, installing one or two broadband stations (i.e., 0.00833 to 0.05 Hz corner frequency) is a good choice. If large (M>4) earthquakes from an active volcano flank or nearby fault or subduction zone are possible, some broadband stations are preferred.

If an array or a network of arrays is to be installed, a mixture of three-component broadband and short-period one-component seismometers will be sufficient (especially when considering that there is no straight forward technique available which involves directly 3D seismic array data). A possible four station array would consist of a central three component station while the three satellite stations are equipped with vertical component sensors only.

13.6.3 Digital telemetry and satellite communication

Most of today's established monitoring networks at volcanoes are designed for transmitting the data "on-line" to a central data center, generally the local volcano observatory. This might be the main technical difference between a short-term seismological experiment and the long-term monitoring of a volcano. From experience worldwide, establishing a reliable radio line is a difficult and time consuming task, which also is subject to changes when new telecommunication facilities are constructed nearby and possibly worsen the data communication.

There are large differences between analog and digital radio transmission regarding data rate, dynamic range and sites to be selected and distance ranges to be covered. If a high resolution is required (e.g., using a 24 or 16 bit A/D converter at the sensor), the only way to exploit the full bandwidth of data is to transmit the signals with a digital radio modem. Meanwhile, several companies offer spread-spectrum modems which transmit in the frequency range of roughly 1 GHz and 2 GHz, respectively. The big advantage of these digital modems is the high data throughput (115,200 baud) and the low power consumption (transmitting power roughly 1 Watt). The high transmission frequency, however, is the main drawback of the digital radios. Commonly, the station and the data center must be in direct line of sight, with no hills, trees or other obstacles between them. This limitation should also be kept in mind when selecting a suitable seismic station site. The problem of obstacles can be circumvented when installing several repeaters on the way to the data center. Even so, the network design depends on intended radio lines (see also Chapter 7, Section 7.3 and Information Sheet IS 8.2).

A disadvantage of analog radio communication is the limited dynamic range and data throughput (usually below 38,400 baud). Most of the installed analog radio systems are barely able to transmit 12 bit and, therefore, the signals must be bandpass filtered (e.g., 1 - 20 Hz) before transmitting it. This is not acceptable when installing a broadband sensor. However, the radios are cheap and the typical frequency bands (100 MHz or 400 MHz) will enable a solid radio link even when the stations are slightly "out of sight".

Wireless LAN technology lately took over a large share in the communication business.

While in many countries the maximum applicable power output is restricted to 100 mW an intelligent use of different antennas for transmitting (low gain) and receiving (high gain) will allow distances of up to 10 km without the use of a repeater.

Even more suited for a communication network at active volcanoes are so called self organizing meshes. These ad hoc networks are able to organize their communication paths by themselves just by giving a central device the IP number of the transmitting station) see Fig. 13.44). If one of the nodes (transmitters) is lost, the network will re-organize itself to reach the stations by a different path. The drawback, however, is the rather complicated setting of the network as well as that potential station sites are chosen based on transmission properties rather than geological/geophysical evidences.

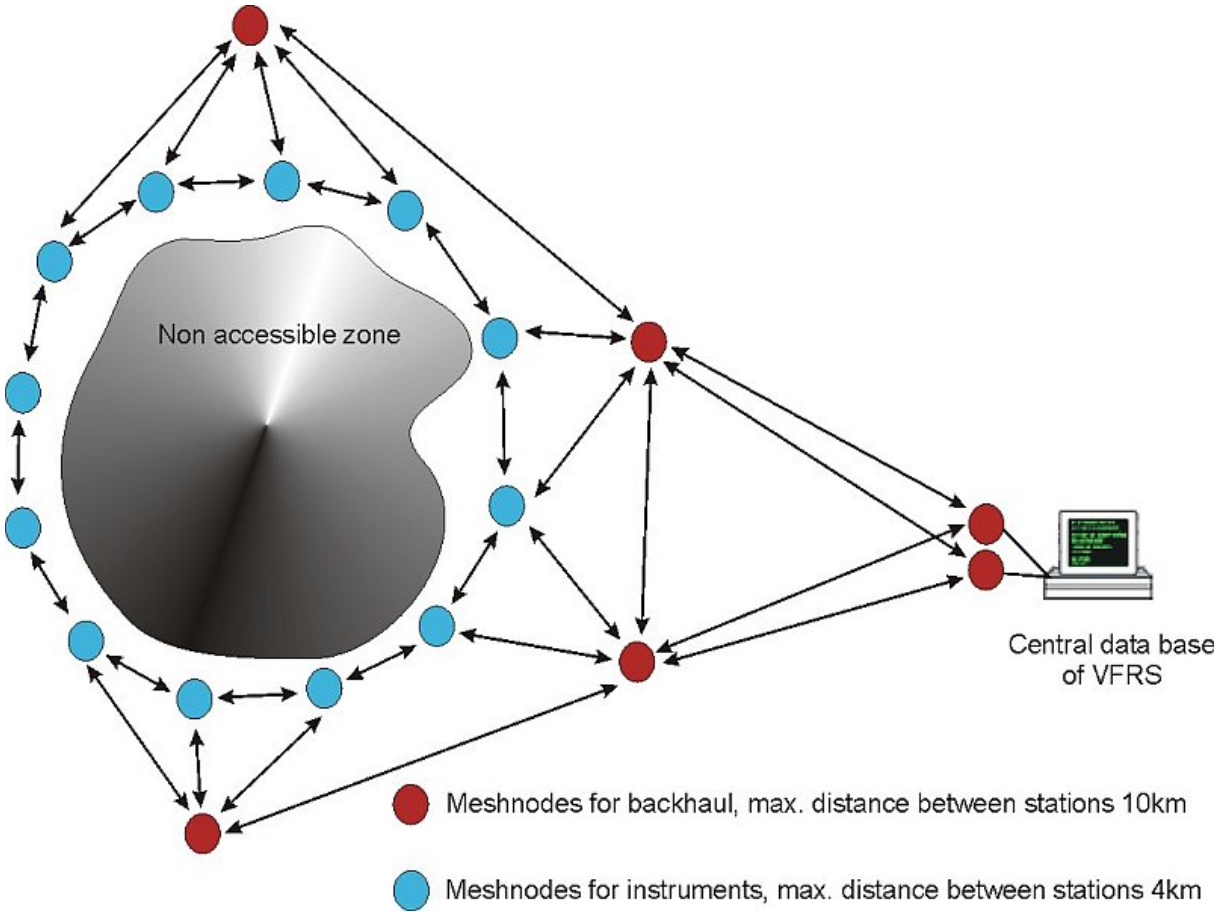

Fig. 13.44 Schematic principle of operation of a Wireless-LAN mesh. In case one of the nodes is not operational the data from a particular station is transmitted using a different path to the data center (courtesy: M. Hort; from: www.exupery-vfrs.de)

Meanwhile also many different satellite communication devices (V-SAT, Sky-DSL) are available. Due to the still high power consumption and rather sensitive equipment the use of these devices is restricted to certain points within the network (e.g., connection of the observatory to the international community; special node of high throughput).

13.6.4 Power considerations

Most of the stations will be remote and no access to a power network will exist. Therefore, the first step is to calculate the expected power consumption of the seismic station. It strongly depends on the kind of digitizer and sensor used, whether the data are transmitted by radio or not and which options for local data storage are desired. Therefore the power consumption of the field equipment should be extensively tested in the lab before constructing the power supply at the site and deploying the instruments. Never trust the optimistic specifications given by the manufacturer!

Most likely the power will be delivered by photo-voltaic (PV) modules, where a variety of different systems is available. All components of a monitoring installation must fit together, including the capacity of batteries and solar charger. Care must be taken, when estimating the amount of solar-modules needed to supply the stations. As a rule of thumb, 10% of the nominal maximum voltage will be supplied by the panels on average (i.e., using a 50 Watt module just 5 W are available on average). Voltage will typically decrease when the panels are installed high up in the mountains. Clouds, snow or ashfall may further reduce the effective power output (i.e., 5% or even less). This significantly increases the number of PV-modules required. To give an example, let the station consume at least 20 W (including radio, some digitizers, SCSI disks for local storage etc.), you will need 400 W panel power in the worst case which is 8 x 50 W panels at this station!

New developments in manufacturing solar-cells increase the efficiency of PV-modules. Especially the CIS technology (Copper, Indium and Selen) in combination with different alignment of the cells makes them more robust against partial shadowing and more efficient in diffusive light condition. The higher costs per panel are balanced by fewer numbers of panels needed to supply power for the monitoring station.

Also the capacity of the battery must be adequate in case no solar power is produced. However, the battery should not be too big in capacity as the PV-modules must be able to recharge the battery in sufficient time. Whenever possible, alternative power sources should be used, such as robust wind generators. It should be kept in mind, however, that a nearby wind generator might increase the noise of a seismic sensor. In case the station is located near running water, a small hydro-power engine could be a good alternative.

A novel and promising approach in building independent power supply which also produce enough power to feed even sophisticated but high power consuming radar devices or satellite dishes originates from the development of fuel cells. Meanwhile there are several different systems of portable fuel cells available. The fuels ranges from classical hydrogen to methanol based systems, which are cheaper and also carry a higher energy to weight factor. Combining PV modules together with fuel cells reduces the usage of fuel by guaranteeing the unbroken power supply. We note however that methanol is a hazardous substance and sometimes difficult to transport on ships and planes.

Care should be taken in the choice of the (programmable) solar charger and the batteries used. Currently Absorbed Glass Mat (AGM) batteries are most suitable for application at a remote site. They are lighter and more easily charged and discharged than common lead-gel batteries but also completely sealed and thus maintenance free. In future lithium air batteries might play an important role in solving the current problems of running monitoring equipment at remote areas.

13.6.5 Data center

All data streams, including those from monitoring techniques in addition to seismic, should be collected, stored and archived in a central facility. In the age of high-performance low-cost PC's, few standard computers will be sufficient to satisfy all needs of data collection, backup systems, automatic and visual analysis. Because continuous recording of all relevant signals is preferred over triggered data, a good backup strategy is crucial for getting complete and long-term data. Continuous recording is indispensable for improving our knowledge about volcanic activity, the underlying physical mechanisms and the relevant parameters to be observed when aiming at improving eruption forecasting. With the advent of DVD disks and CD-ROMS a good solution would be to write images of data sets onto one of these media in a daily or regular manner. CD-ROMS in particular assure a good data safety to price ratio.

Much public domain software is available for either automatic (e.g., EARTHWORM; Johnson et al., 1995) or interactive analysis (SeismicHandler, SAC, IASPEI-Software, PITSA/GIANT). The Orfeus homepage is a good starting point when looking for suitable software and for further contacts (www.orfeus-eu.org)

A very promising new application in the field of "real-time" analysis is distributed as seiscomp3 by the German Research Centre for Geosciences (GFZ-Potsdam). The main advantages are the new design concepts (C++; Python plugins etc) as well as an up-to-date graphical user interface for interactive analysis. In contrast to EARTHWORM, seiscomp3 is directly connected to a SQL-database which can store the analyzed (seismic) event data. The major drawback of this new package lies in the strong focus on seismic real time analysis, which is difficult to change.

A different strategy was chosen during the development of ObsPy (www.obspy.org) and SeisHub (www.seishub.org), which are not real-time packages but form a "near-real-time" system adapted for the need of small to medium sized observatories. All source code parts are completely licensed under GNU and may be altered and changed according to the need of the users.

Obspy/SeisHub together with EARTWORM or seiscomp3 may serve as a good, flexible and easy extendable software solution for a volcano data center.

A special requirement of the data center is the availability of an "uninteruptable power supply" (UPS) to guarantee a loss-less data collection even if the power line of the observatory is broken. Depending on the quality of the power network, a generator could be a good solution to bypass blackouts which may last several hours.

Establishing a "quick-response" volcano observatory during a volcanic crisis of a long-dormant volcano need additional equipment and design criteria of the monitoring network to be deployed. All equipment, including the data center facilities, should be light weighted, robustly made and should have low power consumption. These demands very likely lead to down-grades in resolution and data through-put. A comprehensive description of one realization of mobile monitoring network, the *Mobile Volcano-Monitoring System,* is given by Murray et al. (1996).

Meanwhile several different new applications exist which are designed to react as quickly as possible to new volcanic crisis. An early European initiative EMEWS (European Mobile Early Warning System) was formed in order to define European standards in mobile volcano alarm systems.

A more national approach, which tries to include all possible sets of monitoring parameters, environmental parameters and network metadata is the Exupery-Volcano Fast Response System (VFRS; www.exupery-vfrs.de). The goal of this initative is to record and store all volcano relevant information in a newly developed database (www.seishub.org), to find new strategies of volcanic monitoring (e.g., ground base InSAR; space borne surveillance of active volcanoes) and to aid or guide the local observers and/or decision maker by creating a data vizulation system based on geographic information (GIS) and the estimated monitoring parameters (via EARTHWORM/seiscomp3 – ObsPy/SeisHub). The resulting GIS is also freely available (executable as well as source code) at www.exupery-vfrs.de. Fig. 13.45 gives a snapshot of possible applications. One of the design criteria for the GIS was its platform independence and easy handing.

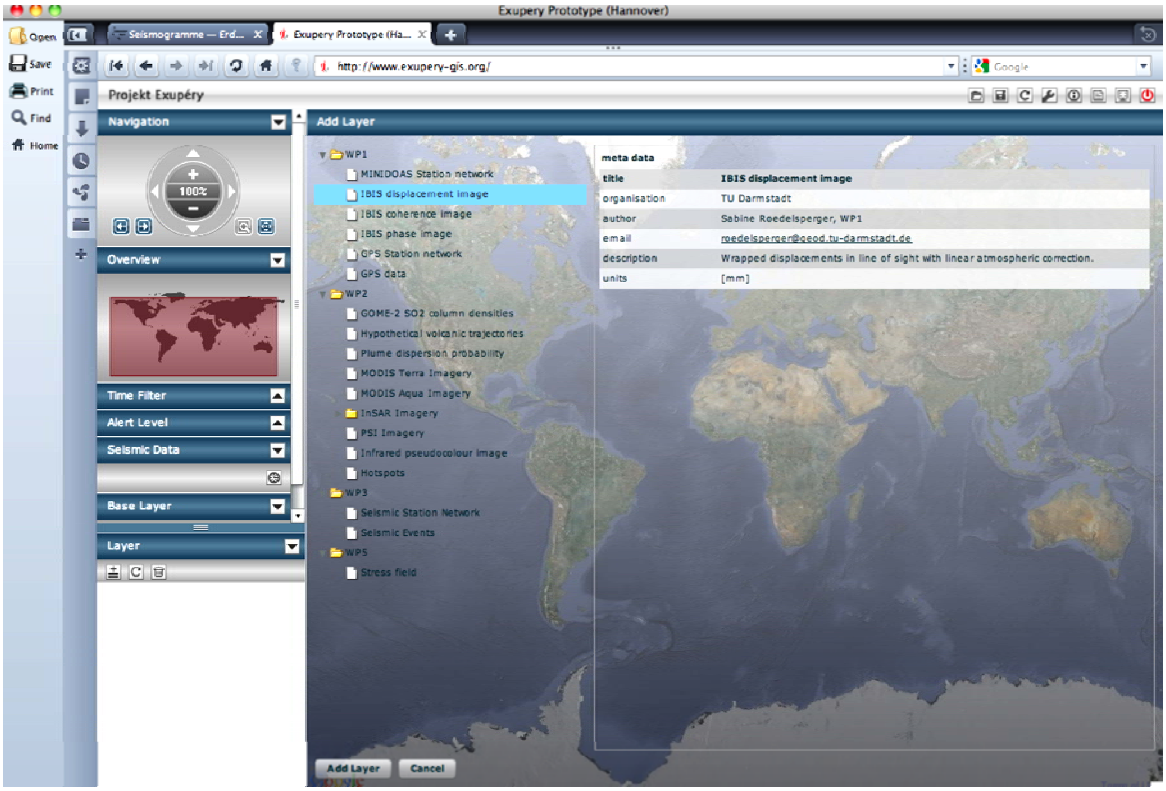

Fig. 13.45 Snapshot of the Exupery GIS. The browser-based application can include ground-based parameter sets and data as well as display 2D InSAR sections and 3D models.

The more and more common storage of multi-parameter data together with environmental data makes the application of "data mining" much more attractive. First steps in this direction are the application of automatic alert level systems based on Bayesian Belief Networks (BBN), which were introduced in volcanology by Aspinall et al. (2003) and Marzocchi et al. (2008). Fig. 13.46 shows the graphical network representation of a BBN build in into the Exupery VFRS. The output of this network consists of a simple alert level estimation which

should only guide the local authorities in their decision. One of the key advantages of this probabilistic belief networks lies in the specification of uncertainties of parameters which lead to a decision. With the interactive tools now available (e.g., GeNie, http://genie.sis.pitt.edu) and open source library (smile, http://genie.sis.pitt.edu) an observer is able to compute the level of probability once a BBN has been constructed and interactively change the BBN output by putting weights on different nodes, when additional information (e.g., field observation, "expert knowledge") is at hand.

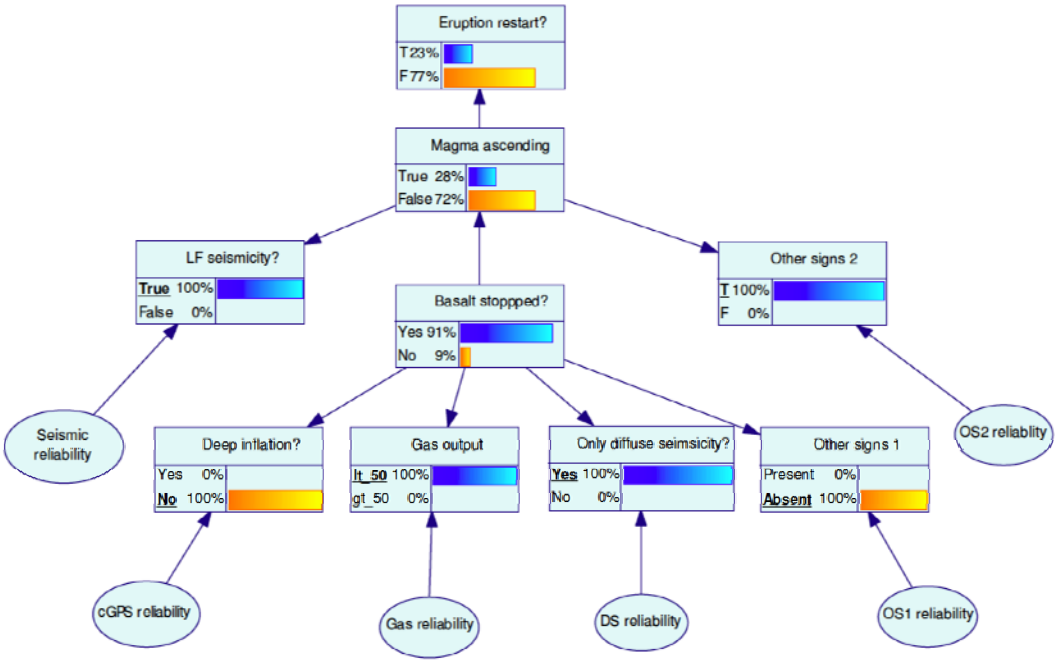

Fig. 13.46 Bayesian Belief Network used for automatic alert level estimation within the Exupery VFRS. This BBN is a modified version of a graphical network designed by Aspinall (courtesy of the author, from: www.exupery-vfrs.de).

Acknowledgments

I am grateful to the reviewers F. Klein, R. Scarpa and R. Tilling for their helpful comments and corrections to the first version, M. Hort and C. Bean for the revised manuscript, which improved the text significantly. I also thank P. Bormann for additional editing of this chapter. Without his continuous effort and labor this chapter never would have been realized. Furthermore leaving the figures and seismograms of E. Gottschämmer, S. Falsaperla, S. McNutt and M. Ohrnberger are highly appreciated. A lot material was taken from the Exupery project homepage (www.exupery-vfrs.de).

Recommended overview readings

Civetta, L., Gasparini, P., Luongo, G., and Rapolla, A. (Eds.), 1974. *Physical volcanology, developments in solid earth geophysics*, 6, *Elsevier*, Amsterdam.

Kawakatsu, H. and Yamamoto, M., 2007. Volcano Seismology, in *Treatise on Geophysics Vol.4*, pp. 389–420, ed. Schubert G., *Elsevier*, Oxford.